Effects of the Dielectric Environment on the Electrical Properties of Graphene

by

Rastko Anicic

A thesis
presented to the University of Waterloo
in fulfillment of the
thesis requirement for the degree of
Master of Mathematics
in
Applied Mathematics

Waterloo, Ontario, Canada, 2013

I hereby declare that I am the sole author of this thesis. This is a true copy of the thesis, including any required final revisions, as accepted by my examiners.

I understand that my thesis may be made electronically available to the public.

Abstract

This thesis provides the study of graphene's electrostatic interaction with the substrate surrounding it. Mathematical models based on current experimental configurations of graphene field-effect transistors (FET) are developed and analyzed. The conductivity and mobility of charge carriers in graphene are examined in the presence of impurities trapped in the substrate near graphene. The impurities encompass a wide range of possible structures and parameters, including different types of impurities, their distance from graphene, and the spatial correlation between them. Furthermore, we extend our models to analyze the influence of impurities on the fluctuations of the electrostatic potential and the charge carrier density in the plane of graphene. The results of our mathematical models are compared with current experimental results in the literature.

Acknowledgements

I am truly grateful towards Prof. Mišković for his continuous support and help in my research, and for the helpful and thoughtful advice he has given me.

I would also like to thank all my friends in Waterloo who have made my time here enjoyable, and my family for being with me throughout the bad and the good times.

Table of Contents

List of Figures

Chapter 1

Introduction

1.1 History

Carbon is the most ubiquitous element in nature. The 6^{th} element of the periodic table shows up in everything from the building blocks of our cells to the strongest known materials. Carbon by itself forms a variety of different crystal structures, called allotropes. The varying structure of the allotropes is responsible to the different properties of the material. Diamond is an example of an allotrope of carbon in which the atoms form a hexagonal crystal system. Such a structure makes it one of the strongest materials known. Recent experimental discoveries have given rise to new allotropes of carbon whose properties have been evaluated theoretically. The experimental discovery of these allotropes of carbon confirmed theoretical predictions. The first carbon allotrope to be discovered in the lab was buckminsterfullerene [37], a 60 atom carbon molecule formed into a highly symmetric ball shape. The team led by Sir Harold Kroto, Robert Curl and Richard Smalley, who made the discovery in 1985, was awarded the Nobel prize in chemistry in 1996. The discovery was surprising, as it confirmed that new forms of carbon crystal exist. Since its discovery, buckminsterfullerene and its variants have found some applications in chemistry as a lubricant and a catalyst. Another allotrope of carbon, the carbon nanotube, was discovered by Iijima in 1991 [30]. Carbon nanotubes are long cylinders of different radii formed entirely of carbon, sometimes one cylinder being contained within another. Due to its small radius, they can be thought of as an almost one-dimensional crystal. This crystal structure gives it great strength while maintaining its relatively small mass. Carbon nanotubes are the strongest materials in terms of tensile strength, and multi-walled carbon nanotubes have been shown to have strengths of 63 GPa [51], the equivalent of 6.2 metric tons for a cable with cross section $1mm^2$. Due to its high strength and very low density, carbon nanotubes have been proposed to be used as threading in a space elevator. Other potential applications of carbon nanotubes are staggering, and range from increasing electron conductivity in wires to making lightweight protective vests. The integration of carbon nanotubes into consumer products is still in its infancy and it is expected to be seen on shelves within the decade.

The most recently discovered carbon allotrope is graphene. Graphene is a two dimensional honeycomb lattice made of carbon atoms. It is a long sought after material due to its unique

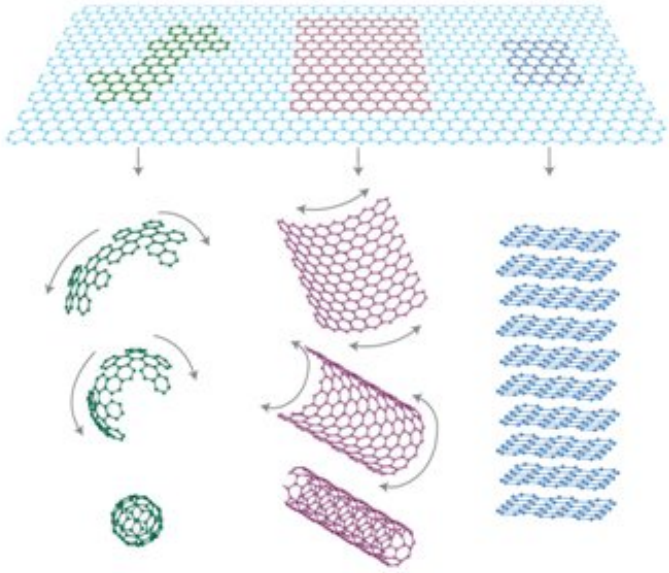

Figure 1.1: Allotropes of carbon formed from a sheet of graphene. From left to right we have buckminsterfullerene, carbon nanotubes and multi-layer graphene sheets. All of these can be formed from a single, large, sheet of graphene. Adapted from [10]

and versatile properties which were derived theoretically in the 1960s. The discovery of graphene in 2004 by a team from the University of Manchester surprised the physics community, and won them the Nobel prize in 2010. Since its discovery, experiments have confirmed graphenes theoretical predictions, and thousands of reports and articles dealing with its properties and possible applications have been published. In 2012 the European Union has pledged a €1B grant for development and research in graphene devices. Recent reports indicate that graphene based devices, such as e-paper and flexible touch screens, are due to hit the shelves as early as 2020, and its integration into high-performance logic circuits is expected by 2030 [48]. The wide gamut of graphene's properties have led it to be dubbed the material of the 21st century.

1.2 Properties and applications of graphene

Graphene has the potential to revolutionize many technologies in use today. Its properties have applications in both theoretical physics and material engineering. Graphene has shown to be an ideal, cheap testbed for various problems in quantum electrodynamics and condensed matter physics. Furthermore, adding a small amount of electrical energy to graphene makes the electron quasi-particles in it behave as though they were relativistic particles traveling at three-hundred times slower than the speed of light. The properties of these particles can be examined through the use of the Dirac equation in quantum electrodynamics, and hence the particles have been called Dirac fermions. A direct result of electrons behaving as Dirac fermions gives rise to a phenomena called Klein tunneling. With Klein tunneling, relativistic particles are allowed to transmit through potential barriers of any height with probability one. In layman terms this would be like a massless tennis

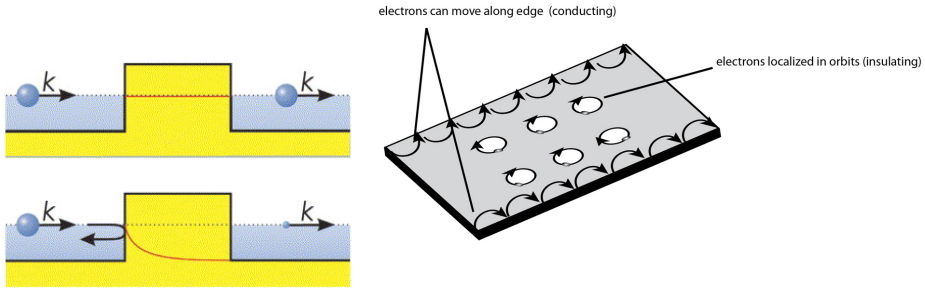

Figure 1.2: (Left) A comparison between relativistic Klein tunneling and regular quantum tunneling. In Klein tunneling, (top case) a massless fermion is transmitted through a potential barrier with probability one. In non-relativistic quantum mechanics, (bottom case) transmission through a barrier exponentially decreases as the length and height of the barrier increases. If the barrier is too high or too long, the transmission probability is negligible. (Right) Schematic overview of the quantum Hall effect. Due to the magnetic field, some electrons are localized in the graphene sheet, circling in orbitals of quantized radius. Other electrons near the edge of the graphene sheet cause a cross-conductance in the material since their quantized orbitals overlap with the boundary of graphene. Obtained from (left) [34] and (right) [31]

ball traveling at the speed of light going through a wall without hindrance. Recent experiments have shown that Klein tunneling in graphene is a realizable phenomenon and its application to semiconductors is being considered [62]. Another interesting property of graphene is its ability to show the quantum Hall effect. The quantum Hall effect is unique to two dimensional systems, and graphene is no exception. When graphene is placed in a transverse magnetic field, the electrons traveling through graphene experience a force in the perpendicular direction to its travel. This force causes the electrons in graphene to orbit in circles of quantized radius, thus reducing the conductivity in graphene. The results of these experiments give insight into the major problems in fundamental physics.

Graphene is an attractive and applicable material due to its high optical conductivity and its linear dispersion in energy near its ground state. By high optical conductivity, we mean that external electric fields induce a strong electrical response in graphene. Furthermore, the range of frequencies which interact with graphene (i.e. its bandwidth) is higher than conventional semiconductors. This implies that graphene could be used as a photodetector and an optical modulator for high bandwidth, high speed optical communications [72]. The linear dispersion in graphene is quite remarkable and is the primary reason for graphene's attractiveness. The linear dispersion implies that there is a linear relation between the so-called crystal momentum of the electrons in graphene and their energy. In most conventional semiconductor devices, the dispersion is parabolic, giving rise to a non-zero effective mass of the electrons. The linear relation gives rise to massless quasi-particles, and allows for Klein tunneling to take place. In addition, the linear dispersion relation allows graphene to be used in tunable mode-locked lasers [4, 65]. Other applications of graphene include its use as an ultracapacitor [64], a biosensors [38], a filtering membrane [11], and most importantly, as a transistors[53].

1.3 Graphene as a transistor

Plenty of research has been devoted to using graphene as a field effect transistor (FET). Through the use of capacitive gating and a back gate in a graphene FET, we can efficiently control the density of charge carriers (electrons or holes) in graphene. Graphene has been shown to have electron mobility an order of magnitude larger than conventional transistors [59]. This, coupled with the fact that graphene transistors would require relatively low amounts of energy to switch between on and off states (i.e. by controlling current through source and drain contacts), could pave the way for new electronic devices with increased execution speed and decreased power consumption. Furthermore, conventional semiconductors suffer from short channel effects. These effects arise from the scaling of the FET below a certain threshold and impair the performance of the transistor significantly. Graphene on the other hand, can overcome these problems due to its one atomic layer thickness [46]. This would greatly increase the miniaturization of transistors and allow the progression of Moore's law in everyday computer chips where conventional semiconductors would fail.

The research is not without problems. Due to the two dimensional structure of graphene, it is highly sensitive to its internal and external surroundings. This causes undesirable impurities to have a big effect on graphenes electrical properties. Charge carriers traveling through graphene can be scattered by external defects, such as charge or dipole impurities in the substrate, or internal defects, such as atomic vacancies in graphene or the crumpling of the graphene sheet itself [5]. This sensitivity makes graphene based transistors difficult to engineer since the level of control needed, in and around graphene, is extremely high. Another hurdle in developing graphene based transistors is the absence of a band gap. A band gap is a material property which implies that a material requires some finite, fixed energy in order for electrons to move within the material and conduct electricity. A band gap is necessary in order for a transistor to have a robust switch with unambiguous on and off states. In theory, graphene is a semi-metallic material (to be shown later) with no band gap. However, in practice, graphene possesses an extremely small band gap due to the material being finite in nature. Considerable work has been done to engineer graphene nanoribbons (GNR), which are sheets of graphene with a small width (10-20 nm), to induce a band gap in graphene devices. So far, no method developed has been able to produce a band gap larger than 360 meV in graphene. A large enough band gap threshold is required for two reasons: to overcome thermal effects, which undesirably increase the energy of the electrons, and to increase the on/off ratio (the ratio of the on state current to the off state current) above 10^4 [59]. An appropriately sized band gap is needed for graphene to be used in future transistors. There is a trade off between mobility and band gap [71]. Decreasing the width of the GNR and hence increasing the band gap, causes a reduction in the electron mobility. High electron mobility is required for logic gate transistors with high switching rate. However, electron mobility is greatly affected by impurities surrounding graphene as they induce scattering in the charge carriers. It has been shown that in suspended graphene, with minimal impurities surrounding it, the electron mobility is at least one order of magnitude larger than graphene on conventional substrates [7]. This large difference requires special attention, and the effects and limitations of the impurities on graphene need to be explored in greater detail.

1.4 Outline of thesis

In this thesis I shall discuss external effects that influence the static, electronic properties of graphene. The main idea is to develop realistic mathematical models and compare them with experimental results. The correlation between my theory and experimental results will shed some light on the still unanswered questions about charge carrier transport in graphene. The mathematical models will use semi-classical physics. In other words, the properties of graphene will be derived using quantum theory and the surrounding material will be modeled using classical electrostatics. Chapter 2 will describe the structure of the graphene lattice and the tight binding model for graphene. The mathematical description of the lattice is used to obtain the energy dispersion relation for quasi-particles in graphene and their density of states will be derived. Next, the experimental methods of modifying the Fermi energy of graphene through charge carrier doping are shown. This gives us a direct link between experimental results and the theory developed in this thesis. Chapter 3 will deal with the random phase approximation (RPA) as a method to derive the linear response function. There I shall describe the electron-electron interactions in graphene with its surrounding and how they contribute to the linear response to an external electric field. Afterwards, a geometric structure of the dielectric environment is presented. The Green's function is derived for the Poisson equation in order to solve for the electric potential in the classical, static case. Chapter 4 will be devoted to the discussion of charge impurities in the substrate near graphene. I shall present different statistical models of impurity correlation and impurity distribution in the substrate. Using the statisitcal description of impurities, the fluctuations in the potential and the fluctuation in the charge carrier density in the plane of graphene will be derived. There I shall show how the effect of charge impurities causes the formation of electron hole puddles in the sheet of graphene for a veriety of models, and a direct comparison to experimental results will be shown. Chapter 5 presents the equation for conductivity of charge carriers through graphene using the energy loss method (ELM). A variety of charge carrier conductivity and mobility profiles in a sheet of graphene is shown for a variety of different geometric models. A comparison between my theoretical results and those obtained experimentally will be shown once again. Finally, Chapter 6 will conclude my thesis and summarize the main points of my work and discuss potential future projects.

Chapter 2

Electronic Structure Of Graphene

2.1 Crystal structure of graphene

Graphene is formed by a two dimensional honeycomb crystal structure made from carbon atoms. It has two carbon atoms per primitive cell which are repeated throughout the lattice. The inter-atomic distance between the nearest atoms has been calculated to be approximately $a \approx 1.42\mathring{A}$ [10]. Figure 2.1 shows what a small portion of the crystal structure of graphene looks like.

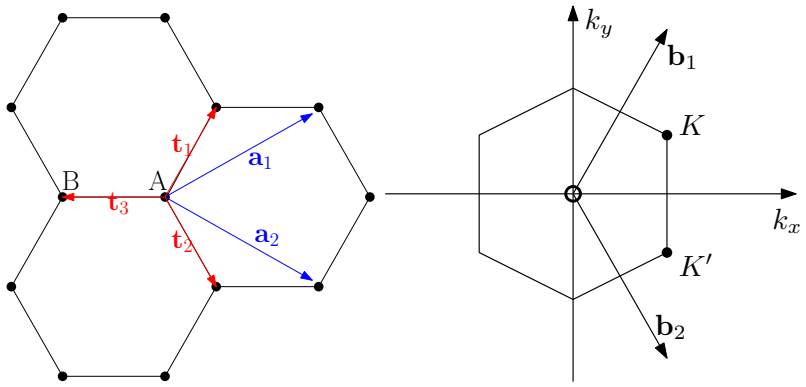

Figure 2.1: (Left) Crystal structure of graphene. The unit cell consists of the two atoms, A and B. The Bravais lattice is formed by repeating the structure of the unit cell using the vectors $\mathbf{a}_1$ and $\mathbf{a}_2$. The location of the nearest neighbour atom sites is determined by vectors $\mathbf{t}_1$,$\mathbf{t}_2$ and $\mathbf{t}_3$. (Right) The first Brillouin zone of the graphene lattice. Vectors $\mathbf{b}_1$ and $\mathbf{b}_2$ denote the reciprocal lattice vectors.

Using simple geometrical arguments we can calculate that the Bravais lattice of graphene is formed by the vectors

$$\begin{aligned} \mathbf{a}_1 &= \frac{a}{2}(3, \sqrt{3}) \\ \mathbf{a}_2 &= \frac{a}{2}(3, -\sqrt{3}) \end{aligned}$$

These vectors define the crystal structure of graphene and are translation vectors between atoms of

the same type. Each atom of type A is connected to three atoms of type B, and vice versa. We need the transition vectors between these two types of atoms in our tight binding calculations. Using similar geometric arguments we calculate that the nearest neighbour transitional vectors are given by

$$\begin{aligned} \mathbf{t}_1 &= \frac{a}{2}(1, \sqrt{3}) \\ \mathbf{t}_2 &= \frac{a}{2}(1, -\sqrt{3}) \\ \mathbf{t}_3 &= -a(1, 0) \end{aligned}$$

Using the vectors that form the Bravais lattice we can calculate the reciprocal lattice and identify the 1st Brillouin zone. The reciprocal lattice vectors are given by,

$$\begin{aligned} \mathbf{b}_1 &= \frac{2\pi}{3a}(1, \sqrt{3}) \\ \mathbf{b}_2 &= \frac{2\pi}{3a}(1, -\sqrt{3}) \end{aligned}$$

and the first Brillouin zone is marked in figure 2.1.

2.2 Tight binding calculations

Now we wish to evaluate the energy dispersion relation of graphene using the tight binding model. We know that graphene is a 2-dimensional honeycomb lattice formed from carbon atoms, so we must examine the structure of the carbon atom first. Each carbon atom consists of six electrons. Two of these electrons are contained in the deepest $1s$ electron orbitals. They are screened from external effects by the other four electrons in the $2s$ and $2p$ orbitals and are tightly bound to the carbon atom giving them limited mobility throughout the lattice. As such, they play no role in the electrical properties of graphene and so we will ignore them. The other four electrons in the $n = 2$ shell have very similar energies and so the electron orbitals will hybridize (i.e. form a superposition of electron orbitals). In order to do a proper tight binding calculation, we would have to include all four $n = 2$ orbitals ($2s$, $2p_x$, $2p_y$, $2p_z$) in the wavefunction. Since the graphene lattice will form a periodic potential, the wavefunction will obey Bloch's theorem [69]. Essentially Bloch's theorem states that for a periodic system, the eigenfunctions will have the form

$$\psi_{\mathbf{k}}(\mathbf{r}) = e^{i\mathbf{k}\cdot\mathbf{r}} u_{\mathbf{k}}(\mathbf{r})$$

where $u_{\mathbf{k}}(\mathbf{r})$ is a periodic function which has the same period as the Bravais lattice (i.e. the potential of the Hamiltonian) and $\mathbf{k}$ is the so-called crystal momentum, which labels the quasi-free electronic states. In addition to the four $n = 2$ orbitals, since there are two atoms per primitive cell of the Bravais lattice our Bloch wavefunction would be a superposition of 8 terms, summed over all Bravais

lattice vectors. With this in mind we can write the wavefunctions as

$$\psi_{\mathbf{k}}(\mathbf{r}) = \sum_{\mathbf{R}} e^{i\mathbf{k}\cdot\mathbf{R}}(b_{As}\varphi_{As} + b_{Ap_x}\varphi_{Ap_x} + b_{Ap_y}\varphi_{Ap_y} + b_{Ap_z}\varphi_{Ap_z} + b_{Bs}\varphi_{Bs} + b_{Bp_x}\varphi_{Bp_x} + b_{Bp_y}\varphi_{Bp_y} + b_{Bp_z}\varphi_{Bp_z}) \tag{2.1}$$

Here φ_{As}, φ_{Ap_x}, etc. are the hydrogen like atomic orbital wavefunctions (whose derivation can be found in [58]) with each one centered at either site A or B in the primitive cell. To keep the notation manageable we have dropped the $\mathbf{r}$ and $\mathbf{R}$ dependence from the atomic orbital wavefunctions. The sum, as usual, is taken over all Bravais lattice vectors. The wavefunction above forms 8 energy bands for each $\mathbf{k}$ in the first Brillouin zone. We can simplify our analysis of the energy dispersion by analyzing the structure of the electron orbitals in graphene more thoroughly. Each carbon atom in graphene is bonded to three other carbon atoms in the x-y plane. This means that the s, p_x and p_y orbitals on each atom must mix together (or hybridize) in such a way to form the covalent bonds between the carbon atoms. Such a mixed orbital state is called sp^2 hybridization since one s orbital mixes with two p orbitals to form a two dimensional hybrid orbital in the x-y plane. The sp^2 orbital states give rise to what are known as σ-bonding bands. Of the eight energy bands in the first Brillouin zone, six are σ-bonding bands of which three are the conduction and three the valence bands. The σ-bonding bands are characterized by having a very high energy gap between the conduction and valence bands and by having the Fermi energy in neutral (i.e. undoped) graphene lie between the two bands. Due to this high energy gap the σ-bonding bands do not contribute much to the electrical properties of graphene near the ground state, and so we will neglect them in our tight binding calculations, but a detailed analysis of the σ-bands can be found elsewhere [73]. The p_z orbitals remain separated from the rest of the orbitals and form what are known as π-bonding bands. The two π-bonding bands in graphene give us the unique electronic properties of graphene and are the primary reason why so much research has been devoted to this substance. Our tight binding calculations will deal with the p_z orbitals and the π-bonding bands, after which we will show why graphene is such an interesting material to study. Ignoring the wavefunctions that contribute to the sp^2 orbitals we can write the wavefunction as a linear combination of p_z orbitals on sites A and B,

$$\Psi_{\mathbf{k}} = a_{\mathbf{k}}\psi_{A,\mathbf{k}} + b_{\mathbf{k}}\psi_{B,\mathbf{k}} \tag{2.2}$$

Here $\psi_{A,\mathbf{k}}$ and $\psi_{B,\mathbf{k}}$ are the Bloch wavefunctions for the p_z orbitals located on sites A and B respectively. The wavefunctions are defined as

$$\psi_{A,\mathbf{k}}(\mathbf{r}) = \frac{1}{\sqrt{N}} \sum_{\mathbf{R}} e^{i\mathbf{k}\cdot\mathbf{R}}\varphi_{Ap_z}(\mathbf{r} - \mathbf{R}) \tag{2.3}$$

where $\mathbf{R}$ are the Bravais lattice vectors for the atoms on site A, and N is the number of unit cells. Similarly, $\psi_{B,\mathbf{k}}$ is defined with the replacement of A and B and summing over Bravais lattice vectors on site B. In order to solve for the energy as a function of $\mathbf{k}$ we start from the Schrodinger equation

in matrix form

$$\begin{bmatrix} \langle\psi_{A,\mathbf{k}}|H|\psi_{A,\mathbf{k}}\rangle & \langle\psi_{B,\mathbf{k}}|H|\psi_{A,\mathbf{k}}\rangle \\ \langle\psi_{A,\mathbf{k}}|H|\psi_{B,\mathbf{k}}\rangle & \langle\psi_{B,\mathbf{k}}|H|\psi_{B,\mathbf{k}}\rangle \end{bmatrix} \begin{bmatrix} a_{\mathbf{k}} \\ b_{\mathbf{k}} \end{bmatrix} = E \begin{bmatrix} \langle\psi_{A,\mathbf{k}}|\psi_{A,\mathbf{k}}\rangle & \langle\psi_{B,\mathbf{k}}|\psi_{A,\mathbf{k}}\rangle \\ \langle\psi_{A,\mathbf{k}}|\psi_{B,\mathbf{k}}\rangle & \langle\psi_{B,\mathbf{k}}|\psi_{B,\mathbf{k}}\rangle \end{bmatrix} \begin{bmatrix} a_{\mathbf{k}} \\ b_{\mathbf{k}} \end{bmatrix}$$

where H is the Hamiltonian of the graphene's atomic lattice. The exact form of the Hamiltonian is not known. What we can do is approximate the matrix elements of the Hamiltonian in the basis of the atomic orbital wavefunctions. The first matrix element is given by

$$\begin{aligned} \langle\psi_{A,\mathbf{k}}|H|\psi_{A,\mathbf{k}}\rangle &= \frac{1}{N}\sum_{\mathbf{R}} e^{i\mathbf{k}\cdot\mathbf{R}} \int d\mathbf{r}^3 \varphi_{Ap_z}(\mathbf{r}-\mathbf{R}) H \varphi_{Ap_z}(\mathbf{r}) \\ &= \int d\mathbf{r}^3 \varphi_{Ap_z}(\mathbf{r}) H \varphi_{Ap_z}(\mathbf{r}) + \sum_{\mathbf{r}_j} e^{i\mathbf{k}\cdot\mathbf{r}_j} \int d\mathbf{r}^3 \varphi_{Ap_z}(\mathbf{r}-\mathbf{r}_j) H \varphi_{Ap_z}(\mathbf{r}) + \cdots \\ &\approx \epsilon_{2p} \end{aligned}$$

In the second line we neglect all the terms after the first one. Here $\mathbf{r}_j$ denotes the nearest carbon atom of type A (i.e. a full unit cell translational vector). The distance between neighbouring type A atoms is large enough that all the integrals involving orbitals on different atoms of type A are negligible, and so we will drop them. What we are left with is the on site energy of the $2p_z$ orbital which we write ϵ_{2p}. Using the same argument we can show that $\langle\psi_{B,\mathbf{k}}|H|\psi_{B,\mathbf{k}}\rangle = \epsilon_{2p}$ as well. Now using once again only nearest neighbour interactions, the off diagonal matrix elements become

$$\begin{aligned} \langle\psi_{A,\mathbf{k}}|H|\psi_{B,\mathbf{k}}\rangle &= \sum_{i=1}^{3} e^{i\mathbf{k}\cdot\mathbf{t}_i} \int d\mathbf{r}^3 \varphi_{p_z}(\mathbf{r}-\mathbf{t}_i) H \varphi_{p_z}(\mathbf{r}) \\ &= \alpha \sum_{i=1}^{3} e^{i\mathbf{k}\cdot\mathbf{t}_i} \end{aligned}$$

Here α is the nearest neighbour coupling strength between atoms of type A and B and it is defined as $\alpha = \int d\mathbf{r}^3 \varphi_{p_z}(\mathbf{r}-\mathbf{t}_i) H \varphi_{p_z}(\mathbf{r})$ and $\mathbf{t}_i$ is one of the three translational vectors defined in section 2.1. Using the same nearest neighbour integrals on the normalization terms we get

$$\begin{aligned} \langle\psi_{A,\mathbf{k}}|\psi_{A,\mathbf{k}}\rangle &= 1 \\ \langle\psi_{A,\mathbf{k}}|\psi_{B,\mathbf{k}}\rangle &= \beta \sum_{i=1}^{3} e^{i\mathbf{k}\cdot\mathbf{t}_i} \end{aligned}$$

where $\beta = \int d\mathbf{r}^3 \varphi_{p_z}(\mathbf{r}-\mathbf{t}_i)\varphi_{p_z}(\mathbf{r})$. Next we define,

$$f(\mathbf{k}) = \sum_{i=1}^{3} e^{i\mathbf{k}\cdot\mathbf{t}_i} \tag{2.4}$$

In order to find the energy dispersion relation of graphene we need to find non-trivial solutions of the system

$$\left(\begin{bmatrix} \epsilon_{2p} & \alpha f(\mathbf{k}) \\ \alpha f^*(\mathbf{k}) & \epsilon_{2p} \end{bmatrix} - E \begin{bmatrix} 1 & \beta f(\mathbf{k}) \\ \beta f^*(\mathbf{k}) & 1 \end{bmatrix} \right) \begin{bmatrix} a_{\mathbf{k}} \\ b_{\mathbf{k}} \end{bmatrix} = 0$$

giving the secular equation

$$\det \begin{bmatrix} \epsilon_{2p} - E & (\alpha - \beta E) f(\mathbf{k}) \\ (\alpha - \beta E) f^*(\mathbf{k}) & \epsilon_{2p} - E \end{bmatrix} = 0$$

After some algebra we get that the energy dispersion has the form

$$E(\mathbf{k}) = \frac{\epsilon_{2p} \pm \alpha |f(\mathbf{k})|}{1 \pm \beta |f(\mathbf{k})|} \tag{2.5}$$

where we use + to denote the dispersion in the conduction band and − for the valence band. This result is exact when only considering nearest neighbour coupling in the tight binding model. Analysis of the graphene dispersion relations beyond nearest neighbour coupling have been done [54, 32]. Unfortunately including 2nd nearest neighbour interactions in the dispersion causes some properties which make our analytical results manageable, to vanish. Furthermore 2nd nearest neighbour effects are approximately one order of magnitude smaller than equation 2.5, so their contribution to the energy dispersion would be relatively small.

Since the Hamiltonian is not exactly known, the values for ϵ_{2p} and α are not known. However, they can be approximated from experimental results or first principle calculations. Currently admissible values of the parameters are $\alpha = 2.7\,\text{eV}$ and $\beta < 0.1$ with ϵ_{2p} being redundant [54]. The value for β is the overlap integral between the two electron orbitals centered at the two nearest neighbour atoms. For two p_z orbitals a distance $1.42\mathring{A}$ apart from each other their overlap is rather small and so we will approximate it to be zero. Also the on site energy ϵ_{2p}, which specifies the amount of energy required to ionize a carbon atom, shifts our two energy bands up or down by the same amount. We can ignore it since this constant does not change the qualitative description of the energy bands. Evaluating the energy dispersion, $E(\mathbf{k})$, we get

$$\begin{aligned} E(\mathbf{k}) &= \pm\, \alpha |f(\mathbf{k})| = \pm\alpha \left| \sum_{i=1}^{3} e^{i\mathbf{k}\cdot\mathbf{t}_i} \right| \\ &= \pm\, \alpha \sqrt{3 + 4\cos(\frac{\sqrt{3}a}{2} k_y)\cos(\frac{3a}{2} k_x) + 2\cos(\sqrt{3} a k_y)} \end{aligned} \tag{2.6}$$

With these two functions we can graph the surface of the energy dispersion in the first Brillouin zone (fig. 2.2).

Of importance here are the points $\mathbf{K}$ and $\mathbf{K}'$ in reciprocal lattice space. The points $\mathbf{K}$ and $\mathbf{K}'$ specify the location where the conduction and valence bands meet, but do not intersect. In other words the energy gap, between the two bands, is zero only at these two points. A material with no energy gap and negligible density of states at the Fermi level is characteristic of a semi-metal, hence this dispersion makes graphene a semi-metal. Furthermore, the energy dispersion near $\mathbf{K}$ and $\mathbf{K}'$ becomes linearly dependent on the momentum $\mathbf{k}$. These points are called Dirac points. The two

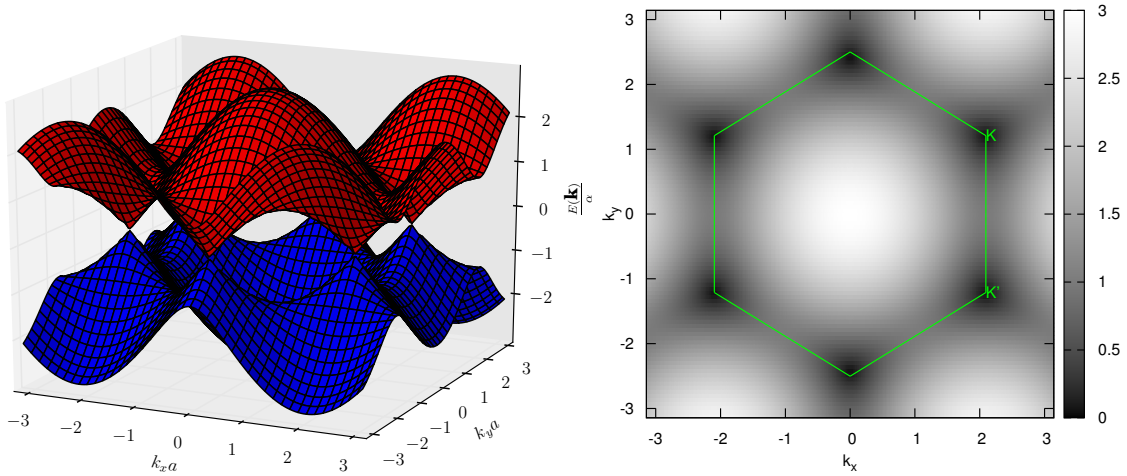

Figure 2.2: (Left) The energy dispersion of the graphene lattice, normalized by the parameter α, in the tight binding model using only the nearest neighbour coupling. No energy gap is present in the band diagram and there are six points where the conduction and the valence bands are touching but not overlapping. (Right) Dispersion of the conduction band overlaid with the first Brillouin zone. The two distinct Dirac points $\mathbf{K}$ and $\mathbf{K}'$ are clearly seen as the minimums of the conduction band, and hence the location where the two bands meet.

Dirac points are located at

$$\begin{aligned} \mathbf{K} &= \frac{2\pi}{3a}(1, \frac{1}{\sqrt{3}}) \\ \mathbf{K}' &= \frac{2\pi}{3a}(1, -\frac{1}{\sqrt{3}}) \end{aligned}$$

To show the linear dispersion of the energy near these points, we Taylor expand the dispersion equation around point $\mathbf{K}$ and keep all the terms up to second order. Defining $k_x = K_x + \delta k_x$, similarly with k_y, gives us

$$\begin{aligned} |f(\mathbf{k})|^2 &= 3 + 4\cos\left[\frac{\sqrt{3}a}{2}(K_y + \delta k_y)\right]\cos\left[\frac{3a}{2}(K_x + \delta k_x)\right] + 2\cos[\sqrt{3}a(K_y + \delta k_y)] \\ &= 3 + 4\cos\left(\frac{\pi}{3} + \frac{\sqrt{3}a}{2}\delta k_y\right)\cos\left(\pi + \frac{3a}{2}\delta k_x\right) + 2\cos\left(\frac{2\pi}{3} + \sqrt{3}a\delta k_y\right) \\ &= 3 - 2 + 3a\delta k_y + \frac{3a^2}{4}\delta k_y^2 + \frac{9a^2}{4}\delta k_x^2 - 1 - 3a\delta k_y + \frac{3a^2}{2}\delta k_y^2 \\ &= \frac{9a^2}{4}(\delta k_y^2 + \delta k_x^2) \end{aligned}$$

So near the Dirac point, $\mathbf{K}$, the dispersion only depends on its distance from the Dirac point. Taking the square root we get that $|f(\mathbf{k})| = \frac{3a}{2}k$ where $k = |\mathbf{k}|$ is redefined as a small displacement in the crystal momentum away from the Dirac point $\mathbf{K}$. We would have come up with the same result if instead of doing the perturbation around point $\mathbf{K}$ we did it around point $\mathbf{K}'$. So for momentum near

the Dirac point the energy dispersion is approximated by

$$E(\mathbf{k}) = \pm\alpha\frac{3a}{2}|\mathbf{k}| = \pm v_F k. \tag{2.7}$$

Here we defined $v_F = \alpha\frac{3a}{2}$, where v_F has units of velocity. We note that the energy dispersion given here is scaled by a factor of $\hbar$. Although this does not change any qualitative description, it is important to keep in mind in order for the units to make sense. The interesting thing about equation 2.7 is that the energy dispersion of electrons in graphene is linear and independent of their mass. The dispersion relation in equation 2.7 also arises from the study of massless fermions traveling at the speed of light. Using the Dirac equation for spin 1/2 fermions one can arrive at equation 2.7 with v_F being the speed of light. In graphene the speed $v_F \approx 10^6 \mathrm{m\,s^{-2}} \approx c/300$ has been calculated experimentally through the use of its cyclotron mass [49, 80]. This relation between graphene and the Dirac equation is the reason why points $\mathbf{K}$ and $\mathbf{K}'$ in the first Brillouin zone are called Dirac points. Equation 2.7 is one of the more important properties of graphene and it is the reason why so much research has been devoted to the material.

Using equation 2.6 we can evaluate the eigenstates of the system and examine how the p_z orbitals on site A and site B are related. Near the Dirac cone $\mathbf{K}$ equation 2.4 becomes, $f(\mathbf{k}) = \frac{3a}{2}(k_x + ik_y)$. So the eigenvectors for a state near the Dirac point $\mathbf{K}$ are solutions to the matrix equation

$$\begin{bmatrix} \pm\alpha k & \alpha(k_x + ik_y) \\ \alpha(k_x - ik_y) & \pm\alpha k \end{bmatrix} \begin{bmatrix} a_k \\ b_k \end{bmatrix} = 0$$

Right away this gives us the normalized eigenvectors

$$\mathbf{u}_\pm = \frac{1}{\sqrt{2}} \begin{bmatrix} 1 \\ \pm\sqrt{\frac{k_x+ik_y}{k_x-ik_y}} \end{bmatrix}$$

Using complex analysis we can simplify the above equation into,

$$\mathbf{u}_\pm = \frac{1}{\sqrt{2}} \begin{bmatrix} 1 \\ \pm e^{i\theta_k} \end{bmatrix} \tag{2.8}$$

where $\theta_k = \tan^{-1}\left(\frac{k_x}{k_y}\right)$ is the polar angle of the vector $\mathbf{k}$. A similar result would have been obtained if the derivation was done around the Dirac point $\mathbf{K}$. So we see that the electron orbitals on sites A and B differ by a phase. This phase differense between the atoms in the unit cell gives rise to pseudospin and is a key component for relativistic like effects [33], which will not be discussed here.

2.3 Density of states

An important quantity needed in semiconductor physics is the density of states (DOS). The DOS gives us the number of states that are accessible for any given energy. With the energy dispersion defined in equation 2.7 we can evaluate the DOS near the Dirac point. The DOS for any given

material is defined as

$$D(E) = \int \frac{d^n\mathbf{k}}{(2\pi)^n}\delta(E - E(\mathbf{k}))$$

where n is the dimensionality of the dispersion relation. For graphene with a two-dimensional dispersion relation function the DOS is given by

$$D(E) = g\int \frac{d^2\mathbf{k}}{(2\pi)^2}\delta(E - E(\mathbf{k}))$$

where the integration is evaluated over the Brillouin zone. The value g is included to account for the degeneracy of the system. In this case we have two degenerate spin states and two Dirac point in the 1^{st} Brillouin zone. So the total degeneracy is 4. For small energies, $E(\mathbf{k})$, near the vicinity of the Dirac points $\mathbf{K}$ or $\mathbf{K'}$ the dispersion will be linear in k (i.e. equation 2.7). Including the $\hbar$ dependence on the energy and integrating over the polar angle we get

$$D(E) = 4\int_0^\infty \frac{dk}{2\pi}\, k\delta(E \pm \hbar v_F k) \tag{2.9}$$

Evaluating this integral gives us the DOS of graphene

$$D(E) = \frac{2|E|}{\pi(\hbar v_F)^2} \tag{2.10}$$

In this case, the density of states is clearly linear and symmetric around the Dirac point. The linear regime of the DOS is only valid for $|E| \lesssim 1.6\,\text{eV}$. Beyond the Dirac cone, the the DOS contains Van Hove singularities (see fig. 2.3). The derivation of the DOS beyond the Dirac cone can be found in [27]. For a more general case, which includes beyond nearest neighbour interactions, the DOS loses some nice properties. While the energy gap near the Dirac cone is still zero, the slope of the DOS for electron doping ($E > 0$) and hole doping ($E < 0$) is different, breaking the electron-hole symmetry of the system, and causing asymmetry of charge carrier doping. Although we do not deal with "beyond the Dirac cone" type problems in this thesis, it is still important to understand the limitations of our derivations. Furthermore, examining these problems can give insight into more general mathematical models describing graphene, and could be useful in the undertaking of future work.

2.4 Capacitive Gating

It is important to know the mechanisms of modifying the electrical properties of graphene in a typical experiment in order for a comparison between theory and experiment to be accessible. As with most other conventional semiconductors, graphene's electrical properties are controlled through the use of the electrical field effect. The electric field effect consists of inducing an external electric field near the material. The external field increases the energy of the charge carriers (electrons or holes) on the surface of the material. The shift in the energy allows for the charge carriers to go from the valence band to the conduction band, thus allowing for current to flow through the

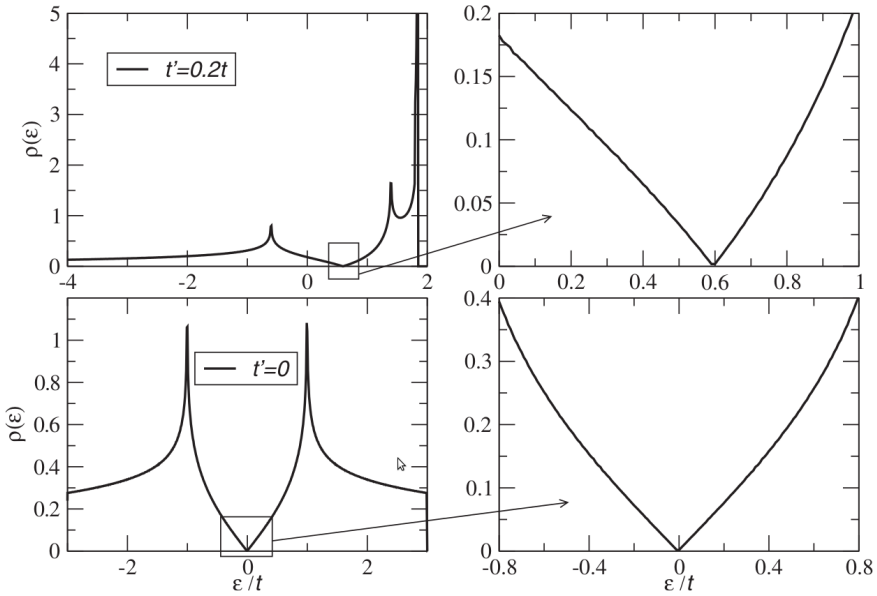

Figure 2.3: The density of states for the graphene lattice. Here $\rho(\epsilon)$ is the DOS defined in this thesis as $D(E)$ and t and t' are the nearest neightbour and nearest-nearest neighbour coupling parameters respectively. (Top) With 2^{nd} nearest neighbour interactions the Dirac point shifts to the right. The DOS is asymmetric around the Dirac point. (Top right) Although there is still no energy gap, the slopes of the DOS is different for hole and electron doping near the Dirac point. (Bottom) The DOS for graphene considering only nearest neighbour interactions. Van Hove singularities can be seen at approximately $E/\alpha = \pm 1$. (Bottom right) The linear DOS near graphene is clearly visible, and has the same slope for both electron and hole doping. Picture adapted from [10]

material. In experiments examining the electrical properties of graphene, graphene is placed on top of a thin, insulating dielectric layer (usually silicon dioxide, SiO_2). Beneath the substrate is a metallic back-gate electrode which is connected to experimental controls. The back-gate electrode is used to produce an electric field, which causes a voltage difference across the insulating, dielectric layer. This layout is fairly similar to that of a capacitor with a parallel-plate geometry (see fig. 2.4). As such, we can use the capacitance to get a simple relation between the charge carrier density (number of charge carriers per unit area) on the graphene sheet and the back-gate voltage,

$$n = \frac{\epsilon_0 \epsilon_r V_g}{te} \tag{2.11}$$

Here ϵ_o is the constant, permittivity of free space, having the value $\epsilon_o = 8.854 \times 10^{-12}$ F/m in SI units, ϵ_r is the relative permittivity of the substrate. In this thesis we will be using Gaussian electrostatic units, which implies that $4\pi\epsilon_0 = 1$. V_g is the back gate voltage, t is the thickness of the dielectric substrate and e is the fundamental electric charge. Equation 2.11 is used in experimental settings as a bridge between theoretical and experimental results. By changing the gate voltage we can alter the charge carrier density in graphene. Graphene needs to be attached to metal contacts at different ends in order for charge carriers to flow and cause a current. In experiments the two contacts are called the source and the drain. In order for current to flow there needs to be a

potential difference between the source and the drain contacts. Usually the current saturates with slight increase in the source-drain voltage difference. Throughout this thesis, we assume that the source-drain voltage is large enough to permit current saturations, as such, we will not deal with the effects of the source-drain voltage in detail.

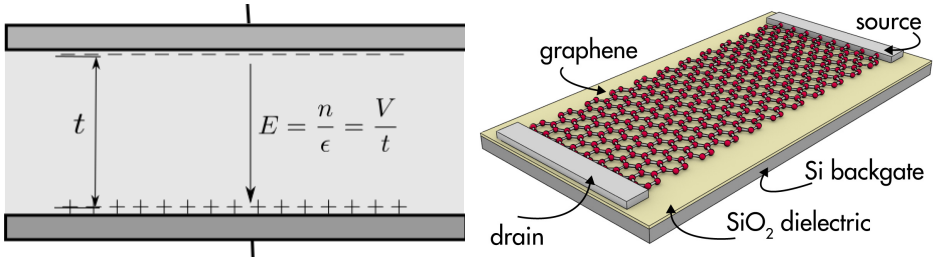

Figure 2.4: (Left) A parallel plate capacitor. Applying a voltage across the dielectric causes charges to accumulate on the different ends. A similar scenario occurs in graphene (Right) Schematic of typical experimental set-up to measure graphene conductivity. Source and drain contacts are attached to different ends of a sheet of graphene, and a dielectric substrate is placed underneath it. A slight potential difference between the two contacts is applied in order for current to flow through graphene. The voltage difference between the back gate and graphene controls the conductivity. In practice the voltage difference between the back gate and one of the contacts is used since the voltage in graphene isn't exactly known. (Right) Adapted from [26]

The charge carriers in graphene can either be electrons (n_e) or holes (n_h). The total charge carrier density is given by the absolute difference between these two values. We can calculate $|n_e - n_p|$ using the density of states in graphene near the Dirac point, and usual Fermi statistics. The number of electrons per unit area in the conduction band is given by

$$n_e = \int_0^\infty dE D(E) f(E)$$

where $D(E)$ is the density of states and $f(E)$ is the Fermi-Dirac distribution. Similarly the number of holes in the valence band is

$$n_h = \int_0^\infty dE D(E)(1 - f(E))$$

Assuming the Fermi energy of graphene is E_F, and using equation 2.10 as the density of states gives us

$$n_e - n_p = \frac{2}{\pi(v_F\hbar)^2}\left[\int_0^\infty dE \frac{E}{1+\exp(\beta(E-E_F))} + \int_{-\infty}^0 dE \frac{E\exp(\beta(E-E_F))}{1+\exp(\beta(E-E_F))}\right]$$

where $\beta = 1/k_B T$. Dividing the second integral by $\exp(\beta(E-E_F))$ and integrating over the positive real axis we get

$$n_e - n_p = \frac{2}{\pi(v_F\hbar)^2}\left[\int_0^\infty dE \frac{E}{1+\exp(\beta(E-E_F))} - \int_0^\infty dE \frac{E}{1+\exp(\beta(E+E_F))}\right] \tag{2.12}$$

These two integrals are called Fermi-Dirac integrals and they show up frequently in solid state

physics. We can express the charge density for an arbitrary temperature as

$$n_e - n_p = \frac{2}{\pi(\beta v_F \hbar)^2} \left[F(E_F) - F(-E_F)\right] \tag{2.13}$$

where

$$F(x) = \int_0^\infty dy \frac{y}{1 + \exp(y - x)}$$

In the zero temperature limit, the Fermi distribution becomes a step function (a Heaviside function) which is evaluated to one for energies less than the Fermi energy and zero otherwise (centered around E_F). In this case our integrals can be simplified to

$$n_e - n_p = \frac{2}{\pi(v_F \hbar)^2} \int_0^{|E_F|} dE E$$

which gives us

$$|n_e - n_p| = \frac{E_F^2}{\pi(v_F \hbar)^2} \tag{2.14}$$

Equation 2.14 gives us the charge carrier density, regardless of charge carrier type (i.e. electron or hole). Defining $\bar{n} = |n_e - n_p|$ as the average total charge carrier density and using the relation between the Fermi energy and the Fermi wavevector, $E_F = \hbar v_F k_F$, we get the direct relation between the Fermi level and the charge carrier density.

$$k_F = \sqrt{\pi \bar{n}} \tag{2.15}$$

In undoped graphene with no external interactions the valence band is full of electrons while the conduction band is full of holes. In this case the Fermi level lies on the Dirac point. Since the Dirac point is a single point of measure zero the density of states at the Dirac point is zero. This means that there are no charge carriers in graphene at the Dirac point. As such the conductivity would be zero. However this is not the case. Experimentally it has been shown that graphene has a minimum conductivity, even at zero charge carrier doping [66]. This paradox can be explained by realizing that flat graphene with no external interactions is an idealistic scenario. External charge impurities and the roughness of the substrate can spontaneously dope graphene. This can cause randomness in the local charge carrier density. It has been proposed that due to this randomness, graphene experiences finite conductivity near the Dirac point. Although equation 2.11 gives us a relation between the charge carrier density and the back gate voltage, one must keep in mind that this charge carrier density is only considered to be the average value, as impurities cause local fluctuations. To limit the effects of impurities near the Dirac point, we only consider the average charge carrier density, $\bar{n}$, in the range $10^{11}\text{cm}^{-2} \lesssim \bar{n} \lesssim 10^{13}\text{cm}^{-2}$. The lower limit on $\bar{n}$ is imposed for a reduction of the effects of impurities while the upper limit is needed so we only consider the two dimensional response function for graphene's π electrons in the approximation of the Dirac cone.

Chapter 3

Linear Response of Graphene

3.1 Random phase approximation

The Random Phase Approximation (RPA) is a widely used general framework for investigating many-electron systems and their response to external electric fields. It has been extensively used in the field of condensed matter to study the dielectric function of a free-electron gas [3], the dissociation behaviour of diatomic molecules [21, 67], atomization energies of small covalent molecules [17], etc. The idea behind the RPA is to examine particle-hole excitations that would result from an external field. A condition required for the RPA to be accurate is that the electron-electron interaction in the material is weak. However, in graphene the quasiparticle interaction is not necessarily weak. The coupling constant, which defines the strength of Coulomb interactions in graphene, is given by $\frac{r_s}{\epsilon} \approx \frac{2.19}{\epsilon}$, where ϵ is the dielectric constant of the material surrounding graphene. The coupling constant shows up in the perturbative expansion of the polarization function using the RPA. The constant $r_s = \frac{e^2}{\hbar v_F} \approx 2.19$ is analogous to the fine-structure constant in QFT. In free graphene ($\epsilon = 1$) the coupling constant is greater than 1, making the perturbative expansion of the interactions questionable, but since the coupling constant is controlled by the dielectric environment surrounding graphene, the value could be reduced to much less than 1 using a suitable substrate. There is still debate surrounding the RPA's validity in graphene [45, 15]. However the literature seems to agree that the problems arise in the case of intrinsic graphene (i.e. undoped graphene with $\bar{n}$ close to zero). In extrinsic graphene, where the Fermi energy is far away from the Dirac point, the logarithmic ultraviolet and infrared divergences, which arise from the momentum integral not including an upper and a lower cutoff respectivley, cancel each other out [15], making the RPA well behaved.

To derive the RPA we will follow the method of Bohm and Pines [6]. We begin this derivation using the most basic properties of the density matrix. The density matrix describes a quantum system in an ensemble of several quantum states. It is the quantum mechanical equivalent to the classical phase space distribution which evaluates the dynamics of the system. The equation that governs the quantum dynamics of the many-electron system is called the Liouville equation and it is given by

$$i\hbar\frac{\partial\rho}{\partial t} = [\mathbf{H}, \rho] \tag{3.1}$$

Here $\mathbf{H}$ is a Hamiltonian operator and ρ is the density matrix, which is also an operator acting on a Hilbert space. Similarly $[*,*]$ is the usual commutation operator. It is usually the case that we can't solve equation 3.1. However we can approximate it through the use of a simpler, solvable Hamiltonian. We would like to expand the Hamiltonian operator into its unperturbed Hamiltonian part and a perturbation potential that would arise from both external and induced internal effects reacting to the external field,

$$\mathbf{H} = \mathbf{H}_0 + V$$

We consider the perturbation potential, V, to be small when compared to the unperturbed Hamiltonian, $\mathbf{H}_0$. Let the states, $|\Psi_k\rangle$, be the eigenstates of the unperturbed Hamiltonian with corresponding energy levels E_k (i.e. $\mathbf{H}_0|\Psi_k\rangle = E_k|\Psi_k\rangle$). Since we are dealing with a many-body system, we note that k in general includes a vector describing the momentum, as well as the band indices, of the many-body system. We expand the density matrix, ρ, as a sum of an unperturbed and a perturbation density matrix,

$$\rho = \rho_0 + \rho_1$$

We assume that ρ_0 determines the dynamics of the unperturbed Hamiltonian and is a solution to equation 3.1, i.e. $i\hbar\frac{\partial\rho_0}{\partial t} = [\mathbf{H}_0, \rho_0]$. As such ρ_0 acting on one of the unperturbed states, $|\Psi_k\rangle$, gives us the probability of the system being in state $|\Psi_k\rangle$, that is $\rho_0|\Psi_k\rangle = f_0(E_k)|\Psi_k\rangle$ where $f_0(E_k)$ is the Fermi-Dirac distribution function. Now we want to approximate the solution to equation 3.1 for the full perturbed system

$$i\hbar\left(\frac{\partial\rho_0}{\partial t} + \frac{\partial\rho_1}{\partial t}\right) = [\mathbf{H}_0 + V, \rho_0 + \rho_1]$$

giving

$$i\hbar\frac{\partial\rho_1}{\partial t} = [\mathbf{H}_0, \rho_1] + [V, \rho_0] + [V, \rho_1]$$

Since both V and ρ_1 are small perturbations we will ignore the last term in the equation above, as it is a second order effect. Evaluating the matrix elements of the equation above in the basis of the unperturbed Hamiltonian gives,

$$\begin{aligned} i\hbar\frac{\partial}{\partial t}\langle\Psi_k|\rho_1|\Psi_{k'}\rangle &= \langle\Psi_k|[\mathbf{H}_0, \rho_1]|\Psi_{k'}\rangle + \langle\Psi_k|[V, \rho_0]|\Psi_{k'}\rangle \\ &= (E_k - E_{k'})\langle\Psi_k|\rho_1|\Psi_{k'}\rangle + (f(E_{k'}) - f(E_k))\langle\Psi_k|V|\Psi_{k'}\rangle, \end{aligned}$$

where the last equality follows from the properties of the eigenstate $|\Psi_k\rangle$ interacting with operators $\mathbf{H}_0$ and ρ_0 which were described earlier. Taking the Fourier transform in the time domain we get,

$$(\omega\hbar + i\nu^+)\langle\Psi_k|\rho_1|\Psi_{k'}\rangle = (E_k - E_{k'})\langle\Psi_k|\rho_1|\Psi_{k'}\rangle + (f(E_{k'}) - f(E_k))\langle\Psi_k|V|\Psi_{k'}\rangle$$

Here ν^+ is a small positive number that is taken to approach zero. It arises from causality, that is initially (in the limit $t \to -\infty$) the system is assumed to be unperturbed and the perturbing potential is applied adiabatically. Collecting the like terms gives,

$$\langle\Psi_k|\rho_1|\Psi_{k'}\rangle = \frac{f(E_{k'}) - f(E_k)}{E_{k'} - E_k + \omega\hbar + i\nu^+}\langle\Psi_k|V|\Psi_{k'}\rangle \tag{3.2}$$

This result is valid under the condition that $|\Psi_k\rangle$ are eigenstated of the unperturbed Hamiltonian. Equation 3.2 gives us the first order correction to the density matrix. Higher order corrections can be obtained using equation 3.2, but we will not consider these in this thesis. Now we can use the first order correction of the density matrix to evaluate the induced charge density at any point in space. First we need to make some assertions about the system we wish to analyze and its eigenstate wavefunctions $|\Psi_k\rangle$. Since this thesis primarily deals with graphene, we assume that our system is a two dimensional crystal with periodic structure that could be described by some primitive basis vectors as derived in Chapter 2. Furthermore we expand on the wavefunctions $|\Psi_k\rangle$ that we will be using. Using the tight binding model we have already calculated the electron wavefunction of graphene near the Dirac points $\mathbf{K}$ and $\mathbf{K}'$ (eq. 2.8) and we know the dispersion of the energy for different momenta (eq. 2.7). Since there are two energy bands we can label the electron wavefunctions as $|\mathbf{k}, l\rangle$. Here $\mathbf{k}$ specifies the two dimensional (2D) momentum of our wavefunctions and l is the index representing one of the two bands of the π bonds. Then we could represent the wavefunctions in position space as

$$\langle \mathbf{r}, z|\mathbf{k}, l\rangle = \Psi_{\mathbf{k},l}(\mathbf{r}, z) = \frac{1}{\sqrt{A}} e^{i\mathbf{k}\cdot\mathbf{r}} u_{\mathbf{k},l}(\mathbf{r}, z)$$

where A is the area of the crystal solid that we wish to examine. Since graphene is a two dimensional material, we are only concerned with momentum waves traveling in the plane of graphene. This implies that $\mathbf{r}$ and $\mathbf{k}$ are two dimensional vectors. Graphene is analyzed in a three dimensional space so we must include the out of plane dependence (the z dependence) on the wavefunction. $e^{i\mathbf{k}\cdot\mathbf{r}}$ is a plane wave with momentum $\mathbf{k}$, which is the momentum of the crystal lattice, and $u_{\mathbf{k},l}(\mathbf{r}, z)$ is a function which is periodic in the x and y coordinates and has the same period as the crystal in position space (i.e. $u_{\mathbf{k},l}(\mathbf{r} + \mathbf{R}, z) = u_{\mathbf{k},l}(\mathbf{r}, z)$, where $\mathbf{R}$ is some two dimensional lattice translational vector of graphene). Furthermore, we follow usual convention and define $l = 1$ for the conduction band and $l = -1$ for the valence band.

An external charge will induce an opposing charge density on the surface of graphene. Now the induced charge density can be expressed as the expectation value of the density matrix of a charged particle in position space,

$$n_{ind}(\mathbf{r}, z) = \langle \mathbf{r}, z|\rho_1|\mathbf{r}, z\rangle \tag{3.3}$$

The dependence of induced charge density on the frequency ω is implied, however we drop it for brevity. We can expand equation 3.3 in momentum space by using the completeness relation $1 = \sum_{\mathbf{k},l} |\mathbf{k}, l\rangle\langle\mathbf{k}, l|$,

$$\begin{aligned} n_{ind}(\mathbf{r}, z) &= \sum_{\mathbf{k}',l'} \sum_{\mathbf{k},l} \langle \mathbf{r}, z|\mathbf{k}', l'\rangle\langle\mathbf{k}', l'|\rho_1|\mathbf{k}, l\rangle\langle\mathbf{k}, l|\mathbf{r}, z\rangle \\ &= \sum_{\mathbf{k}',l'} \sum_{\mathbf{k},l} \Psi^*_{\mathbf{k}',l'}(\mathbf{r}, z)\langle\mathbf{k}', l'|\rho_1|\mathbf{k}, l\rangle\Psi_{\mathbf{k},l}(\mathbf{r}, z) \end{aligned}$$

To evaluate the equation above we will consider a two dimensional Fourier transform of the induced

charge density,

$$\begin{aligned}\tilde{n}_{ind}(\mathbf{q},z) &= \int d^2\mathbf{r} e^{-i\mathbf{q}\cdot\mathbf{r}} n_{ind}(\mathbf{r},z) \\ &= \sum_{\mathbf{k}',l'}\sum_{\mathbf{k},l}\langle \mathbf{k}',l'|\rho_1|\mathbf{k},l\rangle \int d^2\mathbf{r}\Psi^*_{\mathbf{k}',l'}(\mathbf{r},z)e^{-i\mathbf{q}\cdot\mathbf{r}}\Psi_{\mathbf{k},l}(\mathbf{r},z) \end{aligned} \tag{3.4}$$

The matrix elements $\langle \mathbf{k}',l'|\rho_1|\mathbf{k},l\rangle$ are independent of the location $\mathbf{r}$ so they are taken out of the integral. We can simplify our integral using the properties of the Bloch wave functions to get,

$$\begin{aligned} &= \sum_{\mathbf{k}',l'}\sum_{\mathbf{k},l}\langle \mathbf{k}',l'|\rho_1|\mathbf{k},l\rangle\delta_{\mathbf{k},\mathbf{k}'+\mathbf{q}}\int d^2\mathbf{r}\Psi^*_{\mathbf{k}',l'}(\mathbf{r},z)e^{-i\mathbf{q}\cdot\mathbf{r}}\Psi_{\mathbf{k}'+\mathbf{q},l}(\mathbf{r},z) \\ &= \sum_{\mathbf{k}'}\sum_{l,l'}\langle \mathbf{k}',l'|\rho_1|\mathbf{k}'+\mathbf{q},l\rangle\langle \mathbf{k}',l'|e^{-i\mathbf{q}\cdot\mathbf{r}}|\mathbf{k}'+\mathbf{q},l\rangle \\ &= \sum_{\mathbf{k}'}\sum_{l,l'}\langle \mathbf{k}',l'|\rho_1|\mathbf{k}'+\mathbf{q},l\rangle M^{l,l'}_{\mathbf{k}',\mathbf{k}'+\mathbf{q}}(z) \end{aligned}$$

Here we defined $M^{l,l'}_{\mathbf{k}',\mathbf{k}'+\mathbf{q}}(z)$ as the two dimensional Fourier transform of $\Psi^*_{\mathbf{k}',l'}(\mathbf{r},z)\Psi_{\mathbf{k}'+\mathbf{q},l}(\mathbf{r},z)$. Now using equation 3.2 for the matrix elements of the density matrix ρ_1 we expand our equation above to get

$$\tilde{n}_{ind}(\mathbf{q},z) = 2\sum_{\mathbf{k}'}\sum_{l,l'}\frac{f(E_{\mathbf{k}',l'})-f(E_{\mathbf{k}'+\mathbf{q},l})}{E_{\mathbf{k}',l'}-E_{\mathbf{k}'+\mathbf{q},l}+\omega\hbar+i\nu^+}\langle \mathbf{k}',l'|V|\mathbf{k}'+\mathbf{q},l\rangle M^{l,l'}_{\mathbf{k}',\mathbf{k}'+\mathbf{q}}(z) \tag{3.5}$$

We have included the multiple of 2 to account for the spin degeneracy of the electrons. In a more general situations where the spin of the electrons are coupled to the external interactions, the factor of 2 cannot be added and the spin interactions must be accounted for in the energy dispersion $E_{\mathbf{k},l}$. To simplify equation 3.5 even further we need to evaluate the matrix elements of the potential operator V. To do this, we once again look at the Fourier transform of the potential function in position space

$$V(\mathbf{r}',z') = \int \frac{d^2\mathbf{q}'}{(2\pi)^2}e^{i\mathbf{q}'\cdot\mathbf{r}'}\tilde{V}(\mathbf{q}',z')$$

Using this definition of the potential function, the matrix elements in equation 3.5 become

$$\begin{aligned}\langle \mathbf{k}',l'|V|\mathbf{k}'+\mathbf{q},l\rangle &= \int d^2\mathbf{r}'\int dz'\Psi^*_{\mathbf{k}',l'}(\mathbf{r}',z')V(\mathbf{r}',z')\Psi_{\mathbf{k}'+\mathbf{q},l}(\mathbf{r}',z') \\ &= \int\frac{d^2\mathbf{q}'}{(2\pi)^2}\int dz'\tilde{V}(\mathbf{q}',z')\int d^2\mathbf{r}'\Psi^*_{\mathbf{k}',l'}(\mathbf{r}',z')e^{-i\mathbf{q}'\cdot\mathbf{r}'}\Psi_{\mathbf{k}'+\mathbf{q},l}(\mathbf{r}',z')\end{aligned}$$

Now to integrate out the $\mathbf{r}'$ variable we use a similar trick as before. This reduces the above equation to

$$\begin{aligned}\langle \mathbf{k}',l'|V|\mathbf{k}'+\mathbf{q},l\rangle &= \int\frac{d^2\mathbf{q}'}{(2\pi)^2}\int dz'\tilde{V}(\mathbf{q}',z')\delta(\mathbf{q}-\mathbf{q}')\int d^2\mathbf{r}'\Psi^*_{\mathbf{k}',l'}(\mathbf{r}',z')e^{-i\mathbf{q}'\cdot\mathbf{r}'}\Psi_{\mathbf{k}'+\mathbf{q},l}(\mathbf{r}',z') \\ &= \int dz'\,\tilde{V}(\mathbf{q},z')M^{l,l'}_{\mathbf{k}',\mathbf{k}'+\mathbf{q}}(z)\end{aligned}$$

So finally the Fourier transform of the induced charge density has the form

$$\tilde{n}_{ind}(\mathbf{q},z)=2\sum_{\mathbf{k}}\sum_{l,l'}\frac{f(E_{\mathbf{k},l'})-f(E_{\mathbf{k}+\mathbf{q},l})}{E_{\mathbf{k},l'}-E_{\mathbf{k}+\mathbf{q},l}+\omega\hbar+i\nu^{+}}M^{l,l'}_{\mathbf{k},\mathbf{k}+\mathbf{q}}(z)\int dz' M^{l,l'}_{\mathbf{k},\mathbf{k}+\mathbf{q}}(z')\tilde{V}(\mathbf{q},z') \tag{3.6}$$

This is the most general form of the induced charge density for graphene. So far the only assumption we have made about graphene is that it is a two dimensional periodic lattice.

Equation 3.6 is purely the result of using the first order approximation to the density matrix defined in equation 3.2. The function $M^{l,l'}_{\mathbf{k},\mathbf{k}'}(z)$ can be thought of as the average z dependence of the wavefunction. A realistic approach to evaluating it is through the use of the electron orbital structure of graphene which was derived using the tight binding approximation. The π-bonds which are formed from $2p_z$ orbital wavefunctions have an electron density which decays exponentially in the z direction. The spatial decay rate is less than an angstrom so, a distance of a few angstroms away from the graphene surface results in a negligible electron density contribution from the π-bonds. Within the zero thickness approximation of graphene we assume that the function $M^{l,l'}_{\mathbf{k},\mathbf{k}'}(z)$ is localized in the plane of graphene. This is a somewhat idealistic approximation, as impurities near the surface of graphene could significantly overlap with the electron orbitals. We ignore the effects of orbital overlap since they make the analytic calculations less attractive and inseparable. Instead we approximate $\sqrt{A}M^{l,l'}_{\mathbf{k},\mathbf{k}'}(z)\approx\bar{M}^{l,l'}_{\mathbf{k},\mathbf{k}'}\delta(z)$. With this in mind the last factor in equation 3.6 becomes

$$M^{l,l'}_{\mathbf{k},\mathbf{k}+\mathbf{q}}(z)\int dz' M^{l,l'}_{\mathbf{k},\mathbf{k}+\mathbf{q}}(z')\tilde{V}(\mathbf{q},z')=\frac{1}{A}\delta(z)\tilde{V}(\mathbf{q},z)|\bar{M}^{l,l'}_{\mathbf{k},\mathbf{k}+\mathbf{q}}|^2$$

giving us an induced charge density of

$$\tilde{n}_{ind}(\mathbf{q},z)=2\delta(z)\tilde{V}(\mathbf{q},z)\int\frac{d^2\mathbf{k}}{(2\pi)^2}\sum_{l,l'}\frac{f(E_{\mathbf{k},l'})-f(E_{\mathbf{k}+\mathbf{q},l})}{E_{\mathbf{k},l'}-E_{\mathbf{k}+\mathbf{q},l}+\omega\hbar+i\nu^{+}}|\bar{M}^{l,l'}_{\mathbf{k},\mathbf{k}+\mathbf{q}}|^2 \tag{3.7}$$

where we have turned the sum over $\mathbf{k}$ into an integral over the 1st Brillouin zone. This is a valid move since the spacing between consecutive momenta becomes smaller and smaller as the size of the graphene sheet becomes larger. For a theoretically infinite graphene sheet the sum transforms into an integral. In the zero thickness approximation of graphene, the induced charge density resides on the plane of graphene. In Fourier space this density is related to the external potential and the linear response via,

$$\tilde{n}_{ind}(\mathbf{q},z)=\delta(z)\tilde{V}(\mathbf{q},z)\tilde{\chi}_0(\mathbf{q}) \tag{3.8}$$

Although the idea of a zero thickness graphene sheet may seem somewhat *ad hoc* the formalism greatly simplifies our calculations and is very accurate with the limits of k_F discussed in Chapter 2. So the linear response of graphene is equal to,

$$\tilde{\chi}_0(\mathbf{q})=2\int\frac{d^2\mathbf{k}}{(2\pi)^2}\sum_{l,l'}|\bar{M}^{l,l'}_{\mathbf{k},\mathbf{k}+\mathbf{q}}|^2\frac{f(E_{\mathbf{k},l'})-f(E_{\mathbf{k}+\mathbf{q},l})}{E_{\mathbf{k},l'}-E_{\mathbf{k}+\mathbf{q},l}+\omega\hbar+i\nu^{+}} \tag{3.9}$$

Now we need to evaluate the matrix elements of $|\bar{M}^{l,l'}_{\mathbf{k},\mathbf{k}+\mathbf{q}}|^2$ which is the Fourier transform of two

wavefunctions. Expanding the wavefunctions by using the tight binding approximation from equation 2.2

$$\bar{M}^{l,l'}_{\mathbf{k},\mathbf{k}+\mathbf{q}} = \int d^2\mathbf{r} \int dz \left[a^*_{\mathbf{k},l}\psi^*_{A,\mathbf{k}} + b^*_{\mathbf{k},l}\psi^*_{B,\mathbf{k}}\right] e^{-i\mathbf{q}\cdot\mathbf{r}} \left[a_{\mathbf{k}+\mathbf{q},l'}\psi_{A,\mathbf{k}+\mathbf{q}} + b_{\mathbf{k}+\mathbf{q},l'}\psi_{B,\mathbf{k}+\mathbf{q}}\right]$$

The evaluation of this integral is tedious and the reader is invited to see its derivation in the Appendix. Here we shall reiterate the result

$$\bar{M}^{l,l'}_{\mathbf{k},\mathbf{k}+\mathbf{q}} = \frac{1}{2}R(\mathbf{q})\left[1 + (-1)^{l+l'}\frac{f(\mathbf{k})f(\mathbf{k}+\mathbf{q})}{|f(\mathbf{k})||f(\mathbf{k}+\mathbf{q})|}\right]$$

where $R(\mathbf{q})$ is the two-dimensional Fourier transform of the modulus squared of the p_z orbital,

$$R(\mathbf{q}) = \int dz \int d^2\mathbf{r}\, |\varphi_{p_z}(\mathbf{r},z)|^2 e^{i\mathbf{q}\cdot\mathbf{r}} = \left[1 + \left(\frac{a_0 q}{Z_{\text{eff}}}\right)^2\right]^{-3}$$

Here a_o is the Bohr radius and Z_{eff} is the effective charge of the screened nucleus in the carbon atom [60]. Taking the modulus squared of $\bar{M}^{l,l'}_{\mathbf{k},\mathbf{k}+\mathbf{q}}$ results in

$$|\bar{M}^{l,l'}_{\mathbf{k},\mathbf{k}+\mathbf{q}}|^2 = \frac{1}{2}R^2(q)\left\{1 + (-1)^{l+l'}\Re\left[\frac{f(\mathbf{k})f(\mathbf{k}+\mathbf{q})}{|f(\mathbf{k})||f(\mathbf{k}+\mathbf{q})|}\right]\right\}$$

Using equation 2.4 for $f(\mathbf{k})$ near the Dirac point, we can simplify $|\bar{M}^{l,l'}_{\mathbf{k},\mathbf{k}+\mathbf{q}}|^2$, so our polarization function now becomes

$$\tilde{\chi}_0(\mathbf{q}) = R^2(q)\int_{BZ}\frac{d^2\mathbf{k}}{(2\pi)^2}\sum_{l,l'}\left[1 + (-1)^{l+l'}\frac{k + q\cos\theta_{\mathbf{k},\mathbf{q}}}{|\mathbf{k}+\mathbf{q}|}\right]\frac{f(E_{\mathbf{k},l'}) - f(E_{\mathbf{k}+\mathbf{q},l})}{E_{\mathbf{k},l'} - E_{\mathbf{k}+\mathbf{q},l} + \omega\hbar + i\nu^+} \tag{3.10}$$

The evaluation of this integral is rather computationally cumbersome, though straightforward. The results can be found in [29, 70], and a partial derivation is in the Appendix. Here we will just cite the results of the first order linear response of graphene. Define the two complex functions

$$F(q,\omega) = \frac{1}{4\pi}\frac{\hbar v_F^2 q^2}{\sqrt{\omega^2 - v_F^2 q^2}}$$
$$G(x) = x\sqrt{x^2-1} - \ln(x + \sqrt{x^2-1})$$

then

$$\chi_0(\mathbf{q},\omega) = \chi_0^-(\mathbf{q},\omega) + \chi_0^+(\mathbf{q},\omega) \tag{3.11}$$

where,

$$\chi_0^-(\mathbf{q},\omega) = i\pi\frac{F(q,\omega)}{(\hbar v_F)^2}$$
$$\chi_0^+(\mathbf{q},\omega) = -\frac{2E_F}{\pi\hbar^2 v_F^2} + \frac{F(q,\omega)}{\hbar^2 v_F^2}\left\{G\left(\frac{\hbar\omega+2E_F}{\hbar v_F q}\right) - H\left(\frac{2E_F-\hbar\omega}{\hbar v_F q}-1\right)\right.$$
$$\left.\times\left[G\left(\frac{2E_F-\hbar\omega}{\hbar v_F q}\right)-i\pi\right] - H\left(1-\frac{2E_F-\hbar\omega}{\hbar v_F q}\right)G\left(\frac{\hbar\omega-2E_F}{\hbar v_F q}\right)\right\}$$

and E_F is the Fermi energy of doped graphene and $H(x)$ is the Heaviside function. The polarization function of graphene is still subject to intense research. Second order, and beyond the Dirac cone, effects, and their contribution to the polarization function, are currently being examined [61, 35, 63, 77]. For this thesis, first order effects will be sufficient.

Furthermore, we make a note of the factor $R(q)$. According to Zener [78], the effective charge of the carbon atom is $Z_{\text{eff}} \approx 3.18$. With the Bohr radius being approximately 0.53 Å, we get a ratio $a_0/Z_{\text{eff}} \approx 0.167$ Å. This implies that the wavevector q needs to be on the order of 5 Å^{-1} before $R(q)$ has a significant effect. However, due to the limitations imposed on the Fermi wavevector in Chapter 2, forcing $k_F \lesssim 0.1$ Å^{-1}, we can ignore the factor $R(q)$ since it will be almost 1 over the region of interest.

3.2 Dielectric function

Perhaps the most important property of the polarization function of graphene, is its use in the dielectric function. The dielectric function is versatile in the sense that it describes many properties of the material. For graphene in a medium with a relative dielectric constant ϵ_r, the dielectric function is given by

$$\epsilon(\mathbf{q},\omega) = 1 - v_q\chi_0(\mathbf{q},\omega) \tag{3.12}$$

where $v_q = \frac{2\pi e^2}{\epsilon_r q}$ is the 2D Fourier transform of the Coulomb potential. For more complicated system, the dielectric function changes to include the Green's function of the surrounding system, as will be shown later. One of the important properties that the dielectric function gives is the plasmon (i.e. oscillations of charge density) dispersion relation. Solving

$$\epsilon(\mathbf{q},\omega+i\gamma) = 0 \tag{3.13}$$

gives a relation between ω and $\mathbf{q}$, defined as $\omega_p(\mathbf{q})$, which tells us how the collective electron excitation modes called, plasmons, disperse in the material. The value γ is the decay rate of the plasmon. The dielectric function in the long wavelength limit $q \to 0$, $\omega > v_F q$ is particularly important in optical spectroscopy and plasmon dispersion. This limit tells us the interaction between photons impinging on graphene and graphene's response to them. Although plasmons are not studied here, we mention that they are an important and active area of research, particularly in the optical properties of graphene [75, 20, 8].

Another property that the dielectric function tells us, is the screening of external charges. Exter-

nal charges usually are composed of slowly moving, or static, massive charge carriers that interact with the material via Coulomb interaction. Since the external charges are slow and massive, we use the dielectric function in the static limit, $\omega = 0$. The external particles cause an induced charge density to be formed in the material. For a point charge on graphene, the induced charge density is given by

$$n_{\text{ind}}(\mathbf{r}) \propto \int d^2\mathbf{q} \left[\frac{1}{\epsilon(\mathbf{q},0)} - 1\right] e^{i\mathbf{q}\cdot\mathbf{r}} \tag{3.14}$$

where the static polarization function of graphene is,

$$\chi_0(\mathbf{q},\omega\to 0) = -\frac{2k_F}{\pi\hbar v_F}\left\{1 + H(q-2k_F)\left[\frac{q}{4k_F}\arccos\left(\frac{2k_F}{q}\right) - \frac{1}{2}\sqrt{1-\left(\frac{2k_F}{q}\right)^2}\right]\right\} \tag{3.15}$$

Using this in our dielectric function 3.12 we get

$$\epsilon(q,0) = 1 + \frac{2r_s}{\epsilon_r}\frac{1}{x}\left\{1 + H(x-1)\left[\frac{x}{2}\arccos\left(\frac{1}{x}\right) - \frac{1}{2}\sqrt{1-\left(\frac{1}{x}\right)^2}\right]\right\}$$

where we defined the dimensionless parameters $r_s = \frac{e^2}{\hbar v_F}$ and $x = \frac{2k_F}{q}$. As mentioned earlier r_s is the coupling constant of the quasi particles in graphene. The dielectric function has a discontinuous derivative at $x = 1$, which gives rise to Friedel oscillations in the induced charge density in equation 3.14. Friedel oscillations are often found in a Fermi gas, and are analogous to electron screening in a quantum mechanical system. They are characterized by decaying oscillations whose wavevector is proportional to the Fermi wavevector of the material. As was shown earlier, the average charge density is dependent on an external potential. With the inclusion of an external charge in our model, we expect charge density oscillations in the plane of graphene.

3.3 Green's function of nearby dielectrics

In this thesis we consider the interaction of graphene with its surrounding material. As such, a proper treatment of the geometric structure surrounding graphene must be considered. We have already discussed the process of using graphene as a field effect transistor in experiments. So we would like to model the material surrounding graphene after conventional experimental set-ups. First we will consider the geometry of the material surrounding graphene and derive a Green's function for its Poisson equation. After that we will introduce graphene as a two dimensional, zero thickness material and derive a general Green's function by considering the linear response of graphene as a boundary condition.

Consider a three dimensional medium with a discontinuous dielectric boundary at $z = 0$. The upper medium has a dielectric constant of ϵ_2 and the lower medium has a dielectric constant of ϵ_1. Below the lower medium is a metallic electrode with infinite dielectric constant (see figure 3.1). The metallic material is analogous to a back gate in an experimental setting. The model is considered to be translationally invariant and isotropic in the x-y plane. We will use $\mathbf{r}$ to specify a two dimensional vector in the x and y coordinates, and we will denote $r = |\mathbf{r}|$. We want to obtain the electric potential, given an external charge density. This motivates us to use the Poisson equation.

$$\nabla \cdot \epsilon(z) \nabla \Phi = -4\pi\rho \tag{3.16}$$

Our three-dimensional Poisson equation can be decomposed into two equations, one above $z = 0$ and one below,

$$\epsilon_1 \triangle \Phi_1 = -4\pi\rho_1$$
$$\epsilon_2 \triangle \Phi_2 = -4\pi\rho_2$$

where $\triangle = \nabla^2$ is the Laplacian. We require that the two potentials Φ_1 and Φ_2 satisfy the regular conditions of continuity across the discontinuous dielectric surface and we require them to vanish as $z \to \infty$ and $z = -L$, where $-L$ is the location of the metallic plate in the z axis. We also require the electric displacement field to conserve the charge density along the $z = 0$ plane. We can write these boundary conditions mathematically as

$$\begin{aligned} \Phi_1(\mathbf{r}, 0) &= \Phi_2(\mathbf{r}, 0) \\ \Phi_1(\mathbf{r}, -L) &= 0 \\ \Phi_2(\mathbf{r}, \infty) &= 0 \\ \epsilon_1 \frac{\partial \Phi_1}{\partial z}\bigg|_{z=0} - \epsilon_2 \frac{\partial \Phi_2}{\partial z}\bigg|_{z=0} &= 0 \end{aligned}$$

In essence we would like to solve for the Green's function of the differential equation 3.16. In that way we can obtain the scalar potential for any external charge distribution, ρ, by evaluating an integral equation. Since our system is isotropic in the x and y directions we can take the two

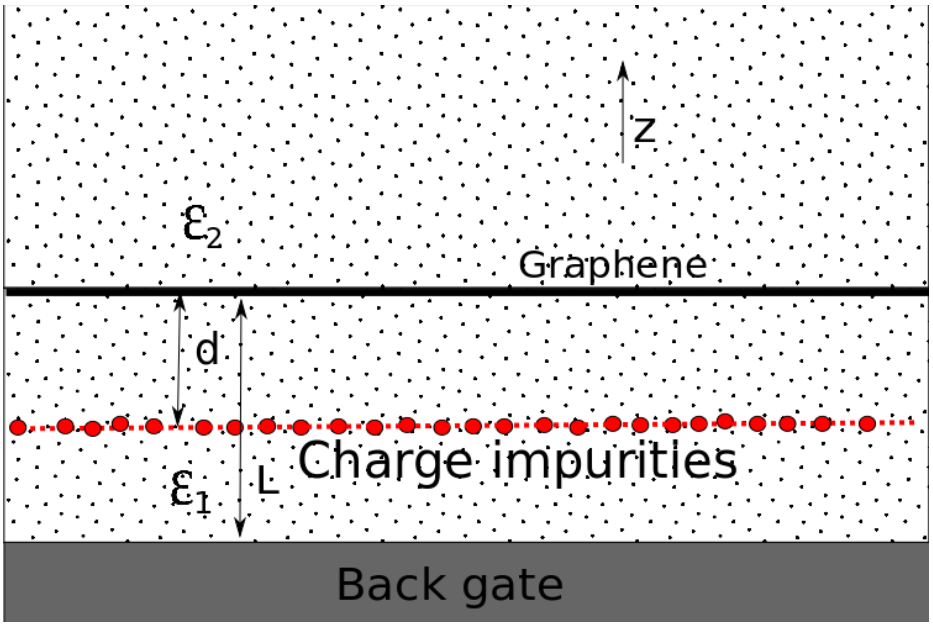

Figure 3.1: The geometry of the model considered with graphene included, which in this case, is sandwiched between two dielectric substrates. Below the bottom substrate lies the back-gate, which is metallic. Charged impurities are placed in the bottom substrate at a distance d away from graphene. The treatment of impurities will be considered in Chapter 6.

dimensional Fourier transform in $\mathbf{r}$. Now our differential equations become:

$$\left(\frac{\partial^2}{\partial z^2} - q^2\right)\tilde{\Phi}_1(\mathbf{q}, z) = -\frac{4\pi}{\epsilon_1}\tilde{\rho}_1(\mathbf{q}, z)$$
$$\left(\frac{\partial^2}{\partial z^2} - q^2\right)\tilde{\Phi}_2(\mathbf{q}, z) = -\frac{4\pi}{\epsilon_2}\tilde{\rho}_2(\mathbf{q}, z)$$

Here we denote $\mathbf{q}$ to be a two dimensional vector in Fourier space, and set $q = |\mathbf{q}|$. Furthermore, the tildes denote that the functions have been Fourier transformed in the x-y plane, and that the functions dependence on $\mathbf{q}$ is implied. To solve the above differential equation we seek a Green's function of the form

$$\begin{cases} \left(\frac{\partial^2}{\partial z^2} - q^2\right) G_1(\mathbf{q}, z, z') = -\frac{4\pi}{\epsilon_1}\delta(z - z') & (-L < z < 0) \\ \left(\frac{\partial^2}{\partial z^2} - q^2\right) G_2(\mathbf{q}, z, z') = 0 & (z > 0) \end{cases} \tag{3.17}$$

As is conventional in integral operators, the z' variable will denote the source point and z will denote the observation point [43]. In this thesis the sources of the charge distribution will be charged impurities in the substrate. We will only consider charge distributions which are located in the bottom dielectric. So the location of the source points will be in the negative z axis, and so there is no need to have a $\delta(z - z')$ term on the right for the greens function G_2 in equation 3.17.

In general the two Green's functions will have the following boundary conditions

$$G_1(\mathbf{q}, -L, z') = 0 \tag{3.18}$$

$$G_2(\mathbf{q}, \infty, z') = 0 \tag{3.19}$$

$$G_1(\mathbf{q}, z' + \eta, z') = G_1(\mathbf{q}, z' - \eta, z') \tag{3.20}$$

$$G_1(\mathbf{q}, 0, z') = G_2(\mathbf{q}, 0, z') \tag{3.21}$$

$$\epsilon_1 \frac{\partial G_1}{\partial z}\bigg|_{z=0} - \epsilon_2 \frac{\partial G_2}{\partial z}\bigg|_{z=0} = 0 \tag{3.22}$$

$$\frac{\partial G_1}{\partial z}\bigg|_{z=z'+\eta} - \frac{\partial G_1}{\partial z}\bigg|_{z=z'-\eta} = -\frac{4\pi}{\epsilon_1} \tag{3.23}$$

where η is some infinitesimally small positive number. Boundary conditions 3.18, 3.19, 3.21, and 3.22 are a direct result of the boundary conditions imposed on equation 3.16. The other boundary conditions arise as a property of the Green's function. We know that the solutions to 3.17 will be exponential functions, so, using boundary conditions 3.18 and 3.19 we get

$$G_1(\mathbf{q}, z, z') = \begin{cases} A\sinh(q(z+L)) & z' > z \\ Be^{-qz} + Ce^{qz} & z > z' \end{cases}$$

and

$$G_2(\mathbf{q}, z, z') = De^{-qz}$$

With the remaining boundary conditions we get

$$\begin{aligned} A\sinh(q(z'+L)) &= Be^{-qz'} + Ce^{qz'} \\ -Be^{-qz'} + Ce^{qz'} - A\cosh(q(z'+L)) &= -\frac{4\pi}{q\epsilon_1} \\ B + C &= D \\ \epsilon_2(-D) - \epsilon_1(-B+C) &= 0 \end{aligned}$$

After some lengthy algebra

$$\begin{aligned} A &= \frac{4\pi}{\epsilon_1 q}\frac{\epsilon_1\cosh(qz') - \epsilon_2\sinh(qz')}{\epsilon_1\cosh(qL) + \epsilon_2\sinh(qL)} \\ B &= \frac{2\pi}{\epsilon_1 q}(\epsilon_1 - \epsilon_2)\frac{\sinh(q(z'+L))}{\epsilon_1\cosh(qL) + \epsilon_2\sinh(qL)} \\ C &= \frac{2\pi}{\epsilon_1 q}(\epsilon_1 + \epsilon_2)\frac{\sinh(q(z'+L))}{\epsilon_1\cosh(qL) + \epsilon_2\sinh(qL)} \\ D &= \frac{4\pi}{q}\frac{\sinh(q(z'+L))}{\epsilon_1\cosh(qL) + \epsilon_2\sinh(qL)} \end{aligned}$$

Defining $\Gamma_\pm(x) = \epsilon_1\cosh(x) \pm \epsilon_2\sinh(x)$, $z_> = \max\{z, z'\}$ and $z_< = \min\{z, z'\}$ we can express the

Green's functions as

$$G(\mathbf{q},z,z') = \begin{cases} G_1(\mathbf{q},z,z') = \frac{4\pi}{\epsilon_1 q}\frac{\Gamma_-(qz_>)\sinh(q(z_<+L))}{\Gamma_+(qL)} & -L<z<0 \\ G_2(\mathbf{q},z,z') = \frac{4\pi}{q}\frac{\sinh(q(z'+L))}{\Gamma_+(qL)}e^{-qz} & z>0 \end{cases} \tag{3.24}$$

We can test our result by examining the Green's function in the limit of the special case $L \to \infty$. In this case the Green's function reduces to

$$G(\mathbf{q},z,z') = \begin{cases} \frac{2\pi}{\epsilon_1 q}\left(\frac{\epsilon_1-\epsilon_2}{\epsilon_1+\epsilon_2}e^{-q|z+z'|}+e^{-q|z-z'|}\right) & z<0 \\ \frac{2\pi}{q\epsilon_{\text{avg}}}e^{-q|z-z'|} & z>0 \end{cases}$$

Here we define $\epsilon_{\text{avg}} = \frac{\epsilon_1+\epsilon_2}{2}$ as the average dielectric value between the two mediums. An inverse two dimensional Fourier transform of this Green's function for $z<0$ gives the following Green's function in position space,

$$\int \frac{\mathrm{d}^2\mathbf{q}}{(2\pi)^2}e^{i\mathbf{q}\cdot(\mathbf{r}-\mathbf{r}')}G(\mathbf{q},z,z') = \frac{1}{\epsilon_1}\left[\frac{\epsilon_1-\epsilon_2}{\epsilon_1+\epsilon_2}\frac{1}{\sqrt{|\mathbf{r}-\mathbf{r}'|^2+(z+z')^2}}+\frac{1}{\sqrt{|\mathbf{r}-\mathbf{r}'|^2+(z-z')^2}}\right]$$

A quick glance at this Green's function and one notices that it is the sum of two familiar Green's function. The first Green's function on the right side is the image term, which results from a discontinuous dielectric boundary, and as a result causes screening of the external charge. The second term on the right is the standard Green's function for a Poisson equation with a dielectric constant ϵ_1. Similarly, if one were to take the Fourier transform of the Green's function for $z>0$ one would get the usual Poisson equation Green's function with a dielectric constant ϵ_{avg}.

3.4 Adding graphene

Now we use our Green's function, which only considers the discontinuous dielectric boundary, and add the interaction with graphene to derive a new Green's function. We treat the sheet of graphene using the zero thickness approximation, turning the Fourier transformed Poisson equation into

$$\left(\frac{\partial^2}{\partial z^2}-k^2\right)\tilde{\Phi}(z) = -4\pi e^2\chi_0(q,\omega)\delta(z-z_g)\tilde{\Phi}(z)-4\pi\tilde{\rho}(z) \tag{3.25}$$

Here $\chi_0(q,\omega)$ is the linear response of the electrons in graphene derived earlier (equation 3.11). $\tilde{\rho}(z)$ is the external charge density and $\tilde{\Phi}(z)$ is the scalar electric potential, which is the quantity we are interested in. For the sake of brevity, we shall drop the q dependence in those functions. With the zero thickness approximation, the location of graphene is a delta function in the z axis, and in this case graphene is located in the plane $z=z_g$. One notices that the first term on the right in equation 3.25 is in fact the induced charge density in graphene, derived in equation 3.8. So the right side of equation 3.25 could be considered as a charge density which includes both the external impurities and the internal, induced charge density due to the external impurities. The Fourier transformed Poisson equation could be used as the linear operator in equation 3.25. This allows us to use the

Green's function derived above (equation 3.24) to find the scalar potential. Denoting the Green's function from the dielectric substrates as $\tilde{G}^0(z,z')$, and dropping the q dependence for brevity, the potential can be expressed as

$$\begin{aligned}\tilde{\Phi}(z) &= \int dz' \tilde{G}^0(z,z')[\tilde{\rho}(z') + e^2\chi_0(q,\omega)\delta(z-z_g)\tilde{\Phi}(z')] \\ &= e^2\chi_0(q,\omega)\tilde{\Phi}(z_g)\tilde{G}^0(z,z_g) + \int dz' \tilde{G}^0(z,z')\tilde{\rho}(z')\end{aligned}$$

Evaluating the scalar potential at $z = z_g$ we get

$$[1 - e^2\chi_0(q,\omega)\tilde{G}^0(z_g,z_g)]\tilde{\Phi}(z_g) = \int dz' \tilde{G}^0(z_g,z')\tilde{\rho}(z')$$

Solving for $\tilde{\Phi}(z_g)$ and plugging it in the original equation gives us

$$\tilde{\Phi}(z) = \int dz' \left[\tilde{G}^0(z,z') + \frac{e^2\chi_0(q,\omega)\tilde{G}^0(z,z_g)\tilde{G}^0(z_g,z')}{1 - e^2\chi_0(q,\omega)\tilde{G}^0(z_g,z_g)}\right]\tilde{\rho}(z')$$

Now we can define the full Green's function, which incorporates the linear response of graphene as

$$\tilde{G}(z,z') = \tilde{G}^0(z,z') + \frac{e^2\chi_0(q,\omega)\tilde{G}^0(z,z_g)\tilde{G}^0(z_g,z')}{1 - e^2\chi_0(q,\omega)\tilde{G}^0(z_g,z_g)} \tag{3.26}$$

So the final result is given in terms of the linear response function, $\chi(q,\omega)$, and the Green's function for the bare model without graphene, $\tilde{G}^0(z,z')$. The denominator in equation 3.26 is subtly connected to the dielectric function of the material. If we evaluate equation 3.26 in the plane $z = z_g$ we get the Green's function for an observation point on graphene, which is given by $\frac{\tilde{G}^0(z_g,z')}{1-e^2\chi_0(q,\omega)\tilde{G}^0(z_g,z_g)}$. Consequently, the denominator in this case gives us the dielectric function in graphene. In the standard case of free graphene, $e^2\tilde{G}^0(z_g,z_g)$ reduces to the two-dimensional Fourier transform of the Coulomb potential, $\frac{e^2 2\pi}{q\epsilon_r}$. In the more general case for any Green's function $\tilde{G}^0(z_g,z_g)$, the dielectric function is $\epsilon(\mathbf{q},\omega) = 1 - \tilde{G}^0(z_g,z_g)\chi_0(q,\omega)$

We note that, although we have used the zero thickness approximation for graphene, a more general model, with a finite thickness of graphene, could be considered. However the derivation of such a model requires a three dimensional linear response function as well. In this thesis, we neglect the derivation of such a model due to its complexity. Furthermore, we make a note on the limitation of equation 3.26. The Green's function, $\tilde{G}^0(z,z')$, need not be the one derived earlier (equation 3.24) and could be replaced with any other Green's function for a substrate geometry without a sheet of graphene. We make use of this property later on when we consider a vacuum gap model. The vacuum gap model is a more general case where we consider a spatial gap between the two dimensional sheet of graphene and the substrates. The derivation of the Green's function for the vacuum gap model is computationally more involved, although the idea is rather rudimentary. The result is presented in the Appendix. The vacuum gap model assumes a dielectric layer between the the substrates in which the graphene sheet resides (see figure 3.2). There are two advantages to this model. Usually in experiments, between the sheet of graphene and the substrate there are impurities

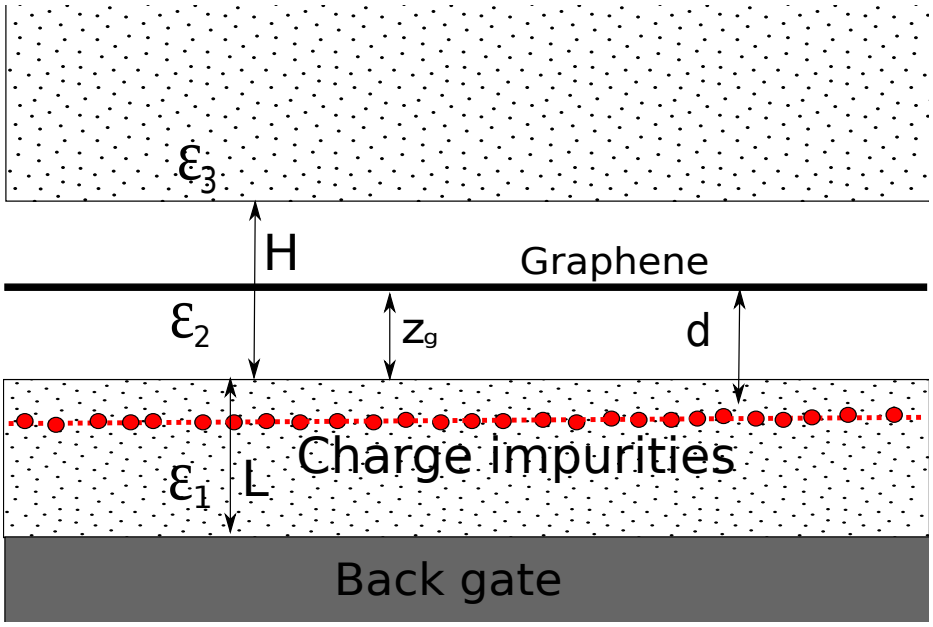

Figure 3.2: The geometry of the the vacuum gap model. Here we have the added parameter h which gives us the distance between the two dielectric surfaces. In the $H = 0$ limit, the vacuum gap model reduces to the simpler model derived earlier.

trapped from the cleaning and manufacturing process. The vacuum gap model has the added utility that it could explore such structures. The other advantage is that the vacuum gap model can be thought of as a simpler way of relaxing the zero thickness approximation of graphene. The out of plane π orbitals decay exponentially and are negligible at a distance of 3Å away from graphene. So we can consider the position of the graphene sheet to be around 3Å away from the substrates. Note that this distance is expected since graphene interacts with the substrate only weakly, usually via Van der Waals interaction, with a typical distance of about 3Å.

Chapter 4

Statistical Properties of Impurities and their Effects

4.1 Types of impurities

Impurities are particles which are confined in a well described material whose properties differ from that of the material itself. Although materials may contain low concentrations of impurities, the properties of the entire system may change. An example of this would be the decrease in the freezing temperature of water by adding certain salts to it. Impurities are an unavoidable consequence in the production of materials. The elimination of all impurities from a material is impossible as it would require reducing the entropy of the system to zero, violating the second law of thermodynamics [22]. As such, we must incorporate impurities in our material analysis. We will only deal with external charged impurities in this thesis. Other types of impurities, such as atomic vacancies in graphene, will not be considered here. In most bulk materials, charged impurities external to the material, cause negligible electronic effects inside the material. With graphene, which can be considered as an ideal surface, this is not the case. It's two dimensional nature gives it tremendous sensitivity to its surroundings. Graphene, being a chemically inert material, does not change its structure due to the external impurities, however, the interaction of the impurities with the crystal lattice alters the electrical properties of graphene. This can be considered both a blessing and a curse. Due to its sensitivity graphene can be an ideal sensor for measuring minute concentrations, of certain chemicals, in its vicinity [47, 57]. However this also causes the undesirable effect of giving false positive results due to unavoidable charged impurities in the substrate surrounding it. This chapter deals with the mathematical description of charged impurities in the vicinity of graphene, as well as their effect on the electric potential and induced charge carrier density in graphene. We will develop mathematical models to describe both the geometric structure of the impurities (i.e distributed in two and three dimensions) as well as the statistical distribution between the impurities (i.e. their pair correlation function).

We assume that the system of external charges contains N particles, with each particle carrying a total charge of $Z_j e$ (where $e > 0$ is the charge of a proton). The particles need not be point charges.

Assuming that the j^{th} particle is centered around the position $\mathbf{R}_j = \{\mathbf{r}_j, z_j\}$, we could consider the charge to be distributed around the center of the particle according to some function $\Delta_j(\mathbf{R})$ under the condition $\int d^3\mathbf{R}\Delta_j(\mathbf{R}) = Z_j$. The entire, external charge density, due to impurities, can be expressed as

$$\rho(\mathbf{r}, z) = e\sum_{j=1}^{N} \Delta_j(\mathbf{r} - \mathbf{r}_j, z - z_j) \tag{4.1}$$

Given that the positions $\mathbf{R}_j$ of external particles, as well as their individual charge densities $\Delta_j(\mathbf{R})$ are statistically distributed, we denote their joint ensemble average by $\langle ... \rangle$. In general Δ_j may consist of different types of distributions for different j. However, in this thesis we assume that the charge around each particle has the same distribution (i.e. $\Delta_j(\mathbf{R}) = \Delta(\mathbf{R})$). The most general N particle density function will be denoted by $F_N(\mathbf{r}_1, z_1, ..., \mathbf{r}_N, z_N)$, and so the average charge density at a point is defined as

$$\langle \rho(\mathbf{r}, z) \rangle = e \int d^2\mathbf{r}_1 \int dz_1 ... \int d^2\mathbf{r}_N \int dz_N F_N(\mathbf{r}_1, z_1, ..., \mathbf{r}_N, z_N) \sum_{j=1}^{N} \Delta(\mathbf{r} - \mathbf{r}_j, z - z_j) \tag{4.2}$$

We will assume translational invariance in the direction of $\mathbf{r}$. This will make the ensemble average, $\langle \rho(\mathbf{r}, z) \rangle$, purely dependent on the z coordinate. If we were to expand out the sum in 4.2, we would have the integral given by

$$\langle \rho(\mathbf{r}, z) \rangle = e \int d^2\mathbf{r}_1 \int dz_1 F_1(\mathbf{r}_1, z_1) \Delta(\mathbf{r} - \mathbf{r}_1, z - z_1) \tag{4.3}$$

By the assumption of translational invariance, the particles will be distributed evenly in the $\mathbf{r}$ direction, so we can express $F_1(\mathbf{r}, z) = \frac{N f_1(z)}{A}$, where A is the area of the x-y plane in which the impurities lie and $f_1(z)$ is a probability distribution which describes how the impurities are distributed in the z direction.

We want to make a clear distinction between the structure of each impurity and their collective distribution. The structure of each impurity is defined through the function $\Delta(\mathbf{R})$. In general, this function can describe a variety of different impurity types. In this thesis we will focus only on two that are applicable to our research. The simplest types of impurities are point particles. Point particles are idealized particles characterized by a delta function in their spatial distribution and are usually used to model particles whose size is not relevant to the problem (e.g. classically interacting electrons). In addition to carrying a total charge of Ze, point particles can be generalized to contain a dipole moment, $\mathbf{D} = e\boldsymbol{\mu}$, where $\boldsymbol{\mu}$ is the displacement vector. With this in mind, the structure of the charge for a point particle impurity is of the form

$$\Delta(\mathbf{R}) = e(Z + \boldsymbol{\mu} \cdot \nabla_{\mathbf{R}})\delta(\mathbf{R}) \tag{4.4}$$

We could express the dipole moment vector in terms of its perpendicular and parallel components with respect to graphene, $\mathbf{D} = D_\perp + \mathbf{D}_\parallel$. In addition, the perpendicular dipole moment component may depend on the local electrostatic field $E_\perp$, which arises form the back gate, according to $D_\perp = \alpha E_\perp$, where α is an effective dipole polarizability near graphene.

Often in experiments, the point particle impurities tend to cluster together as a result of controlled thermal annealing [44]. This clustering of charged impurities can be modeled by an idealized disc of uniformly distributed charge, such that its total charge is still Z. We will only deal with a two dimensional disc, so that the impurities are still fixed in a plane in the z axis. Assuming the disc is of radius $R_{\rm cl}$ in a plane parallel to graphene, we have the following structure of the charge.

$$\Delta_{\rm cl}(\mathbf{R}) = \frac{eZ}{\pi R_{\rm cl}^2} H(R_{\rm cl} - r)\delta(z) \tag{4.5}$$

where $H(r)$ is the usual Heaviside step function. The collective distribution of the particles is governed by the N particle distribution function, $F_N(\mathbf{r}_1, z_1, ..., \mathbf{r}_N, z_N)$. In general this function can be very complicated for interacting particles. Instead we will assume that the impurities are not necessarily independently distributed, and so we will focus on the single particle distribution function described above, and a two particle distribution function defined as

$$F_2(\mathbf{r}_1, z_1, \mathbf{r}_2, z_2) = \frac{N(N-1)}{A^2} f_1(z_1) f_1(z_2) g(\mathbf{r}_2 - \mathbf{r}_1; z_1, z_2)$$

Here $g(\mathbf{r}; z_1, z_2)$ is the pair correlation function between two particles. It is used to describe the probability of finding two particles separated by a distance $\mathbf{r}$ in the x-y plane. The use of the pair correlation function will be discussed later in the thesis, where we relate it to the structure factor. For a large amount of impurities we can make the approximation $N(N-1) \approx N^2$ to simplify our results. Now we describe the distribution of the particles in the z direction. The simplest, and most widely used, model to describe the location of the charge impurities is to assume they are distributed in a plane parallel to the graphene sheet, a distance d below graphene [56, 1, 76, 39]. Assuming that graphene is placed in the plane $z = 0$, this would give us $f_1(z) = \delta(z+d)$. in this case, the impurities are distributed in a two dimensional plane and have an average two dimensional density of

$$n_{\rm imp} = \frac{N}{A} \tag{4.6}$$

Another possible distribution of the impurities, which has not been previously used in the analysis of graphene-impurity interactions, is a uniform, three dimensional distribution of impurities in a substrate of finite thickness. Once again assuming that the charge impurities are at least a distance d away from the graphene sheet the distribution function in the z direction becomes $f_1(z) = \frac{1}{L-d}$. Although now the three dimensional impurity density should be of the form $\frac{N}{A(L-d)}$, however, we will neglect the idea of defining a new impurity density for the three dimensional model. The impurity density for the three dimensional model will be $\frac{n_{\rm imp}}{L-d}$, where we use equation 4.6 as our model parameter to be consistent throughout our analysis.

The external charge density at any given point could be written in the form

$$\rho(\mathbf{R}) = \bar{\rho}(z) + \delta\rho(\mathbf{R}) \tag{4.7}$$

where $\bar{\rho}(z) = \frac{1}{A}\int d^2\mathbf{r} \int dz' f_1(z')\rho(\mathbf{r}, z - z')$ is the average value over the x-y plane at some point on the z axis, and $\delta\rho(\mathbf{R})$ is the fluctuation of the external charge density at some point $\mathbf{R}$. The

quantity we are most interested in is the autocovariance of the fluctuating external charge density (i.e. $\delta\rho(\mathbf{R})$). It is given by

$$\langle\delta\rho(\mathbf{r},z)\delta\rho(\mathbf{r}',z')\rangle = \langle\rho(\mathbf{r},z)\rho(\mathbf{r}',z')\rangle - \bar{\rho}(z)\bar{\rho}(z') \tag{4.8}$$

The importance of this equation will become apparent later. To evaluate this function we break it up term by term. The first term on the right gives,

$$\begin{aligned}\langle\rho(\mathbf{r},z)\rho(\mathbf{r}',z')\rangle =& e^2\int d^2\mathbf{r}_1\int dz_1 ...\int d^2\mathbf{r}_N\int dz_N F_N(\mathbf{r}_1,z_1,...,\mathbf{r}_N,z_N)\\ &\times\left(\sum_{j=1}^{N}\Delta(\mathbf{r}-\mathbf{r}_j,z-z_j)\right)\left(\sum_{j'=1}^{N}\Delta(\mathbf{r}'-\mathbf{r}_{j'},z'-z_{j'})\right)\end{aligned} \tag{4.9}$$

Expanding the sums and collecting like terms yields,

$$\begin{aligned}\langle\rho(\mathbf{r},z)\rho(\mathbf{r}',z')\rangle =& e^2\int d^2\mathbf{r}_1\int dz_1 F_1(\mathbf{r}_1,z_1)\Delta(\mathbf{r}-\mathbf{r}_1,z-z_1)\Delta(\mathbf{r}'-\mathbf{r}_1,z'-z_1)\\ &+e^2\int d^2\mathbf{r}_1\int dz_1\int d^2\mathbf{r}_2\int dz_2\, F_2(\mathbf{r}_1,z_1,\mathbf{r}_2,z_2)\Delta(\mathbf{r}-\mathbf{r}_1,z-z_1)\Delta(\mathbf{r}'-\mathbf{r}_2,z'-z_2)\end{aligned}$$

Since we have already defined $F_1(\mathbf{r}_1,z_1)$ and $F_2(\mathbf{r}_1,z_1,\mathbf{r}_2,z_2)$ we substitute them in to get

$$\begin{aligned}\langle\rho(\mathbf{r},z)\rho(\mathbf{r}',z')\rangle =& e^2 n_{\text{imp}}\int d^2\mathbf{r}_1\int dz_1 f_1(z_1)\Delta(\mathbf{r}-\mathbf{r}_1,z-z_1)\Delta(\mathbf{r}'-\mathbf{r}_1,z'-z_1)\\ &+e^2 n_{\text{imp}}^2\int d^2\mathbf{r}_1\int dz_1\int d^2\mathbf{r}_2\int dz_2\, f_1(z_1)f_1(z_2)g(\mathbf{r}_2-\mathbf{r}_1;z_1,z_2)\\ &\times\Delta(\mathbf{r}-\mathbf{r}_1,z-z_1)\Delta(\mathbf{r}'-\mathbf{r}_2,z'-z_2)\end{aligned}$$

The second term in the sum is just

$$\bar{\rho}(z)\bar{\rho}(z') = e^2 n_{\text{imp}}^2\int d^2\mathbf{r}_1\int dz_1\int d^2\mathbf{r}_2\int dz_2 f_1(z_1)f_1(z_2)\Delta(\mathbf{r}_1,z_1-z)\Delta(\mathbf{r}_2,z_2-z')$$

For the simple case of point particles (equation 4.4), which is the most widely used in this thesis, equation 4.8 becomes

$$\begin{aligned}\langle\delta\rho(\mathbf{r},z)\delta\rho(\mathbf{r}',z')\rangle =& e^2(Z+\boldsymbol{\mu}\cdot\nabla_{\mathbf{R}})^2 n_{\text{imp}}\{\delta(\mathbf{r}-\mathbf{r}')\delta(z-z')f_1(z)\\ &+ n_{\text{imp}}f_1(z)f_1(z')[g(\mathbf{r}-\mathbf{r}',z,z')-1]\}\end{aligned} \tag{4.10}$$

4.2 Geometric structure factor

In this thesis we will deal with two types of correlated impurities, aside from the trivial, uncorrelated ones. Only correlations in two dimensional distribution of the impurities will be considered (i.e. $f_1(z)=\delta(z-z_0)$). As such we can drop the z dependence in the pair correlation function and write $g(\mathbf{r},z,z')=g(\mathbf{r})$. The two models that we consider, contain a single parameter r_c characterizing the

inter-particle correlation distance. They are the step-correlation (SC) model with $g(r) = H(r - r_c)$, where H is a Heaviside unit step function, which was often used in the previous studies of charged impurities in graphene,[76, 39] and the hard-disc (HD) model, in which particles interact with each other as hard discs of the diameter r_c in a many-body Hamiltonian [55]. There are several advantages to using the HD model over the SC model. First, the former model is based on a Hamiltonian equation for the thermodynamic state of a 2D fluid with a well-defined pair potential between impurities, whereas the latter model is an *ad hoc* description of the impurity distribution, made-up for simple, analytic results. That is not to say that the SC model is poor at capturing the interesting results of the electrical properties of graphene with correlated impurities [76, 39], but we think that the HD model is an improvement to obtain more realistic results. The other advantages of the HD model are related to its structure factor, which we describe here.

Instead of the pair correlation functions, we will focus on the structure factor of the impurities in the substrate. The structure factor in two dimensions is defined in terms of the pair correlation function as,

$$I_{2D}(q) = 1 + n_{\text{imp}} \int d^2\mathbf{r}\, e^{i\mathbf{q}\cdot\mathbf{r}}[g(\mathbf{r}) - 1] \tag{4.11}$$

Analogous to the pair correlation function, the structure factor describes the arrangement of external particles in the plane $z = z_0$. The structure factor is a more palpable measure of the particle distribution as it is a direct relation to experimental results in neutron or X-ray scattering [68].

It is well known that $I_{2D}(0)$ is related to the isothermal compressibility of a 2D fluid,[25] which may be expressed as a function of the packing fraction defined by $p = \pi n_{\text{imp}} r_c^2/4$. Thus, p is a key measure of performance of the two models. It was recently shown by Li *et al.*[39] that the SC model gives reliable results for packing fractions $p \ll 1$. This was done by comparing the analytical result for the 2D structure factor in that model, $I_{SC}(q)$, with a numerically calculated structure factor of a hexagonal lattice of impurities. However, the analytical limit $I_{SC}(0) = 1 - 4p$ (see Appendix) shows that the SC model already breaks down for $p \geq 0.25$ because the corresponding compressibility becomes negative at higher packing fractions. On the other hand, it was recently shown that the interaction potential between two point ions near doped graphene is heavily screened and, moreover, exhibits Friedel oscillations with inter-particle distance, giving rise to a strongly repulsive core region of distances on the order of k_F^{-1} that resembles the interaction among hard disks with diameter $r_c \sim k_F^{-1}$ [52]. Therefore, we may estimate that the packing factor in such cases may reach values on the order $p \sim n_{\text{imp}}/\bar{n}$ that may not always be much less than 1, necessitating the use of a model that goes well beyond the SC model.

In that respect, we note that various parameterizations of the HD model extend its applicability to include phase transitions in a 2D fluid as a function of the packing fraction, [41] even going up about $p = 0.9$, corresponding to a crystalline closest packing where hard discs form a hexagonal structure in 2D [24]. We use a simple analytical parametrization for the 2D structure factor in the HD model, $S_{HD}(q)$, provided by Rosenfeld [55] (see Appendix) which works reasonably well for packing fractions up to about $p = 0.69$, just near the freezing point of a 2D fluid.

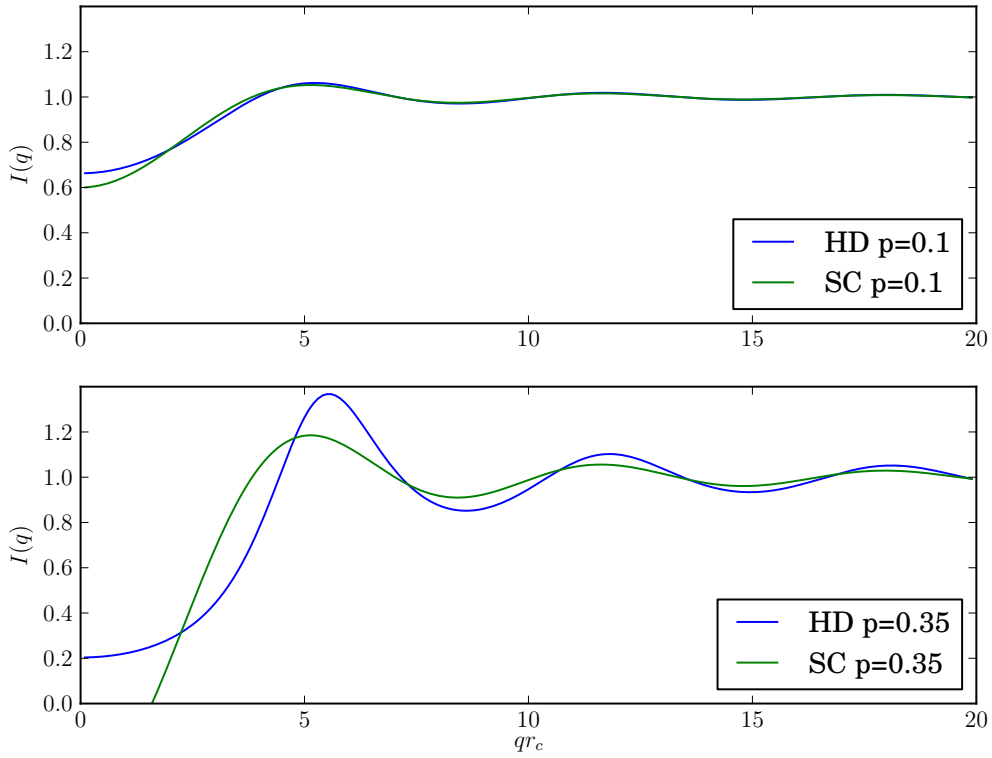

Figure 4.1: The structure factor, $I(q)$, for the step correlation (SC) and hard disc (HD) models, expressed in terms of the unitless parameter qr_c, where r_c is the correlation length of the particles. For small packing fractions (top, $p = 0.1$) the two models agree, with the HD model causing slightly larger oscillations in the structure factor. As we increase the packing fraction past 0.25 (bottom) we see that the two structure factors are qualitatively different. The SC model turns unphysical since $I(0)$ becomes negative.

4.3 Charge carrier and potential fluctuations

Impurities around graphene cause changes to the electrical properties of graphene. How large these changes are depends on many factors including the type of impurities, their location, distribution and concentration near graphene. This poses a problem for experimentalists. The presence of charge impurities, which may be trapped in the substrate or directly absorbed on graphene, render quantitative details of many measurements of graphene's electronic properties 'sample dependent'. We may not know the precise position or type of impurities near graphene, however we can consider their statistical distribution to obtain some qualitative description of their effects on graphene. In an

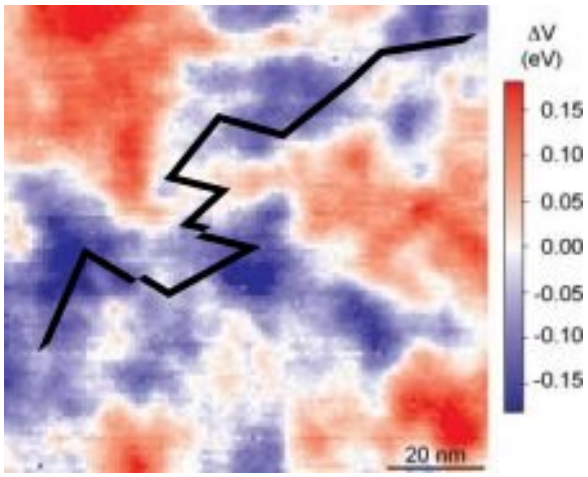

Figure 4.2: Fluctuations in the local potential in the plane of graphene. The randomness of the potential causes two effects. At low charge carrier doping, near the Dirac point, the graphene sheet experiences localized charge carrier density fluctuations, causing a minimum conductivity. At higher charge carrier densities, the impurities cause Coulomb scattering of the charge carriers, reducing their mobility and conductivity. Adapted from [74]

experiment, external gates present an efficient mean for producing concentrations of charge carriers in graphene. External impurities spatially distort the charge carriers and are thought to produce electron-hole puddles in graphene that reduce the resistivity of nominally neutral graphene, which is supposed to be devoid of quasi-free charge carriers and hence present infinite resistivity [79]. This section examines this claim by analyzing the statistics of the electrical potential and charge carrier density in graphene.

Consider the electrical potential defined as

$$\Phi(\mathbf{R}) = \bar{\Phi}(z) + \delta\Phi(\mathbf{R}) \tag{4.12}$$

Here $\delta\Phi(\mathbf{R})$ is the fluctuation or the deviation of the potential from its average in the x-y plane and $\bar{\Phi}(z)$ is the average potential in the x-y plane at some point z which is defined as

$$\bar{\Phi}(z) = \frac{1}{A}\int d^2\mathbf{r}\Phi(\mathbf{R})$$

where A is the area of the plane. Using an appropriate Green's function, the potential fluctuations and charge density fluctuations are related via

$$\delta\Phi(\mathbf{R}) = \int d^3\mathbf{R}' G(\mathbf{R}, \mathbf{R}')\delta\rho(\mathbf{R}')$$

where $\delta\rho(\mathbf{R}')$ was defined in equation 4.7. We don't really know what the Green's function will be in position space. However we do know its Fourier transform in the x-y plane. We will express the potential fluctuation in a rather more complicated form

$$\delta\Phi(\mathbf{R}) = \int \frac{\mathrm{d}^2\mathbf{q}}{(2\pi)^2} e^{i\mathbf{q}\cdot\mathbf{r}} \int dz' G(\mathbf{q}, z, z') \int \mathrm{d}^2\mathbf{r_1} e^{-i\mathbf{q}\cdot\mathbf{r_1}} \delta\rho(\mathbf{r_1}, z') \tag{4.13}$$

What we are interested in is the spatial autocovariance function of the potential fluctuations, that is

$$C(\mathbf{R}, \mathbf{R}') = \langle \delta\Phi(\mathbf{R})\delta\Phi(\mathbf{R}')\rangle \tag{4.14}$$

where the angled bracket indicates an ensemble average over all distributions of the charge density. Since $\delta\Phi(\mathbf{R}) = \Phi(\mathbf{R}) - \bar{\Phi}(z)$, and $\bar{\Phi}(z)$ is the expected value of $\Phi(\mathbf{R})$ in the x-y plane, then equation 4.14 certainly satisfies the usual definition of an autocovariance function. Expanding equation 4.14 by using equation 4.13 gives us the rather long integrals

$$\begin{aligned} C(\mathbf{R}, \mathbf{R}') = \int \frac{\mathrm{d}^2\mathbf{q}}{(2\pi)^2} e^{i\mathbf{q}\cdot\mathbf{r}} \int \frac{\mathrm{d}^2\mathbf{q}'}{(2\pi)^2} e^{i\mathbf{q}'\cdot\mathbf{r}'} \int dz_1 G(\mathbf{q}, z, z_1) \int dz_2 G(\mathbf{q}', z', z_2) \\ \times \int \mathrm{d}^2\mathbf{r_1} e^{-i\mathbf{q}\cdot\mathbf{r_1}} \int \mathrm{d}^2\mathbf{r_2} e^{-i\mathbf{q}'\cdot\mathbf{r_2}} \langle \delta\rho(\mathbf{r_1}, z_1)\delta\rho(\mathbf{r_2}, z_2))\rangle \end{aligned} \tag{4.15}$$

Recall that, we can expand the ensemble average part to get

$$\langle \delta\rho(\mathbf{r_1}, z_1)\delta\rho(\mathbf{r_2}, z_2)\rangle = \langle \rho(\mathbf{r_1}, z_1)\rho(\mathbf{r_2}, z_2)\rangle - \bar{\rho}(z_1)\bar{\rho}(z_2)$$

Now we need to commit ourselves to the type of impurities that will be examined. Only point charge impurities will be considered for the calculation of the autocovariance of potential fluctuations and charge carrier density fluctuations. So the geometry of each impurity is of the same form as equation 4.4 with $Z = 1$ and no dipole moment, i.e. $\Delta(\mathbf{r} - \mathbf{r}_j, z - z_j) = \delta(\mathbf{r} - \mathbf{r}_j)\delta(z - z_j)$. Since this case was already derived earlier (equation 4.10) we just cite the result,

$$\langle \delta\rho(\mathbf{r_1}, z_1)\delta\rho(\mathbf{r_2}, z_2)\rangle = e^2 n_{\mathrm{imp}} \left\{\delta(\mathbf{r_1} - \mathbf{r_2})\delta(z_1 - z_2) f_1(z_1) + n_{\mathrm{imp}} f_1(z_1) f_1(z_2)[g(\mathbf{r_1} - \mathbf{r_2}) - 1)]\right\}$$

Seting $\mathbf{r_2} - \mathbf{r_1} = \mathbf{r_3}$ and $e^{-i\mathbf{q}'\cdot\mathbf{r_2}} = e^{-i\mathbf{q}'\cdot(\mathbf{r_2}-\mathbf{r_1})} e^{-i\mathbf{q}'\cdot\mathbf{r_1}}$ and integrating over $\mathbf{r}_1$ and $\mathbf{r}_3$ gives

$$\int \mathrm{d}^2\mathbf{r_1} e^{-i(\mathbf{q}+\mathbf{q}')\cdot\mathbf{r_1}} \int \mathrm{d}^2\mathbf{r_3} e^{-i\mathbf{q}'\cdot\mathbf{r_3}} e^2 n_{\mathrm{imp}} \{\delta(\mathbf{r_3})\delta(z_1-z_2)f_1(z_1) + n_{\mathrm{imp}} f_1(z_1)f_1(z_2)[g(\mathbf{r_3})-1]\}$$
$$= (2\pi)^2\delta(\mathbf{q}+\mathbf{q}')e^2 n_{\mathrm{imp}} \{\delta(z_1-z_2)f_1(z_1) + n_{\mathrm{imp}} f_1(z_1)f_1(z_2)[I(\mathbf{q}')-1]\}$$

where $I(\mathbf{q}) = 1 + n_{\mathrm{imp}} \int \mathrm{d}^2\mathbf{r} e^{-i\mathbf{q}\cdot\mathbf{r}}[g(\mathbf{r})-1]$ is the structure factor. Integrating over $\mathbf{q}'$ leaves us with the substitution of $\mathbf{q}' = -\mathbf{q}$.

$$C(\mathbf{R},\mathbf{R}') = e^2 n_{\mathrm{imp}} \int \frac{\mathrm{d}^2\mathbf{q}}{(2\pi)^2} e^{i\mathbf{q}\cdot(\mathbf{r}-\mathbf{r}')} \left\{ \int dz_1 G(\mathbf{q},z,z_1)G(-\mathbf{q},z',z_1)f_1(z_1) \right.$$
$$\left. + n_{\mathrm{imp}} \int dz_1 \int dz_2 G(\mathbf{q},z,z_1)G(-\mathbf{q},z',z_2)f_1(z_1)f_1(z_2)[I(-\mathbf{q})-1] \right\}$$

Now we assume that our Green's function is radially symmetric in $\mathbf{q}$. This is a valid assumption since our model is isotropic in the x-y plane. The same argument could be used for the structure factor (i.e. there is no preference where the ions are located in the x-y plane). Also we are only interested in the potential correlation in the plane of graphene. So we can set $z = z' = z_g$, where z_g is the location of the graphene plane, in the final equation. Noticing that the final answer only depends on the difference $\mathbf{r}-\mathbf{r}'$, making the autocovariance of the potential a stationary process, we can, without loss of generality, choose $\mathbf{r}' = 0$ to get

$$C(\mathbf{r}) = e^2 \frac{N}{A} \int \frac{\mathrm{d}^2\mathbf{q}}{(2\pi)^2} e^{i\mathbf{q}\cdot\mathbf{r}} \left[\int dz_1 G(q,z_q,z_1)^2 f_1(z_1) \right.$$
$$\left. + \int dz_1 \int dz_2 G(q,z_g,z_1)G(q,z_g,z_2)f_1(z_1)f_1(z_2)(I(q)-1) \right]$$

Using the Green's function derived in equation 3.26 and evaluating it at $z = z_g$ simplifies our calculations to

$$G(q,z_g,z') = G^{(0)}(q,z_g,z') + \frac{e^2\chi_0(q)G^{(0)}(q,z_g,z_g)G^{(0)}(q,z_g,z')}{1-e^2\chi_0(q)G^{(0)}(q,z_g,z_g)} \tag{4.16}$$
$$= \frac{G^{(0)}(q,z_g,z')}{1-e^2\chi_0(q)G^{(0)}(q,z_g,z_g)} \tag{4.17}$$

Now we notice two things. First the terms in the integral only depend on the magnitude q, and second the denominator of the Green's funciton is independent of the location of the source term z'. Integrating $\mathbf{q}$ over the polar angle and taking out the denominator of the Green's function gives us,

$$C_V(r) = e^2 n_{imp} \int_0^\infty \frac{dq}{2\pi} \frac{J_0(qr)q}{\epsilon(q,z_g)^2} S(q) \tag{4.18}$$

where we define

$$S(q) = \int dz_1 G^{(0)}(q, z_q, z_1)^2 f_1(z_1) + \int dz_1 \int dz_2 G^{(0)}(q, z_g, z_1) G^{(0)}(q, z_g, z_2) f_1(z_1) f_1(z_2)(I(q) - 1), \tag{4.19}$$

$$\tag{4.20}$$

and the dielectric function to be

$$\epsilon(q, z_g) = 1 - e^2 \chi_0(q) G^{(0)}(q, z_g, z_g) \tag{4.21}$$

We include the subscript V to specify that this is the autocovariance of the potential fluctuations, and to differentiate from another type of autocovariance function. The above analysis could have been performed to obtain the autocovariance in the fluctuations of the charge carrier density. The fluctuatuon of the charge carrier density in Fourier space is defined as

$$\delta\tilde{n}(\mathbf{q}, z_g) = e\chi_0(\mathbf{q})\delta\tilde{\Phi}(\mathbf{q}, z_g) \tag{4.22}$$

To obtain its autocovariance we are required to transform it into position space and evaluate $\langle \delta n(\mathbf{r}, z_g)\delta n(\mathbf{r}', z_g)\rangle$. We omit this derivation as it is similar to the one done above. The result for the autocovariance of the fluctuation of the charge carrier density is

$$C_n(r) = n_{imp} \int_0^\infty \frac{dq}{(2\pi)^3} J_0(qr) q^3 \left[1 - \frac{1}{\epsilon(q, z_g)}\right]^2 S(q) \tag{4.23}$$

It is quite clear from equation 4.22 that the fluctuations in the potential cause fluctuations in the charge carrier density, through the linear response function $\chi_0(\mathbf{q})$. Recall that $\chi_0(q)$ is constant for $q < 2k_F$, and increases for $q > 2k_F$. So we expect that a larger k_F (which means a greater charge carrier concentration) would yeild smaller fluctuations in the charge carrier density, since the linear response would be smaller over greater values of momentum vecotr q.

4.4 Autocovariance of potential fluctuations and charge carrier density fluctuations in graphene

We first consider a two-dimensional distribution of impurities in the plane $z = -d$, below the surface of graphene, which is placed in the plane $z = 0$. This implies that $f_1(z) = \delta(z+d)$, reducing equation 4.19 to

$$S(q) = G^{(0)}(q, 0, -d)^2 I(q) \tag{4.24}$$

In the uncorrelated case (i.e. $I(q) = 1$) it has been shown that the variance (i.e. $C_V(r = 0)$) experiences a logarithmic divergence as $d \to 0$ [1, 2]. The divergence is expected to persist in the correlated case, as $I(q)$ is independent of distance d. This forces all our calculations to be conducted with the condition $d > 0$. For our calculations we consider $d = 0.3$ nm, which is a reasonable

assumption since this is the typical gap size between graphene and the nearby dielectric. Figure 4.3 shows the autocovariance of the potential fluctuations in the plane of graphene as a function of the distance, r, in nanometers. This model consists of graphene placed on top of a semi-infinite layer of a silicon dioxide substrate ($SiO_2, \epsilon_1 = 3.9$), with air above graphene ($\epsilon_2 = 1$). An areal density of $n_{\text{imp}} = 10^{12}\text{cm}^{-2}$ of impurities is located 0.3 nm below the graphene sheet. For low charge carrier doping (fig. 4.3 (a)), the models with correlated impurities exhibit oscillatory behaviour for small r. The oscillatory behaviour is much more pronounced in the HD model (black) and increases with increase in correlation length between the impurities. In the SC model (blue) the oscillation is almost nonexistent, even at the highest correlation length, $r_c = 5$ nm, while for uncorrelated impurities there is no noticeable oscillation. Therefore, the oscillation in the autocovariance must be a consequence of the structure factor, $I(q)$, and not the conventional Friedel oscillation, which would be present in isolated impurities [52]. In the HD model with the highest packing fraction (i.e. $r_c = 7$ nm and $p \approx 0.38$) an unambiguous first local minimum is noticeable around $r = 5$ nm. Interestingly enough the location of the minimum varies little with change in the charge carrier density.

As we increase the charge carrier density (fig. 4.3 (a)→(c)), a number of different effects are taking place, giving a significant change in the qualitative description of the autocovariance. First we notice that the spatial decay of the autocovariance is much faster for highly doped graphene (i.e. the autocovariance approaches zero faster). This can be explained through the use of screening. It was shown elsewhere [52] that the screening length of the electrostatic potential induced in graphene by a point charge is approximately proportional to $1/k_F$. Thus, the screening of external charges is much stronger in highly doped graphene, so the effects of the impurities on the fluctuations of the potential will have much shorter range. The autocovariance seems to be spatially decaying in an exponential manner in all three charge carrier densities, implying the absence of long-range order and that the potential in the plane of graphene is, in fact, disordered. Another interesting property that emerges in the highly doped cases is the existence of anticorrelation. In fig. 4.3 (b) the autocovariance curve for the HD model with the highest correlation length, is negative in the range $4\,\text{nm} \lesssim r \lesssim 7\,\text{nm}$ and then again in the range $12\,\text{nm} \lesssim r \lesssim 15\,\text{nm}$ (see inset). The negative value in the autocovariance is quite significant as it implies that the potential fluctuations at close distances are opposite sign, giving a possible indication for electron-hole puddles. A negative autocovariance of the potential has been experimentally observed [9, 16], however, the most recent literature does not explain these results from a mathematical modeling point of view [2]. As we increase the charge carrier density to $\bar{n} = 10^{13}$ cm^{-2} we see that the negative autocovariance is present in all models with correlated impurities. An interesting pattern can be noticed in the HD model. The autocovariance of the potential fluctuations switches from negative to positive near a value of $r \approx r_c$ (see 4.3 (c) inset). This is a somewhat expected trend. Since the minimum distance between two charged impurities is r_c, the possibility of finding a point charge impurity a distance $r < r_c$ away from your observation point is zero. So, for a sufficiently short screening length, it is likely that the signs in the values of the potential fluctuation at two points a distance $r < r_c$ away are different, giving rise to a range of negative values of $C_V(r)$. This property, however, is absent from the SC model, possibly due to it being a poor thermodynamic model (i.e. is not derived from a Hamiltonian).

Figure 4.4 gives us the autocovariance of the charge carrier density fluctuations scaled by a factor

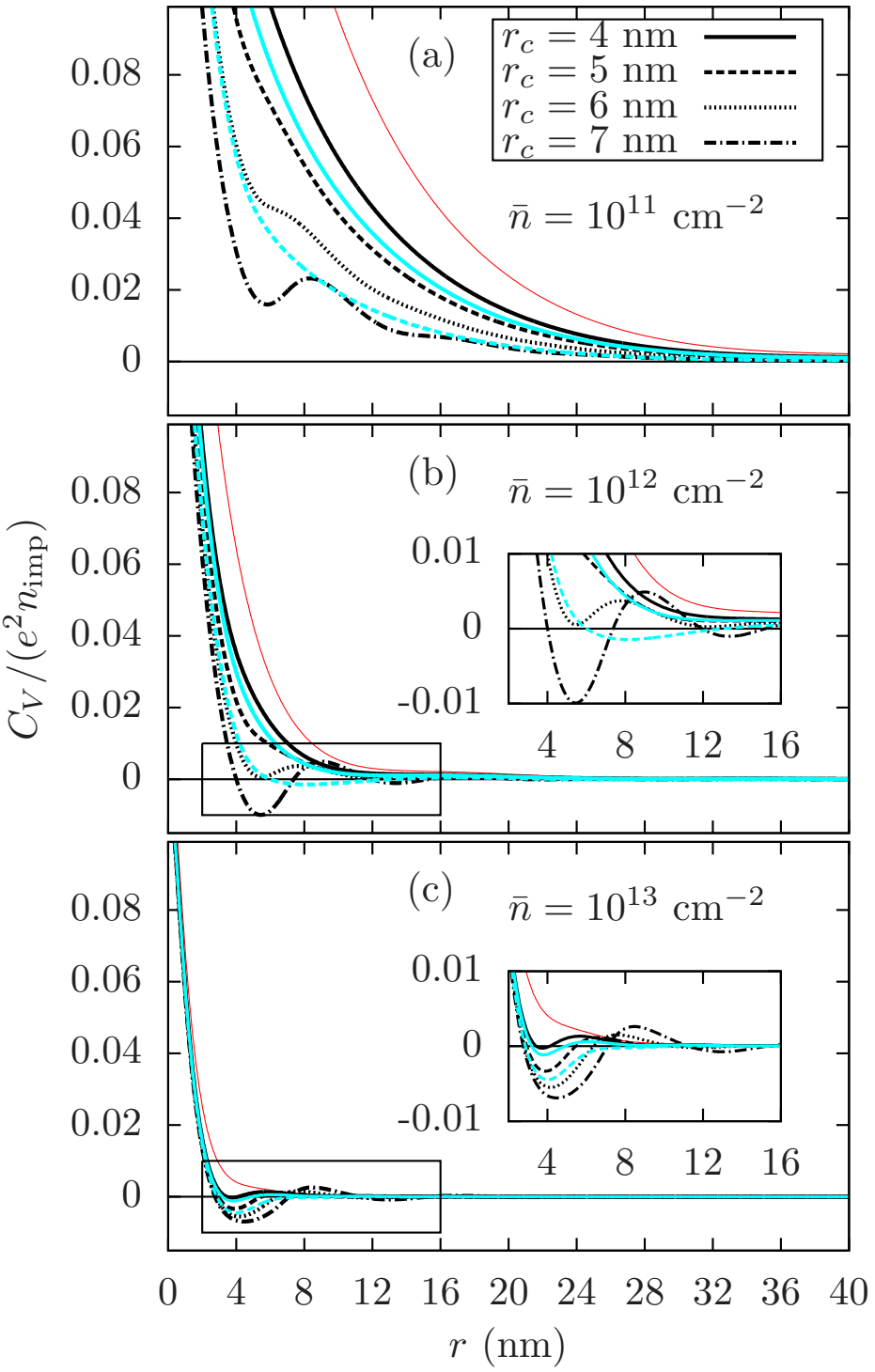

Figure 4.3: Autocovariance of the potential fluctuation in the sheet of graphene placed on top of a semi-infinite silicon dioxide substrate. The hard disc (black) and step correlation (blue) models are compared with the uncorrelated impurities (red) model for different correlation lengths of the impurities.

of $k_F^2 n_{\text{imp}}$. We can see that the oscillations in this autocovariance are present for all correlated impurity models, but absent for the uncorrelated impurity model. Once again this implies that the oscillations are a result of the charged impurity distribution, and not Friedel oscillations. The general profiles of the autocovariance functions seem to be approximately independent from charge carrier doping, $\bar{n}$, with slight variation in the size of the oscillation. However, quantitatively, increasing the charge carrier doping decreases the size of autocovariance of the charge carrier density fluctuations by the same factor. The reason behind such a large decrease of the autocovariance of the charge carrier density fluctuations is still not very well understood, and could point towards a poor choice of scaling. The same property of the autocovariance having a zero at $r \approx r_c$, is present in the HD model. The most interesting result is the similarities between figure 4.4 (c) and figure 4.3 (c) (see inset). The similarities imply that for highly doped graphene, impurities are being strongly screened and having smaller effect on graphene when the charge carrier concentration is high.

We also consider the case of impurities being distributed in a three dimensional volume of finite thickness. For this we use the distribution $f_1(z) = \frac{1}{|L-d|}$, where the impurities are uniformly distributed between $z = -d$ and $z = -L$, where in this case $d = 0.3$ nm. We plot the autocovariance of the fluctuations in the potential as a function of the reduced length $k_F r$ in figure 4.5 for both a 2D and a 3D distribution of the impurities. In this model, we assume graphene is placed between a hafnium dioxide (HfO_2, $\epsilon_1 = 22$) substrate of finite thickness L and a semi-infinite layer of SiO_2. As we increase the charge carrier density we see that the variance (i.e. $C_V(r = 0)$) of the fluctuations of the potential decreases for every model considered. This is because greater charge carrier density has a stronger screening effect on the impurities, causing a smaller amount of randomness [2]. More importantly we see a decrease in the variance from the 2D model to the 3D model. In fact, the 2D, uncorrelated impurities model and the 3D model are qualitatively similar, but quantitatively different by a factor of around 4. This is expected, since essentially the 3D model has the same amount of impurities, but they are spread over the entire volume of the substrate. So the impurities further away from graphene have a weaker effect due to the dielectric screening of the substrate and hence cause smaller fluctuations in graphene. As we increase the substrate thickness from $L = 2$ nm to $L = 10$ nm the autocovariance of the potential fluctuations in most cases increases as well, with some exception in the 3D case. In the 2D cases (i.e. fig. 4.5 (c) to (f)) we see that the increase in the substrate thickness is consistent with a greater increase in the autocovariance for samples with low charge carrier doping. A thicker substrate implies that the metallic back gate is further away from the charged impurities. The charged impurities experience a weaker image force from the metallic gate when it is further away, hence, causing a greater external potential on the graphene sheet. For the 3D impurity model, the increase in the substrate thickness causes two things to happen. The distribution of the impurities is now stretched out over a larger volume, and the screening from the metallic gate is weaker. The interplay between these two effects has a somewhat unexpected consequence, where the autocovariance decreases for large charge carrier doping, but increases for smaller carrier doping. Another interesting phenomena are the changes in the autocovariance for the correlated impurities, with correlation length $r_c = 6$ nm, when the substrate becomes thicker. When the substrate is thin (fig. 4.5 (e)) the autocovariance of the potential fluctuations oscillates around the zero value, indicating statistical possibility for electron-hole puddles. However this property is

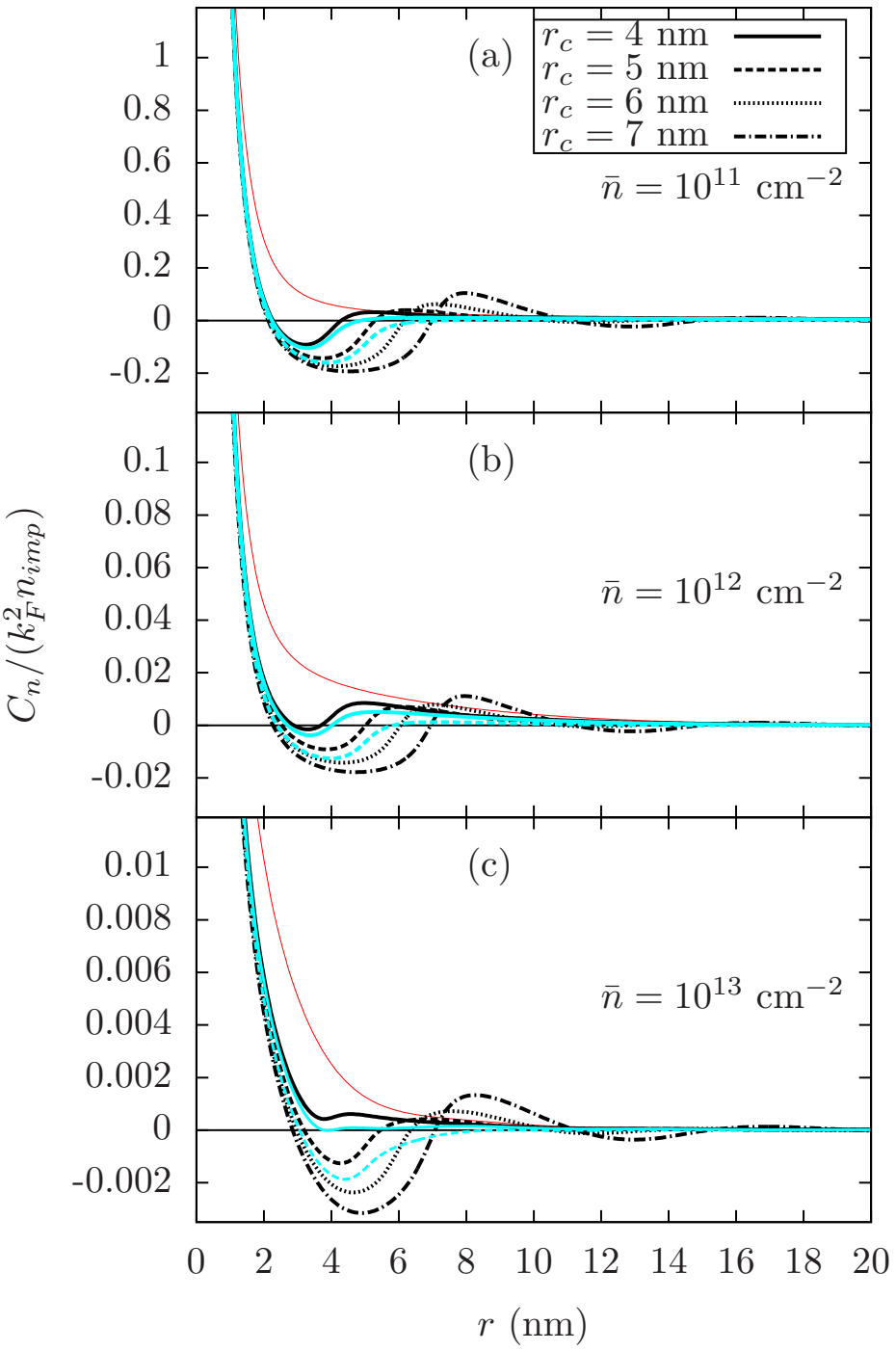

Figure 4.4: Autocovariance of the charge density fluctuation in the sheet of graphene placed on top of a semi-infinite silicon dioxide substrate. The hard disc (black) and step correlation (blue) models are compared with the uncorrelated impurities (red) model for different correlation lengths of the impurities.

absent when the substrate thickness is increased. Although the absence of the autocovariance being negative for such a impurity correlation length may seem in stark contrast to the results obtained in figure 4.3, we note that in this case the large dielectric constant of the substrates dampens the effects of impurities. The reason why increasing the substrate thickness decreases the possibility of electron-hole puddles is still not fully understood.

Figure 4.6 is a comparison between our theoretical models and experimental results obtained by Castellanos-Gomez, *et. al.* [9]. The experimental results were obtained using a combined scanning tunneling and electron force microscope. Their results obtained local potential variations in the plane of graphene which are formed due to trapped charge impurities in the SiO_2 substrate. The variation in the potential was used to calculate the autocorrelation (i.e. $C_V(r)/C_V(0)$) of the potential fluctuations in the plane of graphene. We compare a HD and a SC model to their experimental data. It is quite clear that the HD model gives a better fit to the experimental results. As mentioned earlier the HD model contains much stronger oscillations than the SC model, which agrees with the experimentally observable results. Also important is the comparison between the experimental and theoretical model parameters. The theoretical parameters, $n_{\text{imp}} = 2.1 \cdot 10^{11}\text{cm}^{-2}$ and $\bar{n} = 2.5 \cdot 10^{11}\text{cm}^{-2}$ are in close proximity to the experimentally observed values, $n_{\text{imp}} = (2.9 \pm 0.6) \cdot 10^{11}\text{cm}^{-2}$ and $\bar{n} = (2.6 \pm 0.5) \cdot 10^{11}\text{cm}^{-2}$. However the impurity correlation length between the two models is significantly different. For the HD model we had $r_c = 15.9$ nm ($p = 0.42$) while for the SC model we had $r_c = 12.3$ nm ($p = 0.25$). The mean length between impurities found in the article was 22 ± 2 nm, although the minimum length between impurities, which would correspond to our value r_c, was not evaluated. The inset shows the conductivity of the two models. The conductivity was not evaluated in the paper, so there was no experimental results to compare it to. However it is still interesting to compare the conductivity between the two models. The HD model clearly shows linear dependence for low charge carrier doping, with some saturation near $6 \cdot 10^{11}\text{cm}^{-2}$. The SC model, on the other hand, saturates into a linear relation after a small charge carrier doping. We note that, although it may seem like the SC model has a finite conductivity at zero charge carrier doping, this is not the case. What is actually happening is that the SC model is becoming unphysical since p is close to 0.25. This makes us doubt the validity of the SC model at such a high packing fraction. The conductivity in graphene will be discussed with more detail in the next chapter.

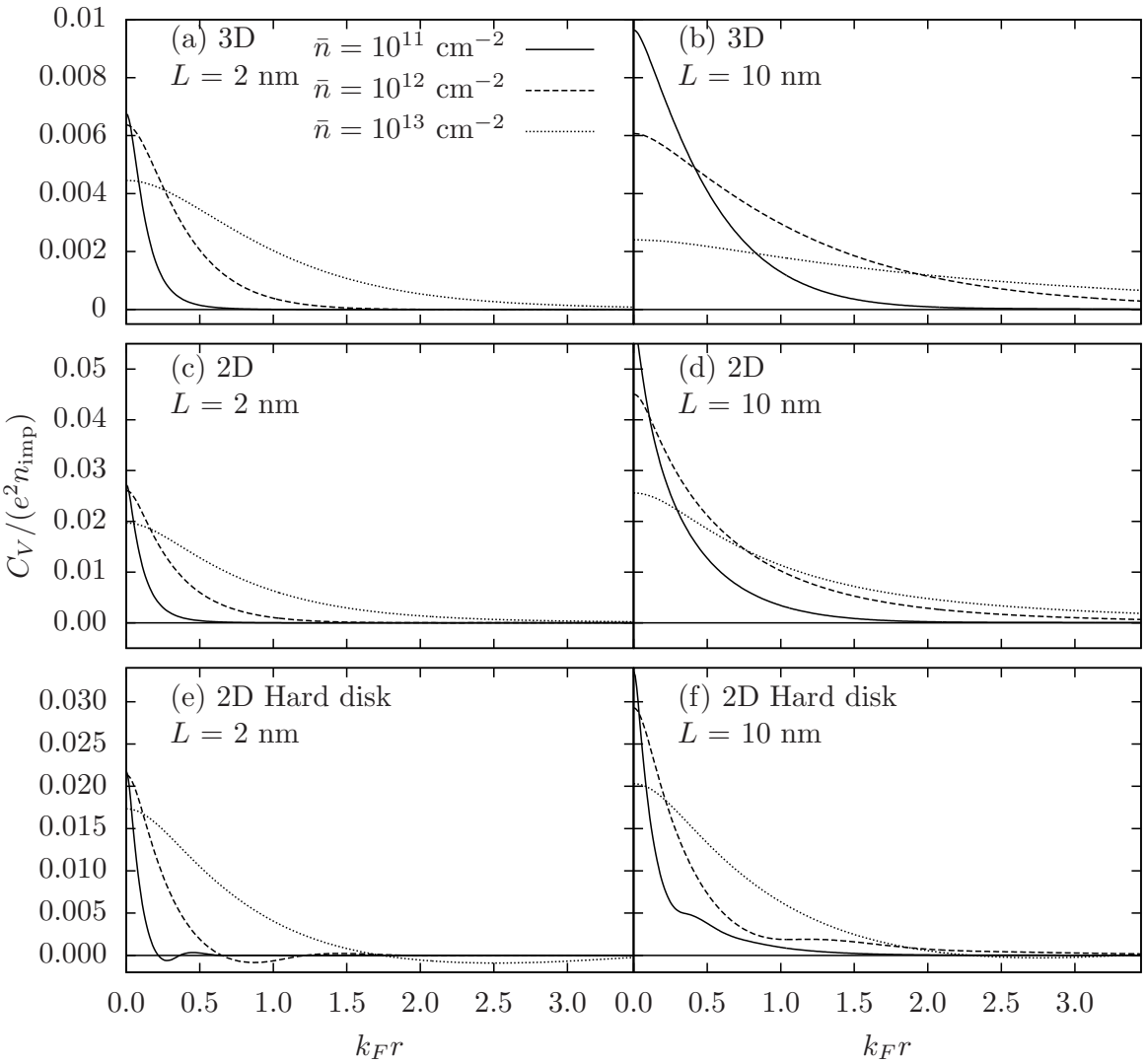

Figure 4.5: Autocovariance of the potential fluctuation in the sheet of graphene. Graphene was placed on top of a HfO_2 substrate ($\epsilon_1 = 22.0$) with finite thickness and a SiO_2 substrate ($\epsilon_2 = 3.9$) was placed on top of grpahene. The column on the left denotes models with a bottom substrate thickness of $L = 2$ nm while the column on the right has a substrate thickness of $L = 10$ nm. Plots (a) and (b) used a three dimensional distribution of the impurities in the substrate. Plots (c) and (d) used a two dimensional distribution with uncorrelated impurities while plots (e) and (f) used a hard disk model with a correlation length of $r_c = 6$ nm. In all six cases the distance between graphene and the impurities was $d = 0.3$ nm.

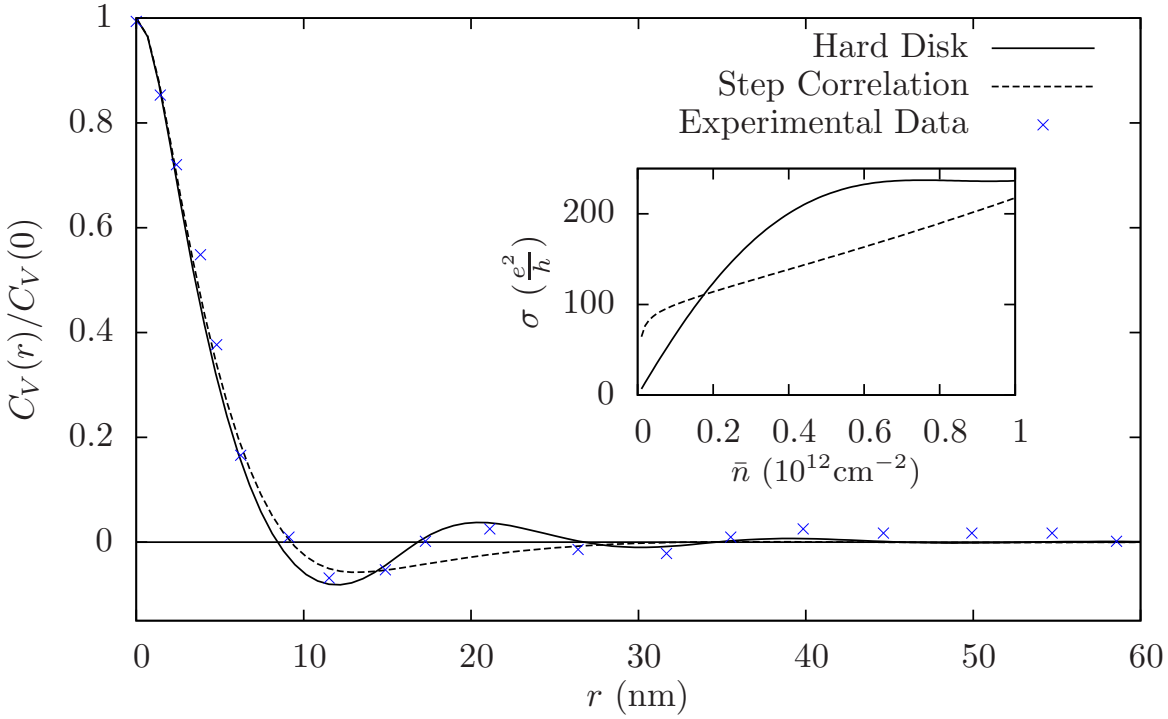

Figure 4.6: A comparison of our theoretical model with experimental results obtained by Castellanos-Gomez *et. al.* [9] The y axis represents the normalized autocorrelation of the fluctuation of the potential on the surface of graphene. We compare two theoretical fits to the experimental data. Using the hard disk model (solid) we are able to get a better fit to the experimental data as opposed to the step correlation model (dashed). The hard disk model has parameters $p = 0.42$, $n_{\text{imp}} = 2.1{\cdot}10^{11}\text{cm}^{-2}$, $\bar{n} = 2.5 \cdot 10^{11}\text{cm}^{-2}$ and the step correlation model has parameters $p = 0.24$, $n_{\text{imp}} = 2.1 \cdot 10^{11}\text{cm}^{-2}$, $\bar{n} = 2.5 \cdot 10^{11}\text{cm}^{-2}$. In both cases we had $d = 1$ nm. The experimental parameters quoted in the paper were $n_{\text{imp}} = (2.9 \pm 0.6) \cdot 10^{11}\text{cm}^{-2}$ and $\bar{n} = (2.6 \pm 0.5) \cdot 10^{11}\text{cm}^{-2}$

Chapter 5

Conductivity

5.1 Energy loss method

As mentioned before, we consider a single-layer graphene sheet sandwiched between a dielectric substrate which contains charge impurities and a layer above graphene, which may be air or another dielectric material. The system may be considered translationally invariant in the x and y coordinates and so we will denote our three dimensional coordinate system by $\mathbf{R} = \{\mathbf{r}, z\}$. The energy loss method (ELM) considers the rigid, steady, motion of an external charge density near graphene and its induced potential on the graphene sheet itself [23]. The movement of an external charge density gives rise to energy dissipation due to excitation of the charge carriers in graphene. The idea behind the ELM is that the frame of reference between the moving charges and graphene (or in general the laboratory reference frame) can be reversed. This allows us to consider the electric conductivity of graphene by examining its charge carriers movement, which has an opposite velocity to the external charge density. For a sufficiently small speed, the resistivity in graphene (which is inversely proportional to conductivity) is related to the energy dissipated by the charge carriers resulting from their scattering on the potential fluctuations due to the external charge density, which in this case are impurities in the substrate. The energy is dissipated due to scattering from external impurities, giving rise to Ohmic heating in graphene. The ELM was developed for studying the transport properties of semiconductor heterostructures by means of the dielectric response formalism for their conducting electrons. This method has been used successfully in studying the scattering of conduction electrons on interface roughness and polarizable scattering centers, as well as in discussing vibrational damping in adsorbed layers due to surface resistivity, and in studying optical properties of thin films for solar energy materials. We note that the ELM gives an expression for the conductivity of doped graphene, which is identical to that obtained by the semiclassical Boltzmann transport theory, but we chose ELM because it yields the drag force on externally moving charges as a side result that may be more directly used in modeling other processes, such as sliding friction of molecular layers physisorbed on graphene [36] or probing the streaming potential in a flowing electrolyte by a graphene based sensor [47] to mention a few.

The electrical energy loss rate of a system due to an external charge is given by

$$\frac{dW}{dt} = -\int d^3\mathbf{R}\ \mathbf{j}(\mathbf{R},t)\cdot\mathbf{E}_{\text{ind}}(\mathbf{R}(t),t) \tag{5.1}$$

Here $\mathbf{E}_{\text{ind}}$ is the induced electrical field in the material and $\mathbf{j}$ is the current vector associated with the distribution of external charges moving parallel to graphene. The induced electrical field arises from external charges. The induced electric field can be represented by the induced electric potential,

$$\mathbf{E}_{\text{ind}}(\mathbf{R},t) = -\nabla\Phi_{\text{ind}}(\mathbf{R},t)$$

and from the conservation of electric charge we have

$$\nabla\cdot\mathbf{j} = -\frac{\partial\rho}{\partial t}$$

where ρ is the external charge density. Now we recall that the induced electric potential and the current density can be written as a sum of their respective average at a point on the z axis and a fluctuating part. That is $\Phi_{\text{ind}}(\mathbf{R}) = \bar{\Phi}_{\text{ind}}(z) + \delta\Phi_{\text{ind}}(\mathbf{R})$ and $\mathbf{j}(\mathbf{R}) = \bar{\mathbf{j}}(z) + \delta\mathbf{j}(\mathbf{R})$. Substituting these into equation 5.1 we get

$$\begin{aligned}\frac{dW}{dt} &= \int d^3\mathbf{R}\ \mathbf{j}(\mathbf{R},t)\cdot\nabla\Phi_{\text{ind}}(\mathbf{R},t)\\ &= \int d^3\mathbf{R}\ \left(\bar{\mathbf{j}}(z,t)+\delta\mathbf{j}(\mathbf{R},t)\right)\cdot\left(\hat{e}_z\frac{d\bar{\Phi}_{\text{ind}}(z,t)}{dz}+\nabla\delta\Phi_{\text{ind}}(\mathbf{R},t)\right)\end{aligned}$$

where $\hat{e}_z$ is a unit vector in the z direction. Since the average current is parallel to graphene by assumption, we have, $\bar{\mathbf{j}}(z,t)\cdot\hat{e}_z = 0$. What we are interested in is the average dissipation of energy, but the average fluctuations of the current density and potential are zero, so the cross terms cancel out, and what we are left with is

$$\begin{aligned}\left\langle\frac{dW}{dt}\right\rangle &= \int d^3\mathbf{R}\ \bar{\mathbf{j}}(z,t)\cdot\langle\nabla\delta\Phi_{\text{ind}}(\mathbf{R},t)\rangle + \langle\delta\mathbf{j}(\mathbf{R},t)\cdot\hat{e}_z\rangle\frac{d\bar{\Phi}_{\text{ind}}(z,t)}{dz} + \langle\delta\mathbf{j}(\mathbf{R},t)\cdot\nabla\delta\Phi_{\text{ind}}(\mathbf{R},t)\rangle\\ &= \int d^3\mathbf{R}\ \langle\delta\mathbf{j}(\mathbf{R},t)\cdot\nabla\delta\Phi_{\text{ind}}(\mathbf{R},t)\rangle\end{aligned}$$

Since the induced electric potential goes to zero as $\mathbf{R}\to\infty$, we use Gauss's theorem and the conservation of the fluctuation in the electric charge to get

$$\left\langle\frac{dW}{dt}\right\rangle = \int d^3\mathbf{R}\ \left\langle\frac{\partial\delta\rho}{\partial t}\delta\Phi_{\text{ind}}(\mathbf{R},t)\right\rangle \tag{5.2}$$

Using the law of the total derivative we can express 5.2 as

$$\left\langle\frac{dW}{dt}\right\rangle = \frac{d}{dt}\int d^3\mathbf{R}\,\langle\delta\rho(\mathbf{R},t)\delta\Phi_{\text{ind}}(\mathbf{R},t)\rangle - \int d^3\mathbf{R}\ \left\langle\delta\rho(\mathbf{R},t)\frac{\partial\delta\Phi_{\text{ind}}}{\partial t}\right\rangle$$

The first term on the right side denotes the change in the total energy. The total energy is conser-

vative and hence does not contribute to the energy dissipation, so the first term will be zero. Now the induced electric potential can be represented in terms of the total potential and the external potential fluctuations

$$\delta\Phi_{\text{ind}} = \delta\Phi_{\text{tot}} - \delta\Phi_{\text{ext}}$$

where $\delta\Phi_{\text{tot}}$ is the fluctuation in the total potential and $\delta\Phi_{\text{ext}}$ is the fluctuation in the external potential. Both potentials can be expressed using the external charge density and a suitable Green's function. For the total potential we use equation 3.26 as our Green's function, while for the external potential we use $G^0(\mathbf{R}, \mathbf{R}')$, the Green's function of the dielectric substrate without graphene, which is static (i.e. time independent). Thus, the induced potential becomes

$$\delta\Phi_{\text{ind}} = \int d^3\mathbf{R}' \int dt' \, \left[G(\mathbf{R}, \mathbf{R}', t - t') - G^0(\mathbf{R}, \mathbf{R}')\right] \delta\rho(\mathbf{R}', t')$$

Now taking the time derivative gives us the dissipation rate

$$\left\langle \frac{dW}{dt} \right\rangle = \int d^3\mathbf{R} \int d^3\mathbf{R}' \int dt' \, \langle \delta\rho(\mathbf{R}, t)\delta\rho(\mathbf{R}', t')\rangle \frac{\partial}{\partial t}[G(\mathbf{R}, \mathbf{R}', t - t') - G^0(\mathbf{R}, \mathbf{R}')] \tag{5.3}$$

As usual we have to transform the Green's functions into their counterparts in Fourier space. The two Green's function in the brackets can be expressed as

$$G(\mathbf{R}, \mathbf{R}', t - t') - G^0(\mathbf{R}, \mathbf{R}') = \int \frac{\mathrm{d}^2\mathbf{q}}{(2\pi)^2} e^{i\mathbf{q}\cdot(\mathbf{r}-\mathbf{r}')} \int d\omega \, e^{-i\omega(t-t')} \left[\tilde{G}(\mathbf{q}, z, z', \omega) - \tilde{G}^0(\mathbf{q}, z, z')\right] \tag{5.4}$$

Since we know what the Green's functions are in Fourier space, using equation 3.26 we get

$$\tilde{G}(\mathbf{q}, z, z', \omega) - \tilde{G}^0(\mathbf{q}, z, z') = \frac{e^2\chi_0(q, \omega)\tilde{G}^0(q, z, z_g)\tilde{G}^0(q, z_g, z')}{1 - e^2\chi_0(q, \omega)\tilde{G}^0(q, z_g, z_g)}$$

The above relation can be expressed in the more convenient form

$$\frac{e^2\chi_0(q, \omega)\tilde{G}^0(q, z, z_g)\tilde{G}^0(q, z_g, z')}{1 - e^2\chi_0(q, \omega)\tilde{G}^0(q, z_g, z_g)} = \left[\frac{1}{\epsilon(q, \omega)} - 1\right] \frac{\tilde{G}^0(q, z, z_g)\tilde{G}^0(q, z_g, z')}{\tilde{G}^0(q, z_g, z_g)} \tag{5.5}$$

where we define the dielectric function $\epsilon(q, \omega) = 1 - e^2\chi_0(q, \omega)\tilde{G}^0(q, z_g, z_g)$. Taking the time derivative of the Green's function and using substitutions 5.4 and 5.5 into 5.3 gives

$$\begin{aligned}\left\langle \frac{dW}{dt} \right\rangle = &\int dz \int dz' \int d^2\mathbf{r} \int d^2\mathbf{r}' \int dt' \, \langle \delta\rho(\mathbf{R}, t)\delta\rho(\mathbf{R}', t')\rangle \\ &\times \int \frac{\mathrm{d}^2\mathbf{q}}{(2\pi)^2} e^{i\mathbf{q}\cdot(\mathbf{r}-\mathbf{r}')} \int d\omega \, (-i\omega) e^{-i\omega(t-t')} \left[\frac{1}{\epsilon(q, \omega)} - 1\right] \frac{\tilde{G}^0(q, z, z_g)\tilde{G}^0(q, z_g, z')}{\tilde{G}^0(q, z_g, z_g)}\end{aligned} \tag{5.6}$$

Furthermore, we assume that the entire distribution of external charges is moving rigidly with velocity

$\mathbf{v}$ parallel to graphene

$$\left\langle \frac{dW}{dt} \right\rangle = \int dz \int dz' \int d^2\mathbf{r} \int d^2\mathbf{r}' \int dt' \int \frac{d^2\mathbf{q}}{(2\pi)^2} \langle \delta\rho(\mathbf{r} - \mathbf{v}t, z)\delta\rho(\mathbf{r}' - \mathbf{v}t', z')\rangle e^{i\mathbf{q}\cdot(\mathbf{r}-\mathbf{v}t-\mathbf{r}'+\mathbf{v}'t)}$$
$$\times e^{i\mathbf{q}\cdot\mathbf{v}(t-t')} \int d\omega\, (-i\omega) e^{-i\omega(t-t')} \left[\frac{1}{\epsilon(q,\omega)} - 1\right] \frac{\tilde{G}^0(q, z, z_g)\tilde{G}^0(q, z_g, z')}{\tilde{G}^0(q, z_g, z_g)} \tag{5.7}$$

where $\delta\rho(\mathbf{r}, z)$ is the fluctuating part of the external charge density defined in equation 4.1, in the rest frame of reference. The integration over $\mathbf{r}$ and $\mathbf{r}'$ transforms our external impurity density functions into their Fourier transformed counterparts,

$$\left\langle \frac{dW}{dt} \right\rangle = -\,i \int dz \int dz' \int d\omega\, \omega \int \frac{d^2\mathbf{q}}{(2\pi)^2} \left[\frac{1}{\epsilon(q,\omega)} - 1\right] \frac{\tilde{G}^0(q, z, z_g)\tilde{G}^0(q, z_g, z')}{\tilde{G}^0(q, z_g, z_g)}$$
$$\times e^{i\mathbf{q}\cdot\mathbf{v}(t-t')} \int dt'\, e^{i(\mathbf{q}\cdot\mathbf{v}-\omega)(t-t')} \langle \delta\tilde{\rho}(-\mathbf{q}, z)\delta\tilde{\rho}(\mathbf{q}, z')\rangle \tag{5.8}$$

where the tildes indicate a Fourier transform on the x-y plane. So using the definition of the external charge density in equation 4.1 we can express its Fourier transform as

$$\tilde{\rho}(\mathbf{q}, z) = \int d^2\mathbf{r} e^{i\mathbf{q}\cdot\mathbf{r}} \rho(\mathbf{r}, z) = e \sum_{j=1}^{N} \tilde{\Delta}(\mathbf{q}, z - z_j) e^{-i\mathbf{q}\cdot\mathbf{r}_j}$$

and note that $\delta\tilde{\rho}$ are the fluctuations of this quantity. Now taking the integral of the last part of equation 5.8 over t' gives

$$\int_{-\infty}^{\infty} dt'\, e^{i(\mathbf{q}\cdot\mathbf{v}-\omega)(t-t')} \langle \delta\tilde{\rho}(-\mathbf{q}, z)\delta\tilde{\rho}(\mathbf{q}, z')\rangle = 2\pi \langle \delta\tilde{\rho}(-\mathbf{q}, z)\delta\tilde{\rho}(\mathbf{q}, z')\rangle \delta(\omega - \mathbf{q}\cdot\mathbf{v})$$

Substituting this back into equation 5.8 and integrating over ω gives

$$\left\langle \frac{dW}{dt} \right\rangle = -i \int dz \int dz' \int \frac{d^2\mathbf{q}}{(2\pi)^2}\, \mathbf{q}\cdot\mathbf{v} \left[\frac{1}{\epsilon(q, \mathbf{q}\cdot\mathbf{v})} - 1\right] \frac{\tilde{G}^0(q, z, z_g)\tilde{G}^0(q, z_g, z')}{\tilde{G}^0(q, z_g, z_g)} \langle \delta\tilde{\rho}(-\mathbf{q}, z)\delta\tilde{\rho}(\mathbf{q}, z')\rangle$$

Since the Green's function $\tilde{G}^0(q, z, z')$ only depends on the magnitude q and the fluctuations are isotropic in the x-y plane we get that

$$\int dz \int dz' \int \frac{d^2\mathbf{q}}{(2\pi)^2} (\mathbf{q}\cdot\mathbf{v}) \frac{\tilde{G}^0(q, z, z_g)\tilde{G}^0(q, z_g, z')}{\tilde{G}^0(q, z_g, z_g)} \langle \delta\tilde{\rho}(-\mathbf{q}, z)\delta\tilde{\rho}(\mathbf{q}, z')\rangle = 0$$

Using the symmetry properties of the dielectric function $\epsilon(q, \omega) = \epsilon^*(q, -\omega)$ and integrating over $\mathbf{q}$ we get

$$\left\langle \frac{dW}{dt} \right\rangle = \int dz \int dz' \int \frac{d^2\mathbf{q}}{(2\pi)^2}\, \mathbf{q}\cdot\mathbf{v} \Im\left[-\frac{1}{\epsilon(q, \mathbf{q}\cdot\mathbf{v})}\right] \frac{\tilde{G}^0(q, z, z_g)\tilde{G}^0(q, z_g, z')}{\tilde{G}^0(q, z_g, z_g)} \langle \delta\tilde{\rho}(-\mathbf{q}, z)\delta\tilde{\rho}(\mathbf{q}, z')\rangle \tag{5.9}$$

The full dielectric function is not necessary as we are more concerned about its value in the so-called friction regime, which is obtained in the $\mathbf{v} \to 0$ limit. Focusing only on the first order approximation

of the dielectric function in $\mathbf{v}$ by taking the partial derivative of the linear response function (eq. 3.11) gives

$$\begin{aligned}\Im\left[-\frac{1}{\epsilon(q,\mathbf{q}\cdot\mathbf{v})}\right] =& \frac{\Im\left[1+e^2\chi_0^*(q,\mathbf{q}\cdot\mathbf{v})\tilde{G}^0(q,z_g,z_g)\right]}{|\epsilon(q,\mathbf{q}\cdot\mathbf{v})|^2} \\ \approx& e^2\frac{\mathbf{q}\cdot\mathbf{v}}{\pi\hbar v_F^2}\frac{H(2k_F-q)\tilde{G}^0(q,z_g,z_g)\sqrt{\left(\frac{2k_F}{q}\right)^2-1}}{|\epsilon(q,\mathbf{q}\cdot\mathbf{v})|^2}\end{aligned} \tag{5.10}$$

We can readily replace $|\epsilon(q,\mathbf{q}\cdot\mathbf{v})|^2$ with the static case $|\epsilon(q,0)|^2$ since higher order terms in $\mathbf{v}$ will not contribute to the conductivity in limit $\mathbf{v}\to 0$. Substituting equation 5.10 into 5.9 and using the fact that $r_s=\frac{e^2}{\hbar v_F}$ gives us

$$\begin{aligned}\left\langle\frac{dW}{dt}\right\rangle =& \frac{r_s}{v_F}\int\frac{d^2\mathbf{q}}{(2\pi)^2}\frac{(\mathbf{q}\cdot\mathbf{v})^2}{\pi}\frac{H(2k_F-q)\sqrt{\left(\frac{2k_F}{q}\right)^2-1}}{|\epsilon(q,0)|^2} \\ &\times\int dz\int dz'\tilde{G}^0(q,z,z_g)\tilde{G}^0(q,z_g,z')\langle\delta\tilde{\rho}(-\mathbf{q},z)\delta\tilde{\rho}(\mathbf{q},z')\rangle\end{aligned}$$

Now notice that the last term with the integrals over z and z' is quite similar to the earlier defined equation 4.19. In fact

$$S(q)=\frac{1}{e^2N}\int dz\int dz'\tilde{G}^0(q,z,z_g)\tilde{G}^0(q,z_g,z')\langle\delta\tilde{\rho}(-\mathbf{q},z)\delta\tilde{\rho}(\mathbf{q},z')\rangle$$

is the more general case of equation 4.19. Using the fact that $(\mathbf{q}\cdot\mathbf{v})^2=q^2v^2\cos^2(\theta)$ we can integrate over the polar angle of $\mathbf{q}$ to get

$$\left\langle\frac{dW}{dt}\right\rangle = e^2N\frac{2k_Fr_sv^2}{v_F}\int_0^{2k_F}\frac{dq}{(2\pi)^2}\frac{q^2\sqrt{1-\left(\frac{q}{2k_F}\right)^2}}{|\epsilon(q,0)|^2}S(q) \tag{5.11}$$

Using a change of variables $q=2k_Fx$ equation 5.11 becomes

$$\left\langle\frac{dW}{dt}\right\rangle = e^2N\frac{k_F^2r_sv^2}{\pi^2v_F}\int_0^1 dx\,\frac{(2k_Fx)^2\sqrt{1-x^2}}{|\epsilon(2k_Fx,0)|^2}S(2k_Fx)$$

Since $k_F^2=\pi\bar{n}$ and $\frac{e^2}{v_F}=\hbar r_s=2\pi hr_s$, the final expression for the average energy dissipation is

$$\left\langle\frac{dW}{dt}\right\rangle = 2Nh\bar{n}r_s^2v^2\int_0^1 dx\,\frac{(2k_Fx)^2\sqrt{1-x^2}}{|\epsilon(2k_Fx,0)|^2}S(2k_Fx) \tag{5.12}$$

By reversing the frame of reference, we can express the energy loss rate in graphene through the use of the standard expression of classical electrodynamics

$$\left\langle\frac{dW}{dt}\right\rangle = \int d^2\mathbf{r}\,\langle\mathbf{J}\cdot\mathbf{E}\rangle \tag{5.13}$$

where $\mathbf{J} = \sigma\mathbf{E}$ is the current density of the charge carriers in graphene, σ denotes its DC conductivity and $\mathbf{E}$ is the applied external electric field tangentially across graphene. Assuming that the charge carrier density is uniform in graphene, we may write $\mathbf{J} = -e\bar{n}\mathbf{v}$ in the steady-state regime. This gives us an average energy loss rate of

$$\left\langle \frac{dW}{dt} \right\rangle = \frac{A(e\bar{n}v)^2}{\sigma} \tag{5.14}$$

where A is the area of the graphene sheet. Taking the limit as $\mathbf{v} \to 0$, we get the conductivity in graphene as

$$\sigma = \frac{A(e\bar{n}v)^2}{\left\langle \frac{dW}{dt} \right\rangle} = \frac{e^2}{h} \frac{\frac{\bar{n}}{n_{\text{imp}}}}{2r_s^2 \int_0^1 dx \, \frac{(2k_F x)^2 \sqrt{1-x^2}}{|\epsilon(2k_F x, 0)|^2} S(2k_F x)} \tag{5.15}$$

where $\frac{e^2}{h}$ is the inverse of the Von Klitzing constant. With the derivation of the conductivity using the ELM we can easily extend it to evaluate the charge carrier mobility, given by

$$\mu = \sigma / (e\bar{n}) \tag{5.16}$$

5.2 Conductivity in graphene

The conductivity in graphene is a subject of intense interest and current research. Graphene has the potential to revolutionize the semiconductor industry since it allows for extremely high electron mobility on its surface. However, many experimentally observable phenomena of the conductivity through graphene have still not been fully understood. The conductivity in graphene varies quantitatively for different samples of graphene sheets. Before graphene FETs can be implemented, the cause of this variation in the conductivity needs to be examined. Recently it has been shown that the mobility in suspended graphene is 10 times larger than graphene on SiO_2 [7]. The most logical explanation for this is that charged impurities, which are in greater concentrations in a SiO_2 substrate than in air surrounding graphene, play an important role in the conductivity and mobility in graphene. Similarly, increased conductivity and mobility have also been observed with graphene being placed on a high-κ (i.e. high dielectric constant) surface. The high-κ substrate have a stronger screening of trapped charged impurities reducing their effects [28].

Since the discovery of graphene, many mathematical models, which incorporate various kinds of impurities, have been proposed to examine the conductivity [10, 1, 39, 50, 14, 19], most of which seem to agree quantitatively and qualitatively, but have different underlying physics to explain the phenomena. Graphene is known to exhibit a sublinear behaviour in the conductivity for large charge carrier doping [66]. This can be explained from a variety of different models. Atomic vacancies in the structure of graphene cause short range scattering of the charge carriers, and a constant resistance across the sheet of graphene [56]. As such, due to Matthiessen's rule the conductivity would have the form $\sigma = \frac{\bar{n}}{A+B\bar{n}}$, for some material dependent constants A and B. This model certainly does give a sublinear trend to the conductivity for higher $\bar{n}$ (and even saturates for extremely high $\bar{n}$), however the experimental absence of atomic vacancies in graphene casts some doubt as to whether this is the underlying mechanism for the sublinear trend. Another contender for the explanation of

the sublinear conductivity for larger $\bar{n}$ is the so called resonant scattering model. The idea behind the resonant scattering method is that the molecules absorbed on graphene, cause both bound states in graphene, near the Dirac point, and strong short range potentials [19, 12]. Although, there is no direct experimental observation of resonant scattering [56] it does provide a phenomenological model. The models we present here were first developed by Das Sarma, *et. al.* [40]. The models consider the correlation between charged impurities as the main source of charge carrier scattering in graphene for high $\bar{n}$. It is well-known that impurities are present in the substrate and do cause significant effects in graphene, strengthening the argument that long range scatterers are the cause to the sublinear behaviour of the conductivity.

In figure 5.1 we consider a two-layer structure that consists of a semi-infinite SiO_2 substrate ($\epsilon_1 = 3.9$) and a semi-infinite layer of air ($\epsilon_2 = 1$), with graphene placed right between the two dielectrics at $z_g = 0$. We show the dependence of graphene's conductivity, σ, with respect to its average charge carrier density $\bar{n}$. The impurities have a planar distribution a distance d away from graphene (i.e. $f_1(z) = \delta(z + d)$) with a fixed $Z = 1$, which will be used throughout all models, and no dipole moment. In all three cases the areal impurity density is $n_{\text{imp}} = 10^{12}$ cm^{-2}. We show the results for several values of the correlation length r_c among the impurities, which are obtained by using the SC and the HD models through their 2D structure factor. Note that the SC model only yields physical results for $r_c < 5.6$ nm for the given value of n_{imp}, whereas the HD model is meaningful for larger values of r_c. In addition to the case of point-like impurities being placed directly on graphene ($d = 0$ and $R_{cl} = 0$), we also show the effects of point-like impurities embedded at $d = 0.3$ nm inside the SiO_2 substrate (fig. 5.1 (b)), as well as disc-like impurities (see equation 4.5) with fixed radius $R_{cl} = 2$ nm placed on graphene ($d = 0$) (fig. 5.1 (c)).

With regards to the effects of non-zero d and R_{cl}, one notices that in figures 5.1 (b) and (c), they both contribute to an increase in the slope of conductivity at higher $\bar{n}$ values, as expected, where they even give rise to a super-linear dependence of conductivity on $\bar{n}$ for smaller values of the correlation length r_c. Note that the case of uncorrelated discs with $r_c = 0$ is somewhat unphysical as the discs are allowed to overlap. The effects of finite d and R_{cl} are relatively weak and only affect quantitative details of conductivity at higher $\bar{n}$, whereas comparison among the insets in figure 5.1 shows that their effects are barely noticeable at $\bar{n} \lesssim 10^{12}$ cm^{-2}

The most prominent effect in figure 5.1 is a strong increase of the initial slope of conductivity as a function of $\bar{n}$ (and hence an increase in mobility of graphene, $\mu = \sigma/(e\bar{n})$) at low values of $\bar{n}$ as the correlation length r_c increases. From the insets in figure 5.1, one notices that the initial slopes from the SC model are higher than those from the HD model for the same value of r_c because $I_{SC}(0) < I_{HD}(0)$, where $I(q)$ is the structure factor. However, the latter model permits the use of much larger values of r_c than the former model, hence giving rise to rather large initial slopes of the conductivity at the largest packing fractions shown. (Notice that the case with a maximum packing fraction of $p \approx 0.38$ that is shown in figure 5.1 is still well within the interval of confidence for the HD model used here.[55]) As the charge carrier density $\bar{n}$ increases, the conductivity shows a sub-linear dependence on $\bar{n}$ that becomes more pronounced as the correlation length r_c increases. In the case of $d = 0$ and $R_{cl} = 0$ the sub-linear dependence occurs for all $r_c > 0$, whereas in the cases of finite d or R_{cl} values, the sub-linear dependence may even overcome the opposite effect

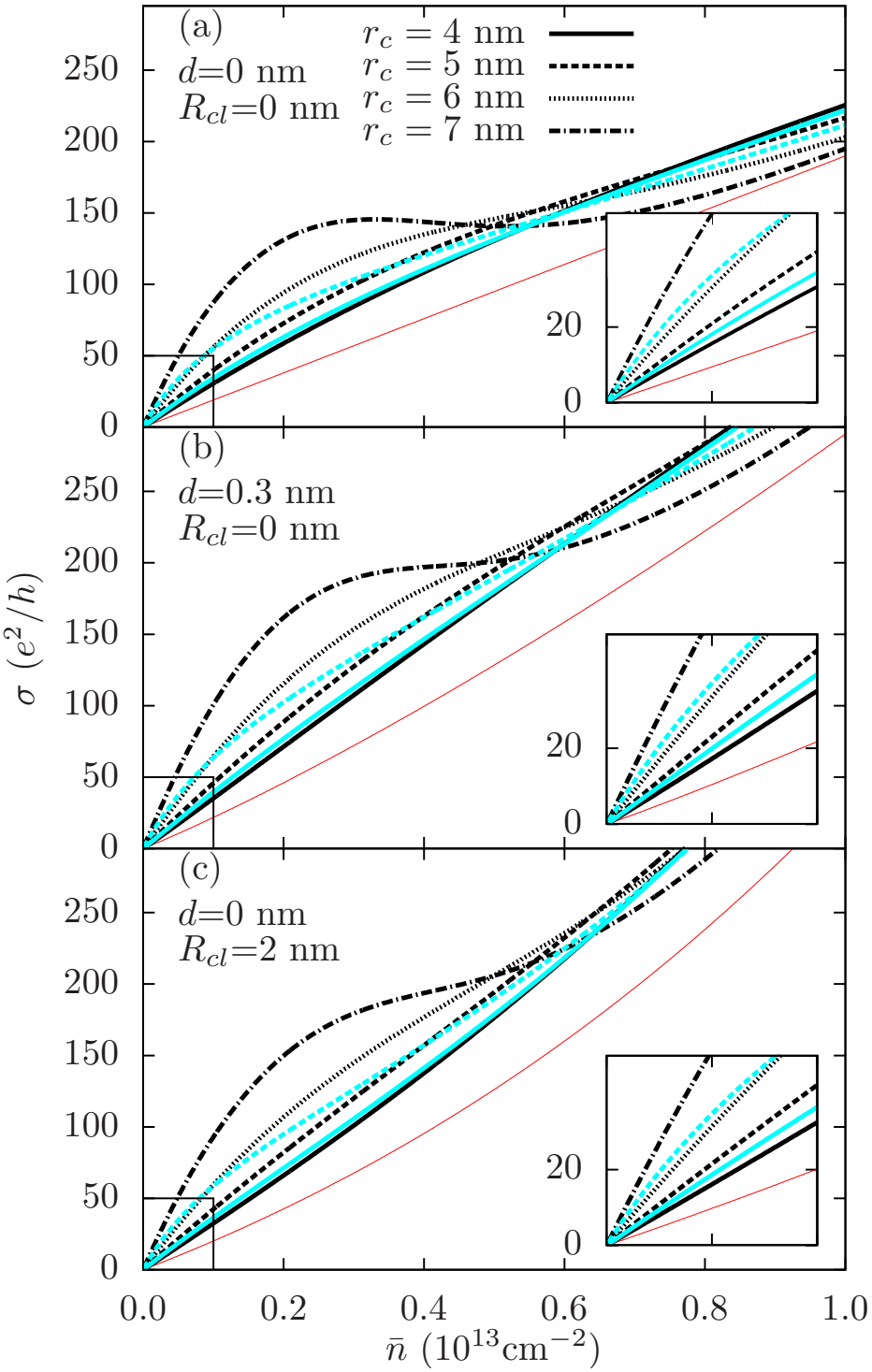

Figure 5.1: Conductivity for various correlation lengths of impurities with $n_{\rm imp} = 10^{12}$ cm^{-2} in the limit $L = \infty$. a) $d = 0$ and no cluster formation. b) $d = 0.3$ nm, no cluster formation. c) $d = 0$ and clusters of radius $R_c = 2$ nm. Black lines denote conductivity using hard disk model and blue lines are for the step correlation model. Thin red line is for uncorrelated impurities.

of super-linear dependence for a sufficiently large r_c. For the largest r_c value shown in figure 5.1, the sub-linear behavior even gives rise to a saturation effect in the conductivity of graphene with increasing $\bar{n}$, which is reminiscent of a similar saturation effect in the conductivity of graphene when the scattering processes on both charged impurities and short-ranged impurities are combined via the Matthiessen's rule [76]. Thus, we may propose that high packing fractions due to large correlation lengths among the charged impurities can give rise to both higher initial slopes of conductivity at lower $\bar{n}$ and a stronger saturation effect at higher $\bar{n}$ with the HD model than those that can be achieved with the SC model. In particular, since $n_{\rm imp}$ is typically used as a fitting parameter that determines the initial slope of conductivity in comparisons with experiments on graphene, the strong effect of the packing fraction of impurities on this slope may cast additional uncertainty in modeling, which could be, in principle, resolved by looking at the degree of saturation in conductivity at higher doping densities.

In figure 5.2 we consider the same configuration of single-layer graphene atop a semi-infinite SiO_2 substrate with a semi-infinite layer of air above it as in figure 5.1, and attempt to model the experimental data for conductivity versus charge carrier density $\bar{n}$ from [66] by using the HD model for a 2D distribution of point charges with $Z = 1$. We select two graphene samples from [66] labeled K17 and K12 and present them in figure 5.2 (a) and (b) respectivly. Both samples exhibit sublinear behaviour with increasing $\bar{n}$, with (a) being symmetric and (b) showing an electron-hole asymmetry (i.e., asymmetry with respect to the sign of $\bar{n}$). The physical mechanism(s) that occasionally give rise to this kind of asymmetry in graphene are still unclear, so we explore here the possibility that the presence of the perpendicular component of a dipole moment in each impurity, $D_\perp$, may give rise to a sizeable asymmetry, as that seen in figure 5.2 (b). We assume $D_\perp = \alpha E_\perp / e$, where α is the effective polarizability and $E_\perp$ is the total perpendicular electric field near graphene. Assuming $n_{\rm imp}$ to be small enough, we may neglect mutual depolarization among the impurities and simply write $E_\perp = 4\pi e\bar{n}/\epsilon_1$, with $E_\perp$ being positive(negative) for electron(hole) doping of graphene [42]. The two samples were fitted in [66] by assuming that the impurities reside in graphene ($d = 0$) and are uncorrelated, and the optimal linear symmetric fits were found with $n_{\rm imp} = 2.2 \cdot 10^{11}$ cm^{-2} for (a) and with $n_{\rm imp} = 4 \cdot 10^{11}$ cm^{-2} for (b). We also assume the impurities to lie in graphene ($d = 0$), and we use $n_{\rm imp}$, r_c and α as fitting parameters. In the case of the symmetric sample, the best fit is found for $n_{\rm imp} = 3 \cdot 10^{11}$ cm^{-2} with $r_c = 6.8$ nm ($p = 0.11$) and $\alpha = 0$, whereas for the asymmetric case the best fit is found for $n_{\rm imp} = 7.4 \cdot 10^{11}$ cm^{-2} with $r_c = 6.3$ nm ($p = 0.23$) and $\alpha = 1150$ Å^3. Both fits obtained with the HD model in figure 5.2 are quite satisfactory as far as the sublinear behavior of conductivity is concerned, and the relatively large values of packing fractions used in both cases suggest the necessity of using the HD rather than the SC model. On the other hand, a good fit in the asymmetric case can only be achieved with a rather large value of α, which indicates that the dipole mechanism may not be the primary cause of the electron-hole asymmetry in conductivity, at least for the experimental setting in [66]. However, we note that the effective polarizability α of a single impurity may be significantly increased by the presence of a nearby conducting surface.[42]

In figure 5.3 we consider a structure that consists of a dielectric material of finite thickness L (we choose HfO_2 with $\epsilon_1 = 22$) and a semi-infinite layer of SiO_2 ($\epsilon_2 = 3.9$) with graphene placed right on their boundary at $z_g = 0$. This configuration may represent the physical situation where single-layer

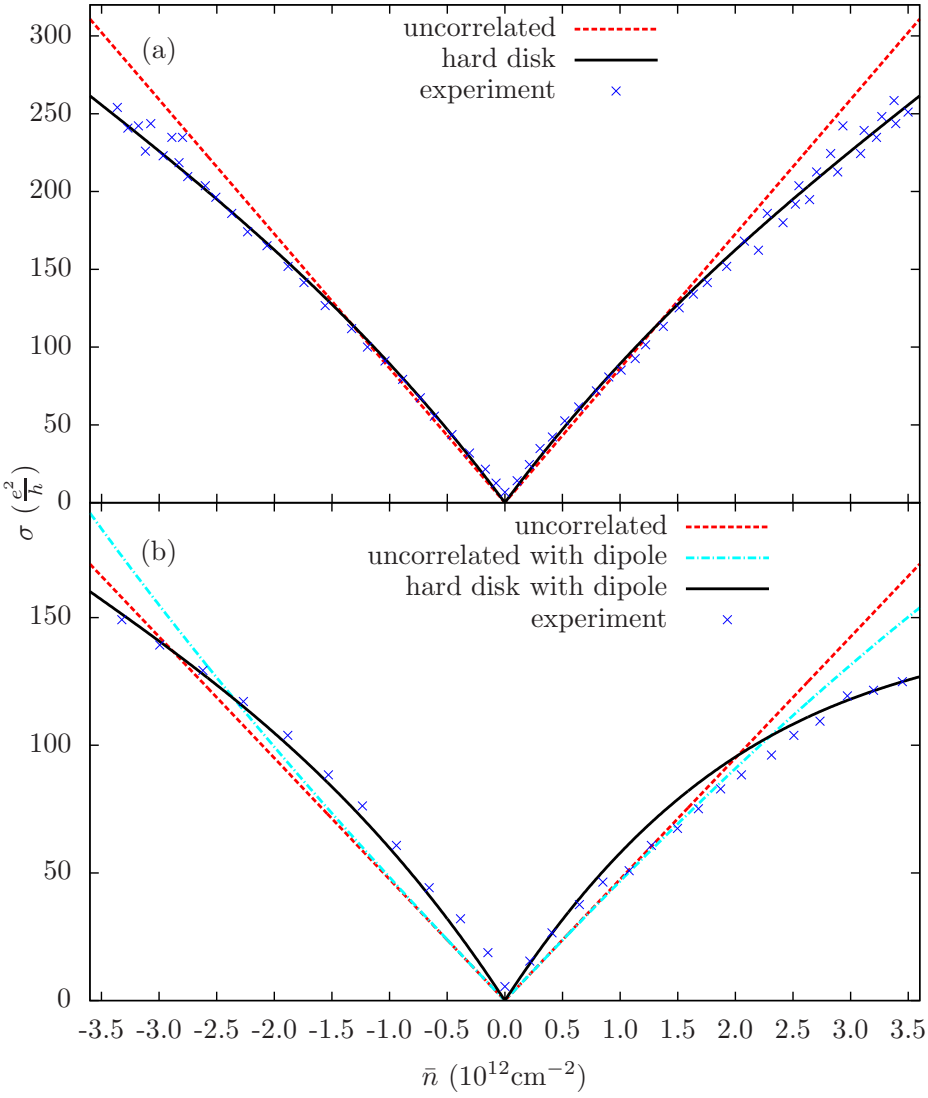

Figure 5.2: Here we compare our theoretical results with experimental results obtained by Tan, Zhang, *et. al.* [66]. In their experiments they used two samples of high quality graphene and measured their conductivity as a they changed the charge carrier density. The linear fit is the theoretical conductivity obtained in the paper and takes only the two dimensional impurity density in the substrate as the fitting parameter. In their paper the densities used were $n_{\text{imp}} = 2.2{\cdot}10^{11}$ cm^{-2} for sample (a) and $n_{\text{imp}} = 4.0{\cdot}10^{11}$ cm^{-2} for sample (b). The linear fit does not explain the sublinear growth of the conductivity for larger carrier densities and the asymmetry of the conductivity around the Dirac point. In our case we consider correlations between the impurities (using a hard disk model) which produce a better fit to the experimental results. For our fitting parameters we used $n_{\text{imp}} = 3.0 \cdot 10^{11}$ cm^{-2} and $p = 0.11$ for sample (a) (top graph). For the bottom graph we show how dipole impurities cause an asymmetric conductivity around the Dirac point (light blue). The fitting parameters for the line of best fit were $n_{\text{imp}} = 7.4 \cdot 10^{11}$ cm^{-2}, $p = 0.23$ and $D = 1100k_F^2$ for sample (b). In both cases we had the impurities on graphene (i.e. $d = 0$ nm). These fits are in excellent agreement with the experimental results. Further more, since these were high quality samples, we expect there to be minimal short-range scattering, so the sub linear behaviour must come from long range scatterers i.e. charge impurities.

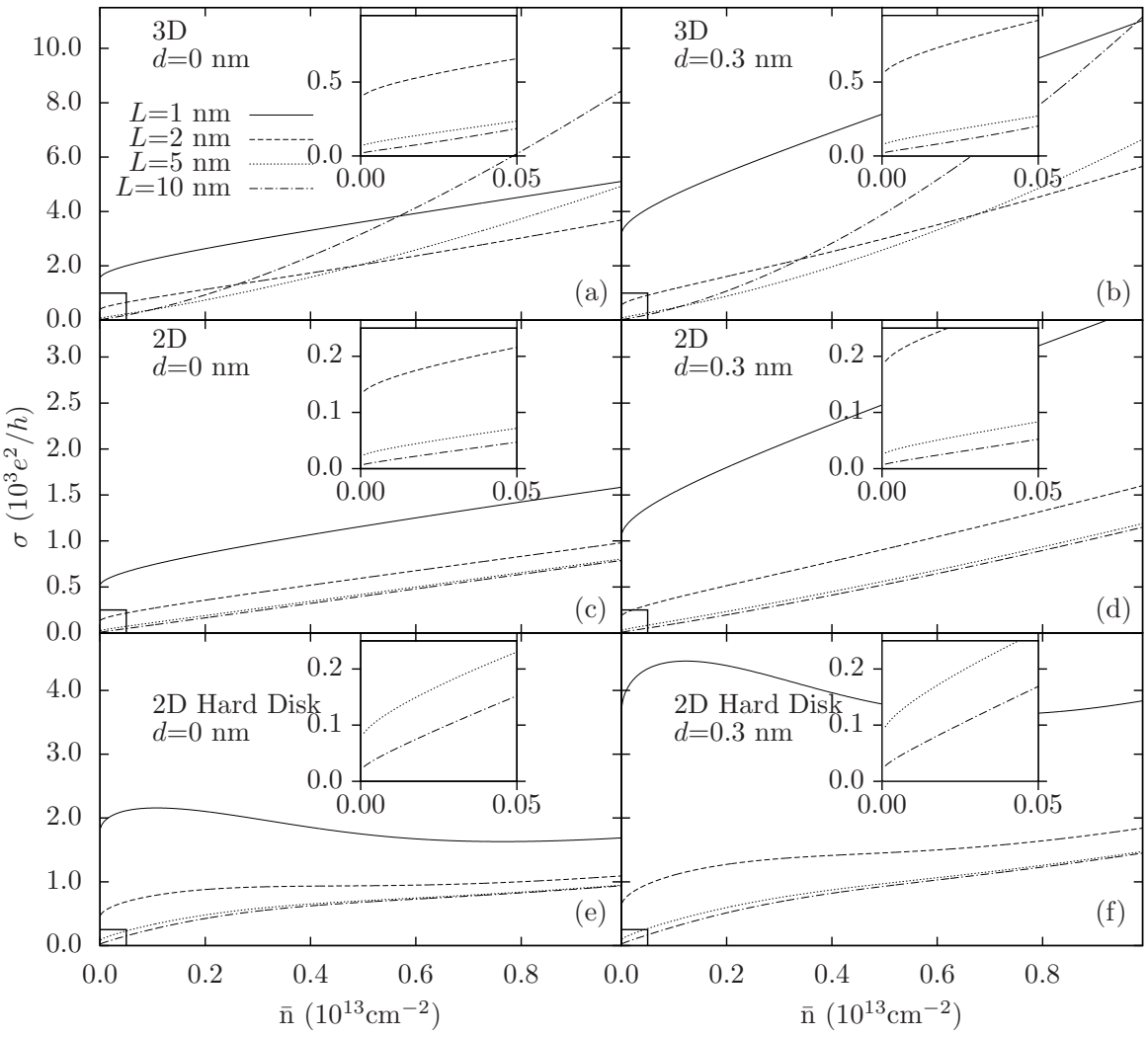

Figure 5.3: Conductivity for various substrate thickness L with $n_{imp} = 10^{12}$ cm^{-2}. We assume graphene is placed between SiO_2 ($\epsilon_2 = 3.9$) and vary the thickness of HfO_2 ($\epsilon_1 = 22.0$). The left column has $d = 0$ while the right column has $d = 0.3$ nm. For the hard disk model we use an impurity correlation length of $r_c = 6$ nm. The insets are a magnification of the conductivity in the range 0 cm$^{-2} \leq \bar{n} \leq 5 \cdot 10^{11}$ cm^{-2}

graphene sits on a thick SiO_2 substrate (with typically $H \sim 300$ nm) and is top-gated through a thin layer of HfO_2 (with $L \lesssim 10$ nm). We show the dependence of the conductivity σ on charge carrier density $\bar{n}$ for several model distributions of point charge impurities in the HfO_2 layer with fixed $Z = 1$ and no dipole moment, having the areal number density $n_{\rm imp} = 10^{12}$ cm^{-2}. We examine the conductivity using a homogeneous 3D distribution of uncorrelated charges throughout the HfO_2 substrate, which extends up to a distance d from graphene, as well as a 2D planar distribution placed in HfO_2 a distance d away from graphene, with both uncorrelated ($r_c = 0$) and correlated ($r_c = 6$ nm, $p \approx 0.28$) charges that are described with the HD model.

One notices in figure 5.3 that finite thickness L exhibits strong effects on conductivity, both in quantitative and qualitative aspects, which are dependent on the underlying structure of charged impurities. First noted is that the overall conductivity is generally increased compared to that seen in figures 5.1 and 5.2, which is expected due to more efficient screening of charged impurities by a high-κ material such as HfO_2. Moreover, the conductivity is seen to increase with decreasing L for all $\bar{n}$ in the 2D cases and only for lower $\bar{n}$ in the 3D case, which may be explained by the more efficient screening of impurities due to the proximity of a metal gate. Furthermore, the conductivity is larger in the 3D case than in the corresponding uncorrelated 2D case because the same number of impurities is spread over larger distances from graphene so that the resulting scattering potential in graphene is weaker. As regards the distance d, one notices similar trends as in figure 5.1, namely, a non-zero d increases both the value of conductivity and its slope (i.e., mobility) in both 3D and 2D models. However, in the case of non-zero correlation length r_c in the 2D models with finite L, one sees little evidence to the increase in the initial slope of conductivity at lower $\bar{n}$, in contrast to the trends seen in figure 5.1, whereas saturation of conductivity at higher $\bar{n}$ seems to get stronger than in figure 5.1 as L decreases. In fact, for the shortest thickness of $L = 1$ nm for both $d = 0$ and $d = 0.3$ nm, this saturation turns into a broad maximum of conductivity around $\bar{n} = 10^{11}$ cm^{-2}, followed by a still broader minimum at higher $\bar{n}$ values.

One remarkable feature seen in figure 5.3 is that the conductivity does not vanish as $\bar{n} \to 0$ for finite L but rather reaches a mimum value $\sigma(0)$. This minimum may be easily estimated for $d = 0$ by using the limiting form of $\frac{S(2k_F x)}{\epsilon(2k_F x,0)^2}$ when $2k_F L \ll 1$ in equation 5.15, which then gives

$$\sigma(0) = \left(\frac{\epsilon_1}{\pi r_s L}\right)^2 \frac{e^2/(2h)}{n_{\rm imp} T}, \tag{5.17}$$

where $T = 1/3$ for the 3D case and $T = I_{2D}(0)$ for the 2D case, where $I_{2D}(0)$ is the structure factor in the long wavelength limit. So in figure 5.3 we would get $T = I_{2D}(0) = (1-p)^3/(1+p) \approx 0.29$ for the correlated 2D case in the HD model.

In figure 5.4 we consider a three-layer structure (implying the use of the substrate model with a gap) that consists of a HfO_2 layer ($\epsilon_1 = 22$) with finite thickness L, a layer of air ($\epsilon_2 = 1$) of thickness $H = 0.6$ nm, and a semi-infinite layer of SiO_2 ($\epsilon_3 = 3.9$), with graphene placed in the air at $z_g = 0.3$ nm, midway between the two dielectrics (see figure 3.2). This configuration is similar to that in figure 5.3 with graphene sandwiched between the HfO_2 and SiO_2 dielectrics, but we introduce in figure 5.4 gaps of air of equal thickness 0.3 nm on both sides of graphene. We investigate the effects of finite thickness L on the mobility of graphene, $\mu = \sigma/(e\bar{n})$, as a function of charge carrier density $\bar{n}$ for a

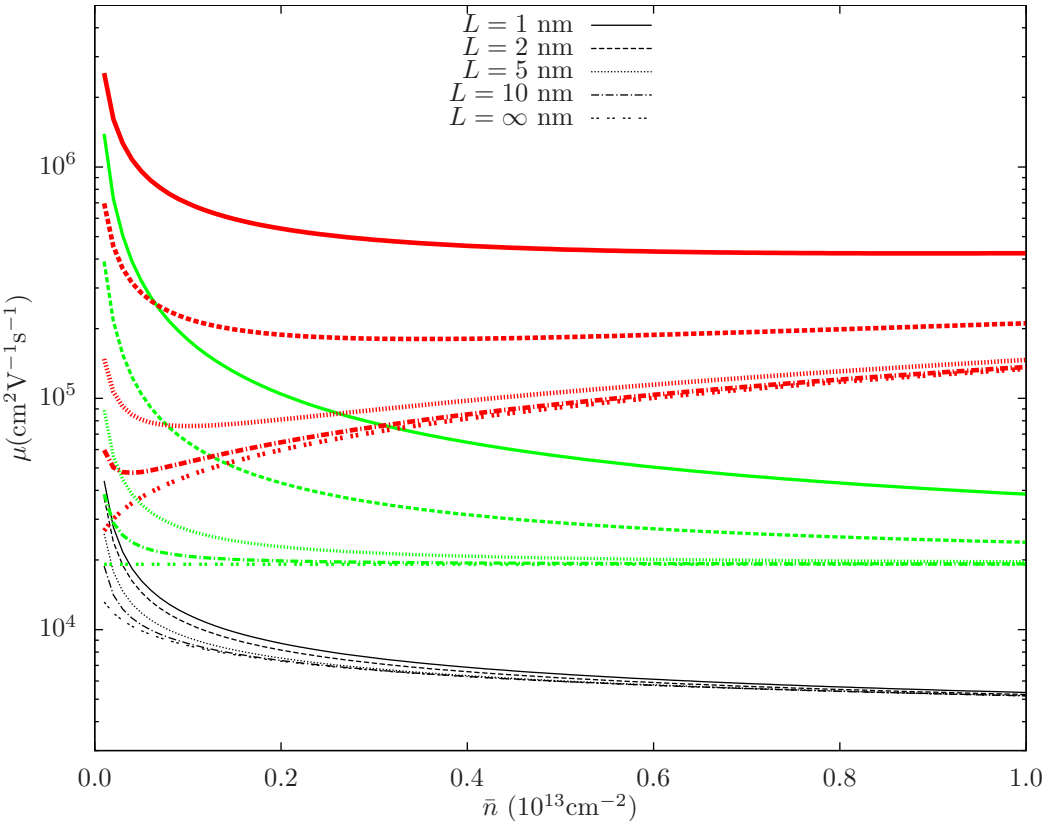

Figure 5.4: Mobility for various thickness of the bottom substrate lengths and $n_{\mathrm{imp}} = 10^{12}$ cm^{-2}. a) (Red) impurities are on the substrate with a vacuum gap of 0.3 nm between graphene and the substrate. (Green) The regular model without a vacuum gap. This is similar to 5.1 (a) where impurities are on the graphene sheet. (Black) Impurities are on the graphene sheet with a vacuum gap of 0.3 nm between the graphene and the substrate.

2D planar distribution of uncorrelated point charges with $Z = 1$ and no dipole moment, having the areal density $n_{\text{imp}} = 10^{12}$ cm^{-2}. We consider three configurations, with the impurities placed either (A) on graphene ($d = 0$) or (B) on the surface of the HfO_2 layer a distance $d = 0.3$ nm away from graphene in the presence of the 0.3 nm gaps, as well as the case (C) from figure 5.3 with zero gaps between graphene and the HfO_2 and SiO_2 dielectrics (i.e. $H = 0$) in the presence of a 2D distribution of uncorrelated charges on graphene ($d = 0$). One may see in figure 5.4 that the mobility increases with decreasing L within each of the three configurations, (A), (B) and (C). This general trend has been experimentally verified by Fallahazad, *et. al.* [18], where the experimental set-up was similar to our theoretical one. However, there is a remarkable differences between the models presented here in the magnitude of the mobility and its dependence on $\bar{n}$. In the configurations (A) and (C) with charge impurities placed on graphene, the mobility generally decreases with increasing $\bar{n}$, whereas in the configuration (B) with the impurities placed on the surface of the HfO_2 layer with a finite gap relative to graphene, the mobilities with higher L values pass through a minimum at a low $\bar{n}$ value and further increase as $\bar{n}$ increases. Moreover, the magnitude of the mobilities with equal L values is seen in figure 5.4 to increase in the order of configurations (A)→(C)→(B), which is also the order of increasing spread of the curves with different L values within each configuration.

One may conclude from figure 5.4 that the existence of a finite gap between graphene and the nearby dielectric, as well as the precise location of impurities within that gap (with the extreme positions being on graphene and on the surface of the dielectric) both have decisive influences on the mobility. Noting that the configuration (A) with impurities on graphene in the presence of gaps was considered by Fischetti and Ong [50], it is remarkable how closing the gaps increases the magnitude of the mobility and increases the spread of its values for different L values, whereas moving the impurities to the surface of a HfO_2 layer in the presence of finite gaps further accentuates those two effects, and even gives rise to a non-monotonous dependence of the mobility on $\bar{n}$ for thicker HfO_2 layers.

5.3 Self-consistent minimum conductivity

We present another phenomenon that occurs in experimental measurements of conductivity through graphene. For graphene with small charge carrier density, the conductivity approaches a non-zero minimum value, σ_{min}. However, in the ELM, equation 5.15 implies that the conductivity, considered a function of the average induced charge carrier density in graphene, $\sigma(\bar{n})$, should vanish in a linear manner close to the neutrality point, i.e., when $\bar{n} \to 0$, as long as $\frac{S(k_F \to 0)}{[\epsilon(k_F \to 0, 0)]^2}$ remains finite. The reason behind a minimum conductivity near the neutrality point could be explained through the fluctuations of the electrostatic potential [76, 66]. As was shown in Chapter 4, the potential in the plane of graphene fluctuates due to the impurities being trapped in the substrate. This fluctuation may form electron-hole puddles in the charge carrier density across graphene, causing finite conductivity, even for zero back gate voltage. An estimate of σ_{min} may be found according to the self-consistent transport (SCT) theory as $\sigma_{\text{min}} = \sigma(n^*)$, where n^* is referred to as a residual charge carrier density that gives a measure of the width of the plateau near the neutrality point where the conductivity minimum is reached [1]. It was shown that n^* may be found as a solution

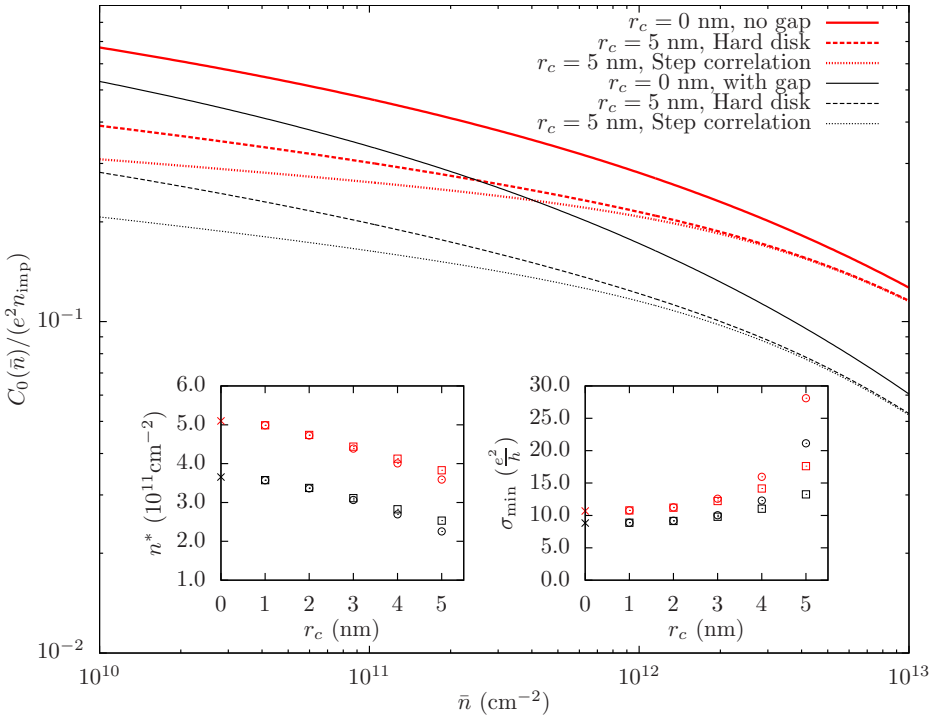

Figure 5.5: We measure the variance of the potential (scaled by $e^2 n_{\rm imp}$) in the plane of graphene as a function of the charge carrier density. Here we denote $C_0(\bar{n}) = C_V(r = 0, \bar{n})$. The variance is shown to decrease with increasing charge carrier doping, and with increase in impurity correlation length, a result which was shown in Chapter 4. The results are obtained using both the zero gap, and non zero gap model, showing that the model with a finite gap causes smaller fluctuations in the potential.

of an equation involving the square of graphene's Fermi energy, $E_F = \hbar v_F k_F$, and the variance of the fluctuating electrostatic potential of graphene derived earlier $C_V(r = 0, \bar{n})$, where we include the dependence of the variance on the charge carrier doping, $\bar{n}$. The residual charge carrier density n^* is the solution to the equation

$$(\hbar v_F)^2 \pi n^* = C_V(r = 0, n^*), \tag{5.18}$$

In this section we turn to studying the conductivity minimum as $\bar{n} \to 0$ due to the presence of electron-hole puddles by solving equation 5.18. We only consider a 2D planar distribution of point charges with $Z = 1$ having no dipole moment. As was mentioned before, $C_V(r)$ experiences a logarithmic divergence as $d \to 0$, whereas equation 5.15 is well behaved in that limit. So in order to make equation 5.18 valid we are forced to assume that charged impurities are placed a finite distance d away from graphene.

In figure 5.5 we consider a configuration similar to that in 5.1, with a semi-infinite SiO_2 substrate ($L \to \infty$ with $\epsilon_1 = 3.9$) and a semi-infinite layer of air ($H \to \infty$ with $\epsilon_2 = 1$), with graphene placed in the air at a distance $z_g \geq 0$ above SiO_2. We show in the main panel of figure 5.5 the $\bar{n}$ dependence of the variance of the potential in the plane of graphene $C_V(r = 0, \bar{n})$ from equation 4.18 for a 2D

distribution of charged impurities with density $n_{\rm imp} = 10^{12}$ cm^{-2} that are placed in/on SiO_2 at a fixed distance $d = 0.3$ nm below graphene. Specifically, we explore the effects of the size of the gap between graphene and the SiO_2 substrate by considering both the zero gap case with $z_g = 0$ (impurities embedded at the depth of 0.3 nm inside SiO_2) and the finite gap case with $z_g = 0.3$ nm (impurities placed on the surface of SiO_2). In addition to considering uncorrelated impurities, we use a finite correlation length of $r_c = 5$ nm ($p \approx 0.2$) allowing us to compare in the main panel the effects of the SC and the HD models on $C_V(r = 0, \bar{n})$. In the insets of figure 5.5, we show the dependence of the residual charge carrier density n^* and the corresponding minimum conductivity $\sigma_{\rm min} = \sigma(n^*)$ on r_c for both the HD and the SC models, in the presence of both zero and finite gaps.

One notices in figure 5.5 that the size of the gap between graphene and the SiO_2 substrate exerts a very strong effect on the magnitude of $C_V(r = 0, \bar{n})$ for all $\bar{n}$, echoing similar conclusion drawn from the results analyzed in figure 5.4. The gap size also strongly affects the values of n^* for all correlation lengths r_c, whereas the effect of the gap size on $\sigma_{\rm min}$ is seen to diminish as r_c decreases. The latter result seems to justify the neglect of graphene–substrate gap, which is implicitly invoked in all simulations of the conductivity minimum in graphene in the presence of charged impurities with small or vanishing packing fractions [1, 76, 40, 13]. As far as the comparison between the HD and SC models is concerned, one sees a noticeable difference in the variance $C_V(r = 0, \bar{n})$ at small $\bar{n}$, which diminishes at large $\bar{n}$ values. The differences between the two models are surprisingly small in both n^* and $\sigma_{\rm min}$, and only become noticeable when the packing fraction p approaches the breakdown value of 0.25 for the SC model for sufficiently large correlation lengths r_c. These results again lend confidence to simulations that use the SC model with short correlation lengths among the charged impurities, which were seen to yield robustly satisfactory interpretations for the conductivity minimum in graphene due to electron-hole puddles [1, 76, 40, 13].

Finally, in figure 5.6 we consider a configuration that was studied in figure 5.3 with graphene sandwiched between a layer of HfO_2 of finite thickness L and a semi-infinite layer of SiO_2, with no gaps between graphene and the two dielectrics, and with a 2D distribution of charged impurities of density $n_{\rm imp} = 10^{12}$ cm^{-2} embedded at a depth $d = 0.3$ nm inside the HfO_2 layer. In the main panel of figure 5.6 we show the dependence of the variance $C_V(r = 0, \bar{n})$ on the charge carrier density in graphene $\bar{n}$, which exhibits an overall reduction in the magnitude of $C_V(r = 0, \bar{n})$ in comparison to figure 5.5 due to a larger dielectric constant of HfO_2, as well as a strong decrease of $C_V(r = 0, \bar{n})$ with decreasing L owing to the screening of impurities by the nearby metallic gate. As a consequence, the resulting residual density n^* is seen in an inset to figure 5.6 to decrease with decreasing L, which indicates that fluctuations in the charge carrier density in graphene due to electron-hole puddles would be gradually erased as the metal gate gets closer to graphene. Finally, in the inset showing $\sigma_{\rm min}$ we explore the contribution of electron-hole puddles to raising the conductivity minimum above its value $\sigma(0)$ that was discussed in figure 5.6 as the limiting value of the expression for conductivity in equation 5.15 when $\bar{n} \to 0$ for a finite thickness L. From that inset one may conclude that the effects of electron-hole puddles in the conductivity minimum of graphene are dominant for dielectric thicknesses $L \gtrsim 10$ nm.

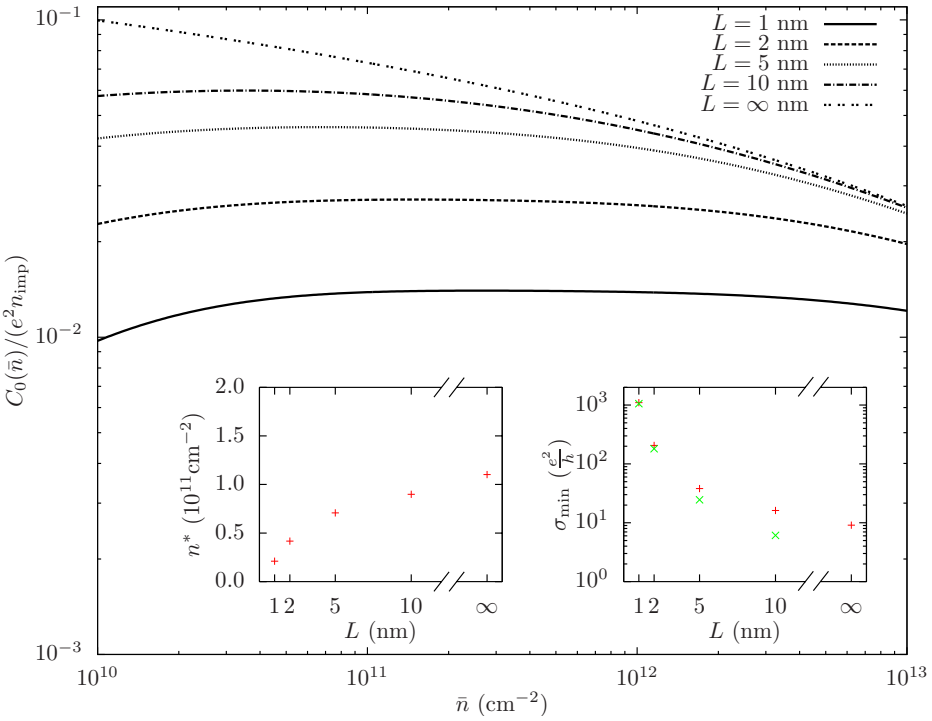

Figure 5.6: We measure the fluctuation of the potential in the plane of graphene as a function charge carrier density and substrate thickness where $C_0(\bar{n}) = C_V(r = 0, \bar{n})$. The model we use is a zero gap model with substrates HfO_2 and SiO_2. The fluctuation decreases with decreasing substrate thickness. The left inset shows the self consistent charge carrier doping as a function of HfO_2 thickness. The right inset shows a comparison of the minimum conductivity obtained using the self-consistent transport theory (red +) and the regular minimum conductivity obtained from finite substrate thickness (green x)

Chapter 6

Conclusion

6.1 Summary

The main goal of this thesis was to study the differences and similarities of various mathematical models that examine the static, electrical properties of graphene. It began with the most basic geometrical and atomic arguments to derive the two dimensional structure of graphene. Using the now derived structure and the tight binding model, the quasi-particle dispersion relation in graphene was obtained, along with the corresponding density of states. A direct correspondence between the charge carrier density in graphene and the back-gate voltage in an experimental setting was shown through the use of capacitive gating. Using this relation enables a direct comparison between experimental and theoretical results. Through the random phase approximation we obtained the linear response of graphene in the zero thickness approximation. Since graphene is affected by external charges trapped in the substrate surrounding graphene, a proper mathematical derivation of the appropriate Green's function for the geometry of the substrate was shown. Using this Green's function and the linear response of graphene, an integral equation between the external charged impurities and the total potential was derived. The external charged impurities which are trapped in the substrate, can have some structure in their distribution. A thorough analysis of the structure and the distribution of the impurities was derived, and a structure factor for the hard disc and step correlation models were presented. The fluctuations in the potential and the charge carrier density were obtained and their respective autocovariance functions were derived. The autocovariance functions gave us a measure of the disorder of the potential and charge carrier density in graphene. Our theoretical results were compared with recent experimental results showing that the hard disc model provided very good agreement with the experimental data. Afterwards, the energy loss method (ELM) was developed to examine the conductivity in graphene. Through the use of the ELM we compare the conductivity in graphene using different structures and distributions of the impurities in the substrate. Theoretical results obtained using a hard disc model are in good agreement with experimental data. Furthermore, we presented the possibility that charged impurities with dipole moments could cause an asymmetric conductivity with respect to electron and hole doping. We also evaluated the charge carrier mobility in graphene using a general substrate geometry which includes

a non-zero gap between the top and the bottom dielectrics. The mobility was shown to be very sensitive to both the location of the charged impurities, and the type of substrate model used. Finally the self-consistent transport theory for graphene was used to evaluate the minimum conductivity in a model with correlated impurities, and a model with changing substrate thickness. There it was shown that correlation between impurities increases the minimum conductivity and increase in the substrate thickness decreases the minimum conductivity.

6.2 Future work

There are many avenues available for the expansion of our current research. While still considering the interaction of graphene with static charged impurities, we could extend our model of graphene beyond the zero thickness approximation. This would require an extended derivation of the linear response of graphene to include the out of plane momentum vector. The use of a graphene model with finite thickness would give a more realistic approach for studying charged impurities near or on the graphene sheet. We could also expand on the idea of impurities distributed in a three dimensional volume to include correlation between the impurities. This addition of the correlation would give a much more realistic model, and a better approach to studying the graphene-impurity interactions.

We can also take another approach for possible future work. Instead of focusing only on the static linear response of graphene, we can consider the full dielectric function and how the addition of different materials surrounding graphene changes the plasmon frequency in graphene. Although the study of plasmons are beyond the scope of this thesis, the analysis is rather straightforward, and results can obtained from the derivations of Chapter 3. Furthermore, we can blend the two research ideas and consider a non-zero thickness of graphene, and how this would effect the plasmon dispersion. The amount of possible directions for future work is endless, and I hope this thesis provides a good introduction for future graduate students conducting research in mathematical models of graphene.

Bibliography

[1] S. Adam, E. H. Hwang, V. M. Galitski, and S. Das Sarma. A self-consistent theory for graphene transport. *Proceedings of the National Academy of Sciences*, 104(47):18392–18397, 2007.

[2] S. Adam, S. Jung, N. N. Klimov, N. B. Zhitenev, J. A. Stroscio, and M. D. Stiles. Mechanism for puddle formation in graphene. *Phys. Rev. B*, 84:235421, Dec 2011.

[3] N. W. Ashcroft and N. D. Mermin. *Solid State Physics*. Thomson Learning, Toronto, 1976.

[4] Q. Bao, H. Zhang, Y. Wang, Z. Ni, Y. Yan, Z. X. Shen, P. Loh, and D. Y. Tang. Atomiclayer graphene as a saturable absorber for ultrafast pulsed lasers. *Advanced Functional Materials*, (19):30773083, 2009.

[5] W. Bao, F. Miao, Z. Chen, H. Zhang, W. Jang, C. Dames, and C. N. Lau. Controlled ripple texturing of suspended graphene and ultrathin graphite membranes. *Nat Nano*, 4(9):562–566, Sep 2009.

[6] D. Bohm and D. Pines. A collective description of electron interactions: III. Coulomb interactions in a degenerate electron gas. *Phys. Rev.*, 92:609–625, Nov 1953.

[7] K. Bolotin, K. Sikes, Z. Jiang, M. Klima, G. Fudenberg, J. Hone, P. Kim, and H. Stormer. Ultrahigh electron mobility in suspended graphene. *Solid State Communications*, 146:351355, 2008.

[8] H. Buljan, M. Jablan, and M. Soljacic. Graphene plasmonics: Damping of plasmons in graphene. *Nat Photon*, 7(5):346–348, May 2013. News and Views.

[9] A. Castellanos-Gomez, R. H. Smit, N. Agrat, and G. Rubio-Bollinger. Spatially resolved electronic inhomogeneities of graphene due to subsurface charges. *Carbon*, 50(3):932 – 938, 2012.

[10] A. H. Castro Neto, F. Guinea, N. M. R. Peres, K. S. Novoselov, and A. K. Geim. The electronic properties of graphene. *Rev. Mod. Phys.*, 81:109–162, Jan 2009.

[11] D. Cohen-Tanugi and J. C. Grossman. Water desalination across nanoporous graphene. *Nano Letters*, 12(7):3602–3608, 2012.

[12] N. J. G. Couto, B. Sacépé, and A. F. Morpurgo. Transport through graphene on $SrTiO_3$. *Phys. Rev. Lett.*, 107:225501, Nov 2011.

[13] S. Das Sarma, S. Adam, E. H. Hwang, and E. Rossi. Electronic transport in two-dimensional graphene. *Rev. Mod. Phys.*, 83:407–470, May 2011.

[14] S. Das Sarma and E. H. Hwang. Density-dependent electrical conductivity in suspended graphene: Approaching the dirac point in transport. *Phys. Rev. B*, 87:035415, Jan 2013.

[15] S. Das Sarma, B. Yu-Kuang Hu, E. Hwang, and W. Tse. Electron-electron interactions in graphene. *arXiv*, 2007.

[16] A. Deshpande, W. Bao, Z. Zhao, C. N. Lau, and B. J. LeRoy. Imaging charge density fluctuations in graphene using coulomb blockade spectroscopy. *Phys. Rev. B*, 83:155409, Apr 2011.

[17] H. Eshuis, J. Yarkony, and F. Furche. Fast computation of molecular random phase approximation correlation energies using resolution of the identity and imaginary frequency integration. *The Journal of Chemical Physics*, 132(23):234114, 2010.

[18] B. Fallahazad, S. Kim, L. Colombo, and E. Tutuc. Dielectric thickness dependence of carrier mobility in graphene with HfO_2 top dielectric. *Applied Physics Letters*, 97(12):123105, 2010.

[19] A. Ferreira, J. Viana-Gomes, J. Nilsson, E. R. Mucciolo, N. M. R. Peres, and A. H. Castro Neto. Unified description of the dc conductivity of monolayer and bilayer graphene at finite densities based on resonant scatterers. *Phys. Rev. B*, 83:165402, Apr 2011.

[20] M. Freitag, T. Low, W. Zhu, H. Yan, F. Xia, and P. Avouris. Photocurrent in graphene harnessed by tunable intrinsic plasmons. *Nat Commun*, 4, Jun 2013.

[21] F. Furche. Molecular tests of the random phase approximation to the exchange-correlation energy functional. *Phys. Rev. B*, 64:195120, Oct 2001.

[22] J. S. Galsin. *Impurity scattering in metallic alloys.* Kluwer academic, 2002.

[23] E. Gerlach. Carrier scattering and transport in semiconductors treated by the energy-loss method. *Journal of Physics C: Solid State Physics*, 19(24):4585, 1986.

[24] X. Guo and U. Riebel. Theoretical direct correlation function for two-dimensional fluids of monodisperse hard spheres. *The Journal of Chemical Physics*, 125(14):144504, 2006.

[25] J.-P. Hansen and I. McDonald. *Theory of Simple Liquids.* Academic, London, 1986.

[26] J. Hedberg. http://www.jameshedberg.com/scienceGraphics.php?sort=all&id=graphene-transistor-labeled-cartoon, 2012.

[27] J. P. Hobson and W. A. Nierenberg. The statistics of a two-dimensional, hexagonal net. *Phys. Rev.*, 89:662–662, Feb 1953.

[28] M. J. Hollander, M. LaBella, Z. R. Hughes, M. Zhu, K. A. Trumbull, R. Cavalero, D. W. Snyder, X. Wang, E. Hwang, S. Datta, and J. A. Robinson. Enhanced transport and transistor performance with oxide seeded high-κ gate dielectrics on wafer-scale epitaxial graphene. *Nano Letters*, 11(9):3601–3607, 2011.

[29] E. H. Hwang and S. Das Sarma. Dielectric function, screening, and plasmons in two-dimensional graphene. *Phys. Rev. B*, 75:205418, May 2007.

[30] S. Iijima. Helical microtubules of graphitic carbon. *Nature*, 354(6348):56–58, Nov 1991.

[31] J. Q. Institute. Quantum hall effect and topological insulators, 2011.

[32] J. Jung and A. H. MacDonald. Tight-binding model for graphene π-bands from maximally localized wannier functions. *Phys. Rev. B*, 87:195450, May 2013.

[33] M. Katsnelson. *Graphene: Carbon in two dimensions.* Cambridge Universit Press, 2012.

[34] M. I. Katsnelson. Graphene: carbon in two dimensions. *Materials Today*, 10(12):20 – 27, 2007.

[35] V. N. Kotov, B. Uchoa, V. M. Pereira, F. Guinea, and A. H. Castro Neto. Electron-electron interactions in graphene: Current status and perspectives. *Rev. Mod. Phys.*, 84:1067–1125, Jul 2012.

[36] J. Krim. Friction and energy dissipation mechanisms in adsorbed molecules and molecularly thin films. *Advances in Physics*, 61, 2012.

[37] H. W. Kroto, J. R. Heath, S. C. O'Brien, R. F. Curl, and R. E. Smalley. C60: Buckminsterfullerene. *Nature*, 318(6042):162–163, Nov 1985.

[38] T. Kuila, S. Bose, P. Khanra, A. Mishra, N. Kim, and J. Lee. Recent advances in graphene-based biosensors. *Biosensors & bioelectronics*, 2011.

[39] Q. Li, E. Hwang, and E. Rossi. Effect of charged impurity correlations on transport in monolayer and bilayer graphene. *Solid State Communications*, 152(15):1390 – 1399, 2012.

[40] Q. Li, E. H. Hwang, E. Rossi, and S. Das Sarma. Theory of 2d transport in graphene for correlated disorder. *Phys. Rev. Lett.*, 107:156601, Oct 2011.

[41] C. H. Mak. Large-scale simulations of the two-dimensional melting of hard disks. *Phys. Rev. E*, 73:065104, Jun 2006.

[42] B. L. Maschhoff and J. P. Cowin. Corrected electrostatic model for dipoles adsorbed on a metal surface. *The Journal of Chemical Physics*, 101(9):8138–8151, 1994.

[43] M. Masujima. *Applied mathematical methods in theoretical physics.* Wiley-vch, Weinheim, 2009.

[44] K. M. McCreary, K. Pi, A. G. Swartz, W. Han, W. Bao, C. N. Lau, F. Guinea, M. I. Katsnelson, and R. K. Kawakami. Effect of cluster formation on graphene mobility. *Phys. Rev. B*, 81:115453, Mar 2010.

[45] E. G. Mishchenko. Effect of electron-electron interactions on the conductivity of clean graphene. *Phys. Rev. Lett.*, 98:216801, May 2007.

[46] R. Murali. *Graphene Nanoelectronics: From Materials to Circuits.* Springer, 2012.

[47] A. K. M. Newaz, D. A. Markov, D. Prasai, and K. I. Bolotin. Graphene transistor as a probe for streaming potential. *Nano Letters*, 12(6):2931–2935, 2012.

[48] K. S. Novoselov, V. I. Falko, L. Colombo, P. R. Gellert, M. G. Schwab, and K. Kim. A roadmap for graphene. *Nature*, 490(7419):192–200, Oct 2012.

[49] K. S. Novoselov, A. K. Geim, S. V. Morozov, D. Jiang, M. I. Katsnelson, I. V. Grigorieva, S. V. Dubonos, and A. A. Firsov. Two-dimensional gas of massless dirac fermions in graphene. *Nature*, 438(7065):197–200, Nov 2005.

[50] Z.-Y. Ong and M. V. Fischetti. Charged impurity scattering in top-gated graphene nanostructures. *Phys. Rev. B*, 86:121409, Sep 2012.

[51] B. Peng, M. Locascio, P. Zapol, S. Li, S. L. Mielke, G. C. Schatz, and H. D. Espinosa. Measurements of near-ultimate strength for multiwalled carbon nanotubes and irradiation-induced crosslinking improvements. *Nat Nano*, 3(10):626–631, Oct 2008.

[52] I. Radović, D. Borka, and Z. L. Mišković. Dynamic polarization of graphene by external correlated charges. *Phys. Rev. B*, 86:125442, Sep 2012.

[53] D. Reddy, L. F. Register, G. D. Carpenter, and S. K. Banerjee. Graphene field-effect transistors. *Journal of Physics D: Applied Physics*, 44(31):313001, 2011.

[54] S. Reich, J. Maultzsch, C. Thomsen, and P. Ordejón. Tight-binding description of graphene. *Phys. Rev. B*, 66:035412, Jul 2002.

[55] Y. Rosenfeld. Free-energy model for the inhomogeneous hard-sphere fluid in D dimensions: Structure factors for the hard-disk (D =2) mixtures in simple explicit form. *Phys. Rev. A*, 42:5978–5989, Nov 1990.

[56] S. D. Sarma and Q. Li. Graphene on $SrTiO_3$. *Solid State Communications*, 152(19):1795 – 1799, 2012.

[57] F. Schedin, A. K. Geim, S. V. Morozov, E. W. Hill, P. Blake, M. I. Katsnelson, and K. S. Novoselov. Detection of individual gas molecules adsorbed on graphene. *Nat Mater*, 6(9):652–655, Sep 2007.

[58] R. Scherrer. *Quantum Mechanics: An Accessible Introduction*. Addison-Wesley, 2005.

[59] F. Schwierz. Graphene transistors. *Nature Nanotechnology*, (7):487496, 2010.

[60] K. W. K. Shung. Dielectric function and plasmon structure of stage-1 intercalated graphite. *Phys. Rev. B*, 34:979–993, Jul 1986.

[61] I. Sodemann and M. M. Fogler. Interaction corrections to the polarization function of graphene. *Phys. Rev. B*, 86:115408, Sep 2012.

[62] N. Stander, B. Huard, and D. Goldhaber-Gordon. Evidence for klein tunneling in graphene p-n junctions. *Phys. Rev. Lett.*, 102:026807, Jan 2009.

[63] T. Stauber, J. Schliemann, and N. M. R. Peres. Dynamical polarizability of graphene beyond the dirac cone approximation. *arXiv*, 2010.

[64] M. D. Stoller, S. Park, Y. Zhu, J. An, and R. S. Ruoff. Graphene-based ultracapacitors. *Nano letters*, 2008.

[65] Z. P. Sun. Graphene mode-locked ultrafast laser. *ACS Nano*, 2010.

[66] Y.-W. Tan, Y. Zhang, K. Bolotin, Y. Zhao, S. Adam, E. H. Hwang, S. Das Sarma, H. L. Stormer, and P. Kim. Measurement of scattering rate and minimum conductivity in graphene. *Phys. Rev. Lett.*, 99:246803, Dec 2007.

[67] J. Toulouse, I. C. Gerber, G. Jansen, A. Savin, and J. G. Ángyán. Adiabatic-connection fluctuation-dissipation density-functional theory based on range separation. *Phys. Rev. Lett.*, 102:096404, Mar 2009.

[68] M. E. Tuckerman. *Statistical Mechanics: Theory and Molecular Simulation*. Oxford Graduate Texts, 2010.

[69] N. M. William Jones. *Theoretical Solid State Physics*. Dover Publications, New York, 2011.

[70] B. Wunsch, T. Stauber, F. Sols, and F. Guinea. Dynamical polarization of graphene at finite doping. *New Journal of Physics*, 8(12):318, 2006.

[71] F. Xia, D. B. Farmer, Y. Lin, and P. Avouris. Graphene field-effect transistors with high on/off current ratio and large transport band gap at room temperature. *Nano Letters*, 10(2):715–718, 2010. PMID: 20092332.

[72] F. Xia, T. Mueller, Y. Lin, A. Valdes-Garcia, and P. Avouris. Ultrafast graphene photodetector. *Nature Nanotechnology*, (12):839843, 2009.

[73] Z. Xu, editor. *Graphene: Properties, Synthesis and Applications*. NOVA, 2011.

[74] J. Xue, J. Sanchez-Yamagishi, D. Bulmash, P. Jacquod, A. Deshpande, K. Watanabe, T. Taniguchi, P. Jarillo-Herrero, and B. J. LeRoy. Scanning tunnelling microscopy and spectroscopy of ultra-flat graphene on hexagonal boron nitride. *Nat Mater*, 10(4):282–285, Apr 2011.

[75] H. Yan, T. Low, W. Zhu, Y. Wu, M. Freitag, X. Li, F. Guinea, P. Avouris, and F. Xia. Damping pathways of mid-infrared plasmons in graphene nanostructures. *Nat Photon*, 7(5):394–399, May 2013. Article.

[76] J. Yan and M. S. Fuhrer. Correlated charged impurity scattering in graphene. *Phys. Rev. Lett.*, 107:206601, Nov 2011.

[77] S. Yuan, R. Roldán, H. De Raedt, and M. I. Katsnelson. Optical conductivity of disordered graphene beyond the dirac cone approximation. *Phys. Rev. B*, 84:195418, Nov 2011.

[78] C. Zener. Analytic atomic wave functions. *Phys. Rev.*, 36:51–56, Jul 1930.

[79] Y. Zhang, V. W. Brar, C. Girit, A. Zettl, and M. F. Crommie. Origin of spatial charge inhomogeneity in graphene. *Nat Phys*, 5(10):722–726, Oct 2009.

[80] Y. Zhang, Y.-W. Tan, H. L. Stormer, and P. Kim. Experimental observation of the quantum hall effect and berry's phase in graphene. *Nature*, 438(7065):201–204, Nov 2005.

Appendix A

Appendix

A.1 Derivation of linear response in graphene

Here we derive the linear polarization function of graphene within the Dirac cone approximation. The derivation follows the procedures of [29, 60, 70]. The full polarization function is given by

$$\chi_0(\mathbf{q},\omega) = -\frac{g_s g_v}{8\pi}\int_{k\leq D} d^2\mathbf{k}\sum_{l,l'}\frac{f_l(\mathbf{k}) - f_{l'}(\mathbf{k}')}{E_l(\mathbf{k}) - E_{l'}(\mathbf{k}') + \omega + i\nu}F_{l,l'}(\mathbf{k},\mathbf{k}') \tag{A.1}$$

The factors g_s and g_v count the spin and valley degeneracy of the system, l and l' denote the type of band (i.e. valence or conduction) and can either be $+1$ or -1. The linear response is a function of $\mathbf{q}$, which is related to $\mathbf{k}'$ through $\mathbf{k}' = \mathbf{k}+\mathbf{q}$. $f_l(\mathbf{k})$ is the Fermi-Dirac distribution and $F_{l,l'}(\mathbf{k},\mathbf{k}')$ is the integral overlap between states given by $\frac{1}{2}(1+(l)(l')\cos(\theta_{\mathbf{k}\mathbf{k}'}))$ where $\theta_{\mathbf{k}\mathbf{k}'}$ is the angle between two vectors and l and l' are either 1 or -1 to indicate the conduction and valence bands respectively. The integral is conducted over all $k \leq D$ where D is taken to be the Fermi wavevector in the Dirac cone approximation, and the sums are evaluated over the two types of bands. To compute the integral we break it up into two parts, $\chi_0^+(\mathbf{q},\omega)$ and $\chi_0^-(\mathbf{q},\omega)$ where $\chi_0^+(\mathbf{q},\omega)$ results from the intra-band electron transitions, and $\chi_0^-(\mathbf{q},\omega)$ results from the inter-band electron transitions. Each one is defined as

$$\begin{aligned}\chi_0^-(\mathbf{q},\omega) = -\frac{g_s g_v}{8\pi}\int d^2\mathbf{k}\Bigg[&\frac{[f_-(\mathbf{k}) - f_-(\mathbf{k}')]\,(1+\cos(\theta_{\mathbf{k}\mathbf{k}'}))}{E_-(\mathbf{k}) - E_-(\mathbf{k}') + \omega + i\nu}\\ &+\frac{f_-(\mathbf{k})(1-\cos(\theta_{\mathbf{k}\mathbf{k}'}))}{E_-(\mathbf{k}) - E_+(\mathbf{k}') + \omega + i\nu} - \frac{f_+(\mathbf{k})(1-\cos(\theta_{\mathbf{k}\mathbf{k}'}))}{E_+(\mathbf{k}) - E_-(\mathbf{k}') + \omega + i\nu}\Bigg]\end{aligned}$$

and

$$\begin{aligned}\chi_0^+(\mathbf{q},\omega) = -\frac{g_s g_v}{8\pi}\int_{k\leq D} d^2\mathbf{k}\Bigg[&\frac{[f_+(\mathbf{k}) - f_+(\mathbf{k}')]\,(1+\cos(\theta_{\mathbf{k}\mathbf{k}'}))}{E_+(\mathbf{k}) - E_+(\mathbf{k}') + \omega + i\nu}\\ &+\frac{f_+(\mathbf{k})(1-\cos(\theta_{\mathbf{k}\mathbf{k}'}))}{E_+(\mathbf{k}) - E_-(\mathbf{k}') + \omega + i\nu} - \frac{f_-(\mathbf{k})(1-\cos(\theta_{\mathbf{k}\mathbf{k}'}))}{E_-(\mathbf{k}) - E_+(\mathbf{k}') + \omega + i\nu}\Bigg]\end{aligned}$$

We assume that graphene is at zero temperature and the valence band is full. This implies that $f_-(\mathbf{k}) = 1$. Using the linear dispersion relation near the Dirac cone $\chi^-(\mathbf{q},\omega)$ becomes,

$$\chi_0^-(\mathbf{q},\omega) = -\frac{g_s g_v}{8\pi}\int d^2\mathbf{k}(1-\cos(\theta_{\mathbf{k}\mathbf{k}'}))\left[\frac{1}{-v_F(k+k')+\omega+i\nu}-\frac{1}{v_F(k+k')+\omega+i\nu}\right]$$

Set $\mathbf{k}' = \mathbf{k}+\mathbf{q}$ then, by the law of cosines we have $\cos(\theta_{\mathbf{k}\mathbf{k}'}) = \frac{k-q\cos(\beta)}{k'}$ where β is the angle between $\mathbf{k}$ and $\mathbf{q}$. Define a new variable $u = k+k' = k+\sqrt{k^2+q^2-2kq\cos(\beta)}$. Then

$$\begin{aligned} d\beta =& \frac{u-k}{qk}(1-\cos^2(\beta))^{-1/2} \\ =& \frac{u-k}{qk}\left[1-\left(\frac{k^2+q^2-(u-k)^2}{2kq}\right)^2\right]^{-1/2} \end{aligned}$$

Now our limits of integration are between $u = k+|\mathbf{k}+\mathbf{q}|$ and $u = k+|\mathbf{k}-\mathbf{q}|$, so after some algebra the integral becomes

$$\int_0^\infty\int_{k+|\mathbf{k}+\mathbf{q}|}^{k+|\mathbf{k}-\mathbf{q}|} dk\,du\,\frac{(u-2k)^2-q^2}{\sqrt{(q^2-u^2)[(u-2k)^2-q^2]}}\left[\frac{1}{-v_F u+\omega+i\nu}-\frac{1}{v_F u+\omega+i\nu}\right]$$

Again set $x = u-2k$ and $y = u$ to get

$$\begin{aligned} \chi_0^-(\mathbf{q},\omega) =& -\frac{g_s g_v}{8\pi}\int_q^\infty\int_{-q}^{q} dx\,dy\,\sqrt{\frac{x^2-q^2}{q^2-y^2}}\left[\frac{1}{-v_F y+\omega+i\nu}-\frac{1}{v_F y+\omega+i\nu}\right] \\ =& -\frac{g_s g_v}{4\pi^2}\int_q^\infty dy\,\frac{\pi v_F y q^2}{2\sqrt{y^2-q^2}[(\omega+i\nu)^2-v_F^2 y^2]} \end{aligned}$$

Integrating the final equation and taking the limit $\nu \to 0$ we have

$$\chi_0^-(\mathbf{q},\omega) = i\frac{q^2}{4\sqrt{\omega^2-v_F^2 q^2}} \tag{A.2}$$

The evaluation of $\chi^+(\mathbf{q},\omega)$ is quite tedious and lengthy. We omit its derivation in this thesis, which can be found in [70].

A.2 Derivation of $\bar{M}^{l,l'}_{\mathbf{k},\mathbf{k}+\mathbf{q}}$

The matrix $\bar{M}^{l,l'}_{\mathbf{k},\mathbf{k}+\mathbf{q}}$ is given by the integral,

$$\begin{aligned} \bar{M}^{l,l'}_{\mathbf{k},\mathbf{k}+\mathbf{q}} =& \int d^2\mathbf{r}\int dz\,\Psi^*_{l,\mathbf{k}}(\mathbf{r},z)e^{-i\mathbf{q}\cdot\mathbf{r}}\,\Psi_{l',\mathbf{k}+\mathbf{q}}(\mathbf{r},z) \\ =& \int d^2\mathbf{r}\int dz\left[a^*_{\mathbf{k},l}\psi^*_{A,\mathbf{k}}+b^*_{\mathbf{k},l}\psi^*_{B,\mathbf{k}}\right]e^{-i\mathbf{q}\cdot\mathbf{r}}\left[a_{\mathbf{k}+\mathbf{q},l'}\psi_{A,\mathbf{k}+\mathbf{q}}+b_{\mathbf{k}+\mathbf{q},l'}\psi_{B,\mathbf{k}+\mathbf{q}}\right] \end{aligned}$$

Using equation 2.3 we can express the terms $\psi_{A,\mathbf{k}}$ and $\psi_{B,\mathbf{k}}$ as a sum over the p_z orbitals. Looking at the individual terms without their coefficients and expanding the integral in terms of the p_z orbitals we get,

$$\begin{aligned}(\bar{M}^{l,l'}_{\mathbf{k},\mathbf{k}+\mathbf{q}})^{i,j} &= \int d^2\mathbf{r} \int dz\, \psi^*_{i,\mathbf{k}} e^{-i\mathbf{q}\cdot\mathbf{r}} \psi_{j,\mathbf{k}} \\ &= \frac{1}{N} \sum_{\mathbf{R}} \sum_{\mathbf{R}'} e^{i(\mathbf{k}+\mathbf{q})\cdot(\mathbf{R}+\mathbf{t}_i) - i\mathbf{k}\cdot(\mathbf{R}'+\mathbf{t}_j)} \int d^2\mathbf{r} \int dz\, \varphi^*_{p_z}(\mathbf{r}-\mathbf{R}'-\mathbf{t}_j; z) e^{-i\mathbf{q}\cdot\mathbf{r}} \varphi_{p_z}(\mathbf{r}-\mathbf{R}-\mathbf{t}_i; z)\end{aligned}$$

Here i and j are indices identifying either position A or position B atoms in the sub-lattice, $\mathbf{t}_i$ are the nearest neighbour vectors and $\mathbf{R}$ are the Bravias lattice vectors. The overlap integral between p_z orbitals on different Bravais lattice sites (i.e. $\mathbf{R} \neq \mathbf{R}'$) will be negligible so we will ignore them. This reduces our integral to,

$$\begin{aligned}(\bar{M}^{l,l'}_{\mathbf{k},\mathbf{k}+\mathbf{q}})^{i,j} &= \frac{1}{N} \sum_{\mathbf{R}} e^{i(\mathbf{k}+\mathbf{q})\cdot(\mathbf{t}_i-\mathbf{t}_j) + i\mathbf{q}\cdot\mathbf{t}_j} \int d^2\mathbf{r} \int dz\, \varphi^*_{p_z}(\mathbf{r}-\mathbf{R}-\mathbf{t}_j; z) e^{-i\mathbf{q}\cdot(\mathbf{r}-\mathbf{R})} \varphi_{p_z}(\mathbf{r}-\mathbf{R}-\mathbf{t}_i; z) \\ &= \sum_{\alpha} e^{i(\mathbf{k}+\mathbf{q})\cdot\mathbf{w}_\alpha} \int d^2\mathbf{r} \int dz\, \varphi^*_{p_z}(\mathbf{r}; z) e^{-i\mathbf{q}\cdot\mathbf{r}} \varphi_{p_z}(\mathbf{r}-\mathbf{w}_i; z)\end{aligned}$$

where we define $\mathbf{w}_\alpha = \mathbf{t}_i - \mathbf{t}_j$ to be a difference between nearest neighbour positions within the unit cell. Once again, assuming that the nearest neighbour overlap integral is negligible we are left with

$$(\bar{M}^{l,l'}_{\mathbf{k},\mathbf{k}+\mathbf{q}})^{i,i} = \int d^2\mathbf{r} \int dz\, |\varphi_{p_z}(\mathbf{r}; z)|^2 e^{-i\mathbf{q}\cdot\mathbf{r}}$$

Using the hydrogen like wavefunctions for the p_z orbital we get,

$$(\bar{M}^{l,l'}_{\mathbf{k},\mathbf{k}+\mathbf{q}})^{A,A} = (\bar{M}^{l,l'}_{\mathbf{k},\mathbf{k}+\mathbf{q}})^{B,B} = \left[1 + \left(\frac{a_0 q}{Z_{\text{eff}}}\right)^2\right]^{-3} \tag{A.3}$$

were a_o is the Bohr radius and Z_{eff} is the effective charge of the nucleus of the carbon atom. Now to include the coefficients in our analysis, we recall that the coefficients for sublattice sites A and B are $a_{\mathbf{k},l} = 1$ and $b_{\mathbf{k},l} = \frac{f(\mathbf{k})}{|f(\mathbf{k})|}$ respectively. So the final equation for the matrix is

$$\bar{M}^{l,l'}_{\mathbf{k},\mathbf{k}+\mathbf{q}} = \left[1 + \left(\frac{a_0 q}{Z_{\text{eff}}}\right)^2\right]^{-3} \left[1 + \frac{f(\mathbf{k}) f(\mathbf{k}+\mathbf{q})}{|f(\mathbf{k}) f(\mathbf{k}+\mathbf{q})|}\right] \tag{A.4}$$

A.3 Green's function of vacuum gap model

Here we present the Green's function of the vacuum gap model (fig. 3.2), whose derivation we will omit. The result is an adaptation of the Green's function in [50], with minor changes to account for the geometric difference of the substrate. The Green's function is only valid for source points in the

same layer in which graphene resides. For $0 < z, z' < H$ the Green's function is given by

$$G^0(z,z') = \frac{2\pi}{\epsilon_2 q}\left[e^{-q|z-z'|} + \frac{\lambda_t\lambda_b e^{-2qH}}{1-\lambda_t\lambda_b e^{-2qH}}[e^{-q(z-z')} + e^{q(z-z')}] - \frac{\lambda_t e^{(z+z'-2qh)} + \lambda_b e^{(z+z')}}{1-\lambda_t\lambda_b e^{-2qH}}\right] \tag{A.5}$$

where $\lambda_t = \frac{\epsilon_3-\epsilon_2}{\epsilon_3+\epsilon_2}$ and $\lambda_t = \frac{\epsilon_1\coth(qL)-\epsilon_2}{\epsilon_1\coth(qL)+\epsilon_2}$

A.4 Geometric structure models

Here we present the structure factor for the Hard disc (HD) model without derivation. For a complete derivation and limitations of the model see [55]. The HD model assumes that the pair potential between particles in the Hamiltonian is infinite below some distance r_c and zero otherwise. The statistical mechanics of the model can be described using by the the packing fraction $p = \pi n_{\text{imp}} r_c^2/4$, where $n_{\text{imp}} = N/A$ is their areal number density, and r_c is the disc diameter. The structure factor for the HD model is

$$I_{HD}(q) = \left\{1 + 16a\left[\frac{J_1(qr_c/2)}{qr_c}\right]^2 + 8b\frac{J_0(qr_c/2)J_1(qr_c/2)}{qr_c} + \frac{8p}{1-p}\frac{J_1(qr_c)}{qr_c}\right\}^{-1} \tag{A.6}$$

with

$$\begin{aligned} a &= 1 + x(2p-1) + \frac{2p}{1-p}, \\ b &= x(1-p) - 1 - \frac{3p}{1-p}, \\ x &= \frac{1+p}{(1-p)^3}. \end{aligned}$$

Note that the important long wavelength limit is given by $I_{HD}(0) = 1/x = (1-p)^3/(1+p)$. The expression in equation A.6 should be compared with the structure factor for a model with the step-like pair correlation function,[76, 39]

$$I_{SC}(q) = 1 - \frac{8p}{qr_c}J_1(qr_c), \tag{A.7}$$

which gives $I_{SC}(0) = 1 - 4p$.